LEVEL II

SYSTEMS, SCIENCE AND SOFTWARE

SSS-R-79-3847

AD A069802

SUMMARY OF SEISMIC DISCRIMINATION AND EXPLOSION YIELD DETERMINATION RESEARCH

T. C. BACHE
J. M. SAVINO
S. M. DAY
J. T. CHERRY
H. J. SWANGER
N. RIMER

FINAL REPORT

SPONSORED BY

ADVANCED RESEARCH PROJECTS AGENCY
ARPA ORDER No. 2551

This research was supported by the Advanced Research Projects Agency of the Department of Defense and was monitored by AFTAC/VSC, Patrick Air Force Base, Florida, 32925, under Contract No. F08606-76-C-0041.

APPROVED FOR PUBLIC RELEASE, DISTRIBUTION UNLIMITED.

NOVEMBER 1978

P. O. BOX 1620, LA JOLLA, CALIFORNIA 92038, TELEPHONE (714) 453-0060

2

AFTAC Project Authorization No. VELA/T/7712/B/ETR

ARPA Order 2551, Program Code 8F10

Effective Date of Contract: October 1, 1976

Contract Expiration Date: September 30, 1978

Amount of Contract: $435,087

Contract No. F08606-76-C-0041

Principal Investigator and Phone No.
Dr. Thomas C. Bache, (714) 453-0060, Ext. 337

Project Scientist and Phone No.
Captain Michael J. Shore, (202) 325-7581

UNCLASSIFIED

SECURITY CLASSIFICATION OF THIS PAGE (When Data Entered)

REPORT DOCUMENTATION PAGE	READ INSTRUCTIONS BEFORE COMPLETING FORM
1. REPORT NUMBER	2. GOVT ACCESSION NO.
	3. RECIPIENT'S CATALOG NUMBER (9)
4. TITLE (and Subtitle) (6) SUMMARY OF SEISMIC DISCRIMINATION AND EXPLOSION YIELD DETERMINATION RESEARCH,	5. TYPE OF REPORT & PERIOD COVERED Final Report.
	6. PERFORMING ORG. REPORT NUMBER (14) SSS-R-79-3847
7. AUTHOR(s) (10) T. C. Bache, J. M. Savino, S. M. Day, J. T. Cherry, H. J. Swanger and N. Rimer	8. CONTRACT OR GRANT NUMBER(s) (15) F08606-76-C-0041
9. PERFORMING ORGANIZATION NAME AND ADDRESS Systems, Science and Software P. O. Box 1620 La Jolla, California 92038	10. PROGRAM ELEMENT, PROJECT, TASK AREA & WORK UNIT NUMBERS Program Code No. 6H189 ARPA Order No. 2551
11. CONTROLLING OFFICE NAME AND ADDRESS VELA Seismological Center 312 Montgomery Street Alexandria, Virginia 22314	12. REPORT DATE November 1978
	13. NUMBER OF PAGES 127
14. MONITORING AGENCY NAME & ADDRESS (if different from Controlling Office) (12) 125 p.	15. SECURITY CLASS. (of this report) Unclassified
	15a. DECLASSIFICATION DOWNGRADING SCHEDULE

16. DISTRIBUTION STATEMENT (of this Report)

Approved for Public Release, Distribution Unlimited.

17. DISTRIBUTION STATEMENT (of the abstract entered in Block 20, if different from Report)

18. SUPPLEMENTARY NOTES

19. KEY WORDS (Continue on reverse side if necessary and identify by block number)

Nuclear Explosion Seismology
Seismic Discrimination
Seismic Source Theory
Nuclear Explosion Yield Determination

20. ABSTRACT (Continue on reverse side if necessary and identify by block number)

This report summarizes the work accomplished in a twenty-four month research program directed toward resolution of technical issues arising in the seismic verification of an underground nuclear test ban treaty. Emphasis is on research conducted during the last year in five subject areas: data analysis, source studies, grout experiments, surface wave studies and body wave studies. →

DD FORM 1 JAN 73 1473 EDITION OF 1 NOV 65 IS OBSOLETE

UNCLASSIFIED

SECURITY CLASSIFICATION OF THIS PAGE (When Data Entered)

368 501

20. Abstract (continued)

Results are summarized for thirteen research projects.

The report also includes an appendix in which abstracts are listed for seventeen technical reports submitted under this contract. Also included are the abstracts for twelve reports submitted under a preceding fifteen month contract.

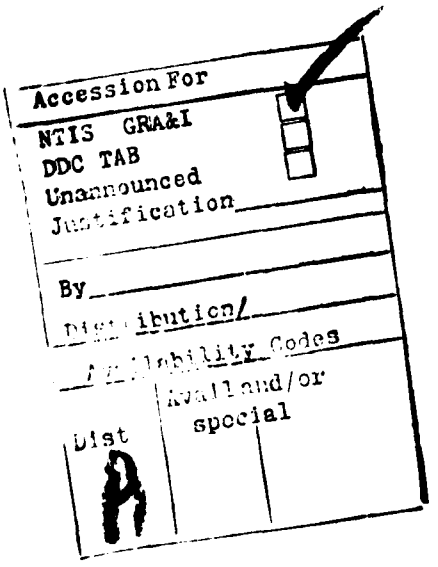

TABLE OF CONTENTS

TABLE OF CONTENTS (Continued)

LIST OF ILLUSTRATIONS

LIST OF ILLUSTRATIONS (Continued)

LIST OF ILLUSTRATIONS (Continued)

LIST OF FIGURES (Continued)

LIST OF TABLES

I. INTRODUCTION

During the past twenty-four months, Systems, Science and Software (S^3) has been conducting a research program directed to resolution of technical issues arising in the seismic verification of an underground nuclear test ban treaty. This report is intended to summarize the work done in this ARPA supported research effort which was monitored by AFTAC/VSC.

The objective of this S^3 research program is to examine the parameters that affect the seismic signals from underground explosions and earthquakes. Our attention is primarily directed to those features of the seismic waveforms that discriminate between the two classes of events and that reliably indicate the explosion yield.

Since 1 October 1976, S^3 has submitted seventeen technical reports to AFTAC/VSC. Seven are required quarterly technical reports. Each of these includes detailed technical descriptions of two to five research projects. These quarterly reports are often used to report research results that, while important, do not seem to warrant separate publication. Some of the work described in the quarterlies is not yet complete and is later published in special reports.

The other ten technical reports submitted to AFTAC/VSC since October 1976 are special technical reports devoted to presentation of results from a completed research project. These reports are intended to be complete and of comparable standard to the referenced literature.

In Appendix A the seventeen technical reports and their abstracts are listed. Also listed in the Appendix are the abstracts for twelve technical reports submitted to AFTAC/VSC under a previous fifteen month contract (1 May 1975 - 1 October 1976). These twenty-nine report abstracts provide

an excellent overview of the range and depth of the S^3 research program in support of United States efforts to monitor a test ban treaty.

In this final contract report we present summaries of thirteen of our most important and interesting research projects. These summaries are divided into five subject areas. A brief description of each of the thirteen projects, together with the principal S^3 scientists concerned with each, is given below.

I. DATA ANALYSIS - Four Projects

A. Discrimination Experiment - We are participating in an experiment to test the effectiveness of the S^3 developed VFM discriminant. Data for Eurasian earthquakes and explosions are being provided for our analysis.

Principal Scientists: J. M. Savino, J. F. Masso and C. B. Archambeau (Consultant, University of Colorado).

B. Spectral m_b and M_s - A new event magnitude based on narrow-band filter amplitudes is being developed and tested. The basic algorithm is based on output from the MARS program used for the VFM discriminant.

Principal Scientists: T. C. Bache, D. L. Lambert and C. B. Archambeau.

C. Multiple Explosion Decomposition - Multiple explosion recordings constructed by scaling, lagging and summing single event records in both the near- and far-field were analyzed to determine how well individual events in an array could be identified.

Principal Scientists: D. G. Lambert, T. C. Bache, J. F. Masso, J. M. Savino and C. B. Archambeau.

D. Analysis of P Wave Residuals - A large data set of world-wide P wave travel time residuals was correlated with heat flow, magnitude residuals and other geophysical parameters.

Principal Scientist: J. M. Savino.

II. SOURCE STUDIES - Four Projects

A. Finite Difference Explosion Modeling - Explosions can be modeled in detail in both one and two dimensions. Most of our work has been in one dimension. We are now studying two dimensional effects.

Principal Scientists: J. T. Cherry and N. Rimer.

B. Transmitting Boundary Condition - A transmitting boundary is an important addition to a finite difference program because it allows substantial reduction of grid size and thus cost. Such a capability has been implemented for high frequency waves impinging on plane boundaries.

Principal Scientist: S. M. Day.

C. ILLIAC Earthquake Modeling - A three-dimensional model of earthquake faulting has been implemented on the ILLIAC computer and several interesting calculations have been completed.

Principal Scientist: S. M. Day.

D. Analytical Continuation of Finite Difference Source Calculations - An analytical continuation scheme has been developed to link two-dimensional source calculations including free surface effects with the analytical wave propagation techniques of theoretical seismology.

Principal Scientists: T. G. Barker and H. J. Swanger.

III. GROUT EXPERIMENTS

Small-scale explosion experiments in grout blocks were carried out to model three classes of events: free-field, contained (at roughly the scaled depth of nuclear tests) and cratering. The results were analyzed and modeled with finite difference methods.

Principal Scientists: J. T. Cherry, P. L. Coleman and S. M. Day.

IV. SURFACE WAVE STUDIES - Two Projects

A. Surface Wave Inversion - An improved method for determining plane-layered earth models that accurately represent the important features controlling the amplitude and waveform of surface waves was developed and applied to two paths; NTS-Albuquerque and NTS-Tucson.

Principal Scientists: T. C. Bache, W. L. Rodi and D. G. Harkrider (Consultant, California Institute of Technology).

B. Source Amplitudes from Surface Waves - Using the models of the previous project, synthetic

seismograms were compiled and compared to data to infer the source characteristics of NTS explosions.

Principal Scientists: T. C. Bache and W. L. Rodi.

V. BODY WAVE STUDIES - Two Projects

A. Analysis of ATI Decoupling Calculations - Results of two finite difference calculations of decoupled nuclear explosions in salt that were done by Applied Theory, Inc., were provided to S^3 for analysis. Equivalent elastic sources were computed for these calculations and then studied to determine the influence of decoupling on the radiated body and surface waves.

Principal Scientists: T. C. Bache and J. F. Masso.

B. Influences of Interfaces on Near-Field Ground Motions - Linear elastic calculations were done to determine the influence of interfaces, particularly the free surface, on the ground motions in the near-field of nuclear explosions. Recommendations were made for the optimum gauge locations for measuring that portion of the source that controls the far-field seismic waves.

Project Scientists: T. G. Barker and T. C. Bache.

II. DATA ANALYSIS

2.1 DISCRIMINATION EXPERIMENT

Our objective in the discrimination experiment is to analyze seismic waveforms from a large population of events in order to identify the events as either earthquakes or underground explosions. The waveforms that we have concentrated on to date are short-period P waves recorded by a global network of seismograph stations. To date we have analyzed some 28 events at up to nine stations.

The variable frequency magnitude discriminant, as proposed by Archambeau, et al. (1974), and first tested by Savino and Archambeau (1974), is the technique that we are using to identify the Eurasian events. The variable frequency magnitudes are computed by the Multiple Arrival Recognition System (MARS) program, especially designed for event detection and discrimination.

The central feature of the MARS signal analysis program is the use of narrow-band frequency filters to break up or decompose a time series consisting of signal plus noise into a set of quasi-harmonic modulated "signals". This set of filtered signals, one for each filter center frequency, can then be used to determine the energy arrival time (the group arrival time, t_g) and amplitude of the signal for each center frequency by analysis of the time modulation of the filter outputs.

Of particular note is the use of Gaussian-shaped narrow-band filters. This particular filter form is selected to satisfy two goals: (1) minimum width in the frequency domain, and (2) maximum ripple suppression in the time domain. As a consequence of the sampling theorem, or uncertainty principle, one cannot simultaneously satisfy these two goals to arbitrary precision. The filter employed was selected for its optimal

time and frequency domain characteristics within this basic limitation.

The narrow-band filtered signal will appear as a quasi-sinusoidal carrier wave contained within a smooth envelope. The MARS program next computes an envelope function by means of the Hilbert transform. The maximum of the envelope function occurs at the time of arrival of energy at the center frequency of the filter and the amplitude of the maximum is proportional to the spectral amplitude of the filtered signal at the filter center frequency. Finally, the variable frequency magnitudes for event discrimination are based on the envelope maxima.

The actual procedure used for discriminating the 28 Eurasian events received during this reporting period was to estimate $\bar{m}_b$ values at several different frequencies within the teleseismic band pass (i.e., 0.3 to several hertz). Given these estimates, we then construct $m_b(f_1)$ versus $m_b(f_2)$ plots, with $f_1 << f_2$, for different sensor-source region combinations and test for event discrimination. Toward the end of this reporting period we introduced procedures for making noise corrections and obtaining more stable $\bar{m}_b(f)$ estimate by averaging over a high and low frequency band. These newly implemented procedures will be used on all events analyzed in the future.

Table 1 summarizes the event identifications that have been made to date based on results from nine of the stations contributing data to this experiment. The highest number of stations that contributed seismograms for any one event is 7. This explains the blanks that occur throughout this table. The most important thing to note in this table is the fairly consistent dichotomy of most of the events. Of the four events (47, 49, 62 and 63) which cross population boundaries, the majority of stations predict that three (47, 49 and 62) are earthquakes and the fourth (63) explosion-like. The

TABLE 1

PRELIMINARY EVENT IDENTIFICATION

EARTHQUAKES (EVENT NUMBER)							
ANMO	BFAK	CHTO	CTAO	ILPA	KAAO	KSRS	LAO
	36						
	38			38			
				41			
47	47			47			47
				48			
49		49	49		49	49	49
50	50				50	50	
				55			
			56	56			
	57			57			
	58			58			
				59			
	60						
	61						
62							
				63			
	64			64	64		

EXPLOSION-LIKE EVENTS (EVENT NUMBER)							
ANMO	BFAK	CHTO	CTAO	ILPA	KAAO	KSRS	LAO
1	1	1			1	1	
14	14	14			14		
16	16					16	
	17						
18		18		18		18	
19		19		19	19	19	19
20		20	20	20	20	20	
21	21		21	21	21	21	
22				22	22	22	
	33			33			33
		47	47				
				49			
53	53		53	53	53		
63	63				63		

locations of these four events along the Japan and Kurile Island arc systems suggest that these events are most likely to be earthquakes. This then leads to the remaining point about Table 1. Those events which are presumed explosions, namely, events 1, 14, 16, 17, 18, 19, 20, 21, 22, 23, 33 and 53, in no case cross population boundaries. These eleven events are consistently identified as explosions at each and every one of the stations at which they are recorded. After the data base increases, we will try multi-station discrimination techniques which should improve the discrimination results.

2.2 SPECTRAL MAGNITUDES: $\hat{m}_b$ AND $\hat{M}_s$

The purpose of the work described in this section is to define a new measure of seismic magnitude. We are not concerned with the procedure by which individual station magnitudes are combined to define an event magnitude, but rather with the processing of individual seismograms. Current practice requires: (1) selection of the phase to be measured, (2) time domain measurement of the amplitude (A) and period (T) of this phase, (3) correction of the amplitude for the instrument amplification at the measured period, and (4) calculation of log A or log A/T which is added to some empirical range and station correction to obtain the magnitude m_b or M_s.

There are many reasons to question the reliability of the conventional magnitude measure described above. However, it remains the preferred method for several reasons, not the least of which is the fact that no better way has been found. Our criteria for a "better" method are as follows: (We assume that the data are available in digital form.)

- The method should be able to be automated. That is, allowing for some guidance by an analyst, it should be able to select the phase to be measured and automatically compute the magnitude.

- The magnitude should be as good or better an indicator of source amplitude as the conventional magnitude. It should not be strongly sensitive to noise, interfering phases, coda amplitude, etc.

A magnitude measure that seems to satisfy these criteria has been defined and is now being tested on body wave recordings of NTS explosives. The magnitudes are called $\hat{m}_b$ and $\hat{M}_s$ and are a natural result of the data processing of our MARS (Multiple Arrival Recognition System) program. This is the same program being used for the discrimination experiment described in Section 2.1. The MARS program is also used as a signal detector.

Briefly described, the MARS algorithm is as follows. The seismogram is Fourier transformed and filtered by a narrow band, Gaussian filter. The Hilbert transform of the filtered spectrum is then constructed and inverse transformed to obtain the envelope function. The peaks of the envelope function indicate phase arrivals of energy in a narrow band of frequencies near the filter center frequency. The arrival times are accurately preserved in the times of these peaks and the relative amplitudes of the peaks reflect the relative amplitudes of arriving pulses of energy in the frequency band.

The discrimination algorithm described in Section 2.1 is based on comparison of high and low frequency values of a "variable frequency magnitude" or VFM. The VFM is like a magnitude defined in the usual way with the time domain amplitude/period quotient being replaced by the product of the envelope function peak and filter center frequency. This VFM is frequency dependent since there is a different magnitude for each filter.

The motivation for the definitions for $\hat{m}_b$ and $\hat{M}_s$ is the observation that the VFM provides, for a particular group arrival time, an estimate of the spectral energy in a narrow frequency band. The idea is to, in some sense, average this

quantity in the region of maximum spectral energy which is also the band sampled by the conventional time domain measurements.

In this section we specify our measurement of $\hat{m}_b$ and show some examples. An entirely analogous procedure is used to define $\hat{M}_s$. The set of seismograms to be analyzed to illustrate the $\hat{m}_b$ are plotted in Figure 1. These are HNME recordings of eleven large yield explosions at Pahute Mesa, NTS. These records were processed by MARS and the results are shown in Figure 2. These plots were obtained in the following way.

- Each seismogram was filtered by 48 constant width narrow-band filters with center frequencies (f_c) from 0.2 - 1.6 Hz and specified by $Q = 15\ f_c$. For the lowest frequencies, $Q = 5.25$ and the filter width was f_c dependent; otherwise the filter width was constant.

- Envelope peak amplitudes, $A_c(f_c)$, with group arrival times, $t_g(f_c)$, within a six second window about the P wave arrival time were selected. In many cases there are two or more such peaks.

- The largest peak for $0.35 \leq f_c \leq 1.6$ was identified. Using this peak as a starting point, one peak is then selected for each f_c, with the selection made to maximize the smoothness of t_g versus f_c and A_c versus f_c.

In Figure 2, we show log $(A_c \cdot f_c)$ and t_g versus f_c for each event for f_c between 0.2 and 1.6 Hz. The zero crossing between the first peak and first trough is defined to be at $t_g = 0$. The amplitude quantity plotted in Figure 2 is essentially the VFM (variable frequency magnitude) which is used for event discrimination (e.g., Savino and Archambeau, 1974; Savino, et al., 1975 and Rodi, et al., 1978). The definition of VFM used in the discrimination work is

$$\bar{m}_b(f_c) = \log (A_{c\ max} \cdot f_c) + B(\Delta) \qquad (1)$$

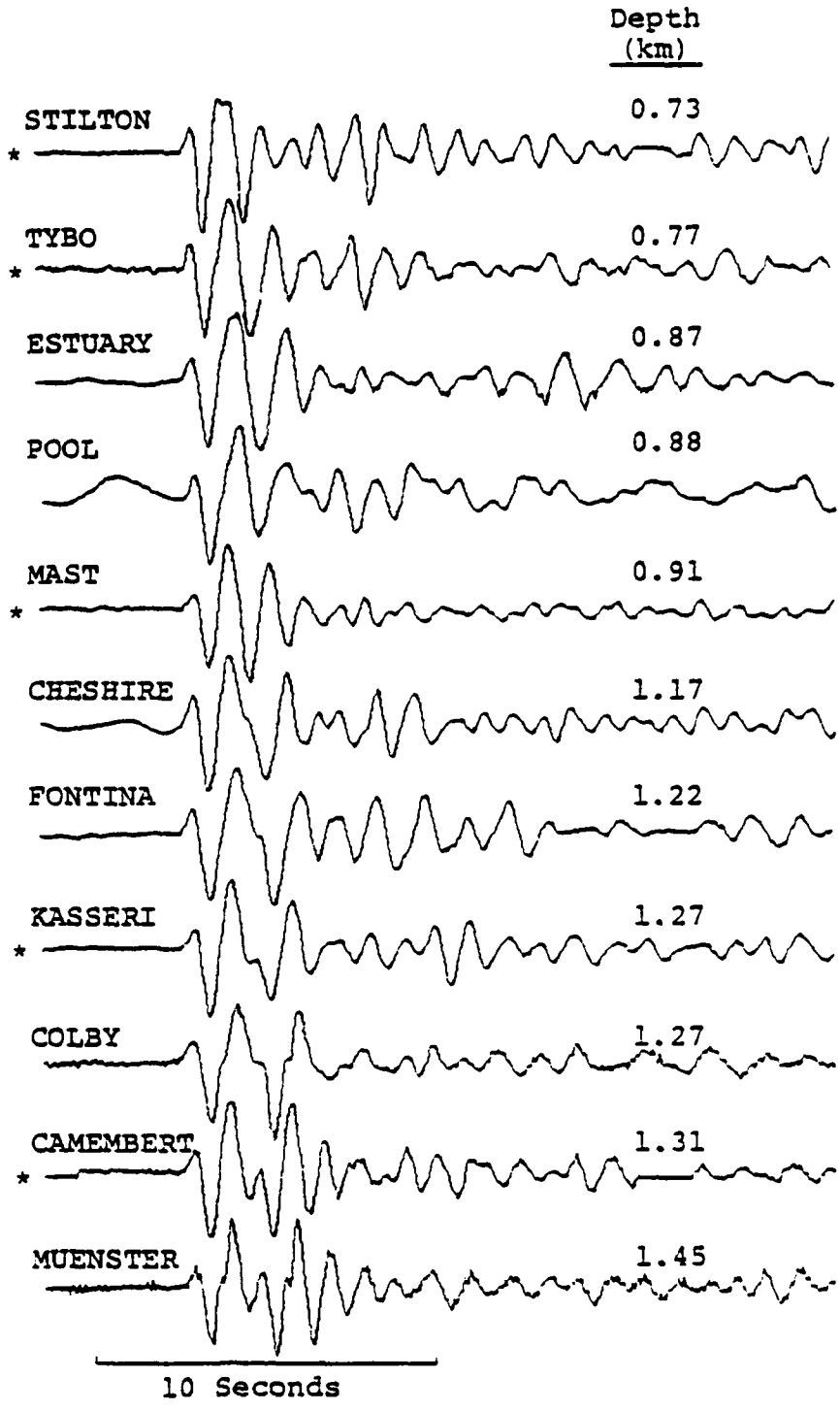

Figure 1. The HNME recordings of eleven Pahute Mesa events are arranged according to increasing depth. The asterisk denotes events recorded by the 18300 seismometer. The others were recorded by the KS36000.

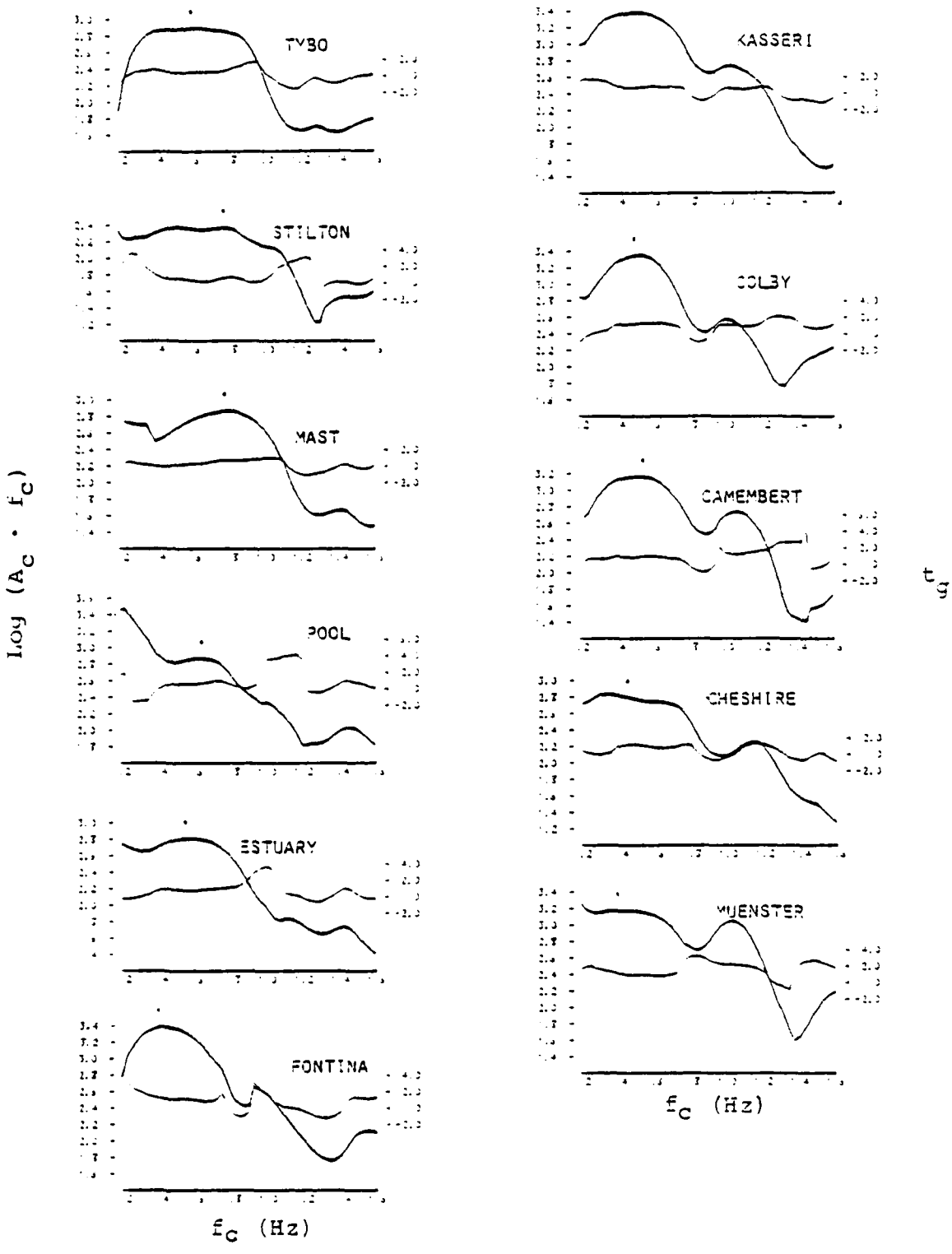

Figure 2. For each of the HNME recordings of Figure 1 we plot log ($A_c \cdot f_c$) and t_g versus filter center frequency, f_c. The t_g scale is at the right on each plot. The band for the $\hat{m}_b$ determination is indicated by small vertical bars. The maximum log ($A_c \cdot f_c$) in this band is marked with an asterisk.

where $B(\Delta)$ is the usual Gutenberg-Richter distance correction for peak amplitude. For Pahute Mesa to HNME, $\Delta \approx 36.7°$ and $B(\Delta) = 3.53$. This formula is the frequency domain analog of the standard formula for time domain m_b.

The log $(A_c \cdot f_c)$ is a velocity-like quantity. Since the instrument response has been removed and the geometric attenuation is nearly independent of frequency, the only important filter applied to the data should be the Q operator; that is, $\exp [- \pi f_c t^*]$ where t^* is the travel time divided by the effective Q for the path. Thus, the log $(A_c \cdot f_c)$ falls off at high and low frequency and has the peaked character seen.

The data plotted in Figure 2 are used to define $\hat{m}_b$. There are several possibilities for how this might be done. In each case we define $\hat{m}_b$ according to

$$\hat{m}_b = \mathcal{A} + B \ , \qquad (2)$$

where B is the Guttenberg-Richter distance correction plus (possibly) some empirically determined station correction. Possible definitions for $\mathcal{A}$ include:

1. $\mathcal{A}$ is log $(A_c \cdot f_c)$ at a single frequency;
2. $\mathcal{A}$ is the maximum value of log $(A_c \cdot f_c)$ in a particular f_c band;
3. $\mathcal{A}$ is the average log $(A_c \cdot f_c)$ over a fixed band;
4. $\mathcal{A}$ is the average value of log $(A_c \cdot f_c)$ in an f_c band defined by requiring that t_g remain within specified limits.

These alternatives are being evaluated by testing their application to actual data like that in Figure 1. Preliminary indications are that the fourth definition is to be preferred. As implemented, this definition requires selection of the

peak log ($A_c \cdot f_c$) for $f_c \geq 0.35$. This peak is indicated by a "*" on the plots in Figure 2. The end points of the band about this value are then the nearest points at which the t_g is more than one second different from that at the peak. This band is indicated in Figure 2 by small vertical bars.

Results of the testing of $\hat{m}_b$ and $\hat{M}_s$ will be reported to VSC during the next contract (FY'79). Our intention is to evaluate this technique for possible implementation in an automated detection/discrimination/yield determination system.

2.3 MULTIPLE EXPLOSION DECOMPOSITION

During the contract, S^3 completed two studies which were intended to test our capabilities to identify and describe multiple explosion configurations from seismic data. The first of these studies, "Simulation and Decomposition of Multiple Explosions", by D. G. Lambert, T. C. Bache and J. M. Savino, was concerned with the decomposition of close-in data. The second study, "Identification of Individual Events in a Multiple Explosion from Teleseismic Short Period Body Wave Recordings", by D. G. Lambert and T. C. Bache, was concerned with teleseismic data. The important results from these studies will now be summarized.

2.3.1 Near-Field Data

In the near-field experiment, several multiple explosion configurations were simulated using vertical velocity recordings of the Pahute Mesa events MAST, COLBY and POOL from ranges less than 20 km. These data were then analyzed with MARS to determine event time separation and amplitude scaling. Three distinct types of simulations were done.

The first kind of simulated multiple event can be considered to be comprised of an array of three closely spaced, equal-sized explosions observed along two close-in station

arrays. For these composites we summed the individual station seismograms with themselves. Thus, we did not account for path differences between the individual explosions and the receiver. Application of the narrow-band filtering technique (frequency range from 3 to 100 Hz) to these simulations yielded the following significant results.

- Separation of the individual events was observed to begin at a characteristic frequency that is about 3.5 times the inverse of the explosion lag time. The explosion lag times ranged from 0.034 to 2.0 seconds in the several simulated events studied.

- Accurate separation and relative scaling of events is achieved as long as the signal-to-noise ratio is one or more at the aforementioned characteristic frequency. This requirement is most easily met at stations close to the event, since high frequency energy attenuates rapidly with distance. For single station teleseismic recordings the signal-to-noise ratio is such that separation of events with less than 2.0 second lags was not achieved.

The second kind of multiple event can be thought of as an array of four widely spaced, equal-sized explosions observed at one close-in station. Such an event is simulated by summing seismograms from a linear array of stations that recorded one event. We think of the actual explosion epicenter as the recording station for our simulated event and the actual recording stations are then the epicenters of the events in our simulation. In this way the simulated event includes propagation path differences between the various sources and the receiver. Several such events were constructed and the application of the narrow-band filter technique gives the following results.

- The complexity of the later portion of the simulated event seismograms (i.e., slapdown times and later) increased as compared to those from the closely spaced multiple event.

- Separation of events is achieved by analyzing the first portion of the composite signal. Accurate separation of events is obtained for those detected. Scaling of the detected events gives relative amplitudes varying by about a factor of two from the expected values. Occasionally, larger deviations occur and these are probably due to interference from other signal phases.

- There were two situations in which we were not able to detect an event; one in which the separation was only 0.05 seconds and one in which the main arrival occurred at the same time as the spall closure phase from an earlier event.

The third multiple event configuration is similar to that discussed above. However, we use recordings of several different events and thus introduce more complex propagation path effects as well as different explosion yields.

This is the most complex class of simulated events we studied. The application of the narrow-band filtering technique produced results similar to those described above for the second configuration.

For the second two types of simulated events, the widely spaced explosions, we were unable to realistically construct seismograms at more than one station. Thus, it is not possible to quantitatively evaluate the degree to which an array of stations will aid in the scaling problem. However, qualitatively, it seems clear than an array of stations should considerably improve the resolution of the technique. Tentatively identified events could be correlated from station to station and the signal-to-noise ratio may be improved upon processing data from an array. Even restricting attenuation to the single station data studied, we are able to conclude that our narrow-band filter technique is able to identify and scale closely spaced arrivals from separate events. It should be emphasized that successful use of this technique requires the presence of sufficient signal energy at frequencies greater than 3.5 times the inverse of the separation time.

2.3.2 Teleseismic Short Period Data

For our study of teleseismic data the records to be analyzed were given to us by VSC and the actual solution was unknown during the analysis. Two multiple event records were provided in digital form. The distances (19° and 91°) and azimuths (N117°W and N9°E) from the event were known. We also knew that the multiple event records were constructed by lagging, scaling and summing a single event record at the stations and this single event record was also provided. The data for one of the stations are shown in Figure 3. Again, the data analysis was done by MARS.

A by-product of the analysis is the variable frequency magnitude $[\bar{m}_b(f)]$ for each seismogram. The $[\bar{m}_b(f)]$ values form the basis for a powerful earthquake/explosion discriminant (Savino and Archambeau, 1974). The first question addressed is, do the seismograms appear to be from an explosion? We find that all four seismograms, the two single and the two multiple event records are clearly recordings of an explosion event.

Decomposition of the multiple event record basically requires a cross-correlation of the pattern of phase arrivals on the single event records with those on the multiple event records. The correlation is done automatically by cross-correlating the narrow-band filter output filter-by-filter and summing the resulting correlation functions.

Separation of event arrivals in far-field data is difficult because of the attenuation of high frequency energy in the records. We know from previous experience (Section 2.3.1 and Lambert, et al., 1977) that arrivals can generally be separated only when there is sufficient signal energy at frequencies greater than 3.5 times the inverse of the lag time between arrivals. Therefore, we know at the onset that events

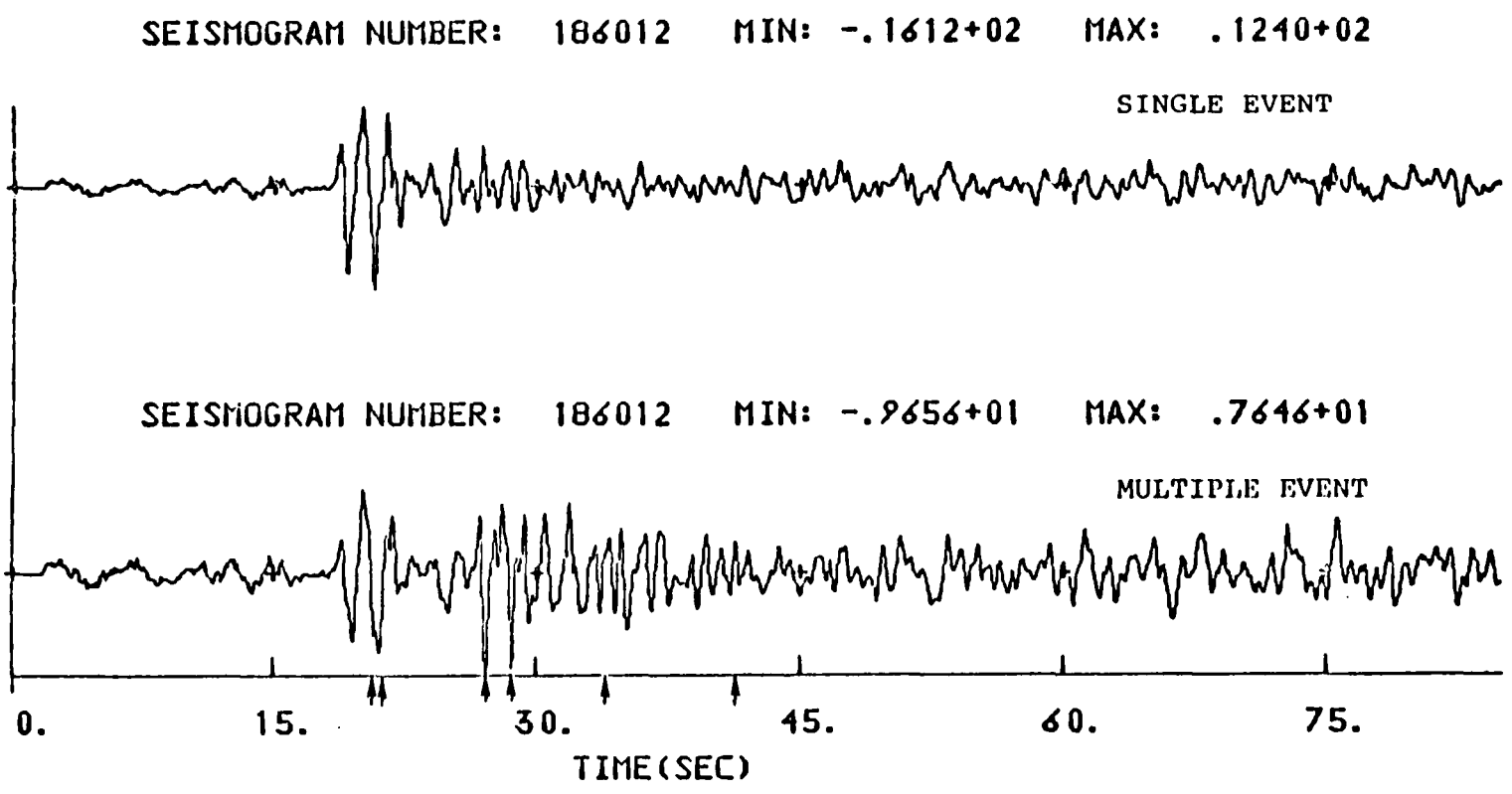

Figure 3. The data for station ANMO are shown. The top record is for the single event and the multiple event record is plotted below.

separated by times on the order of a second or less will be very difficult to detect.

The results are unambiguous in identifying two main groups of events separated by 6.7 or 7.8 seconds, depending on the station azimuth. The longer lag times are seen at ANMO (Δ = 91°), suggesting that the array is oriented more nearly in line with this station, or approximately north-south. Each of the two main groups seems to consist of two or more explosions. All the events identified by the automated cross-correlation are summarized in Table 2.

Also shown in Table 2 are the correct answers; that is, the amplitude and spacing used to construct the composite record. The summed cross-correlation functions used for the event separation are shown in Figures 4 and 5 where the correct answers are also indicated.

Our cross-correlation scheme correctly identified the first four of the six events in the sequence with a maximum error in the lag time of less than 0.1 seconds. The amplitude estimates were correct with 10-20 percent. The last two events were entirely missed, presumably because they are much smaller.

2.4 WORLDWIDE OBSERVATIONS OF P WAVE TRAVEL TIME RESIDUALS AND MAGNITUDE BIASES

A large data set, consisting of mean P wave travel time residuals observed at 524 globally distributed seismograph stations, was compared to body wave magnitude bias data and heat flow observations for several regions of the world with differing geologic and tectonic settings. The travel time data were obtained from Georges Poupinet of the Institute de Physique du Globe, Paris, France, while the magnitude bias information was taken from North (1977). The heat flow observations were taken from a map prepared by the World Data Center A for Solid Earth Geophysics, Boulder, Colorado.

TABLE 2

INDIVIDUAL EVENTS IN THE MULTIPLE EXPLOSION ARRAY

	ANMO				MAIO			
	Lag Time		Normalized Amplitude		Lag Time		Normalized Amplitude	
Event	Actual	Estimated	Actual	Estimated	Actual	Estimated	Actual	Estimated
1	0.0	0.0	0.4	0.45	0.0	0.0	0.4	0.35
2	0.38	0.4	0.4	0.5	0.94	0.90	0.4	0.4
3	7.94	7.90	0.8	0.7	6.82	6.80	0.8	0.75
4	8.69	8.60	0.4	0.35	7.79	7.70	0.4	0.3
5	10.49		0.2		10.53		0.2	
6	10.32		0.2		11.16		0.2	

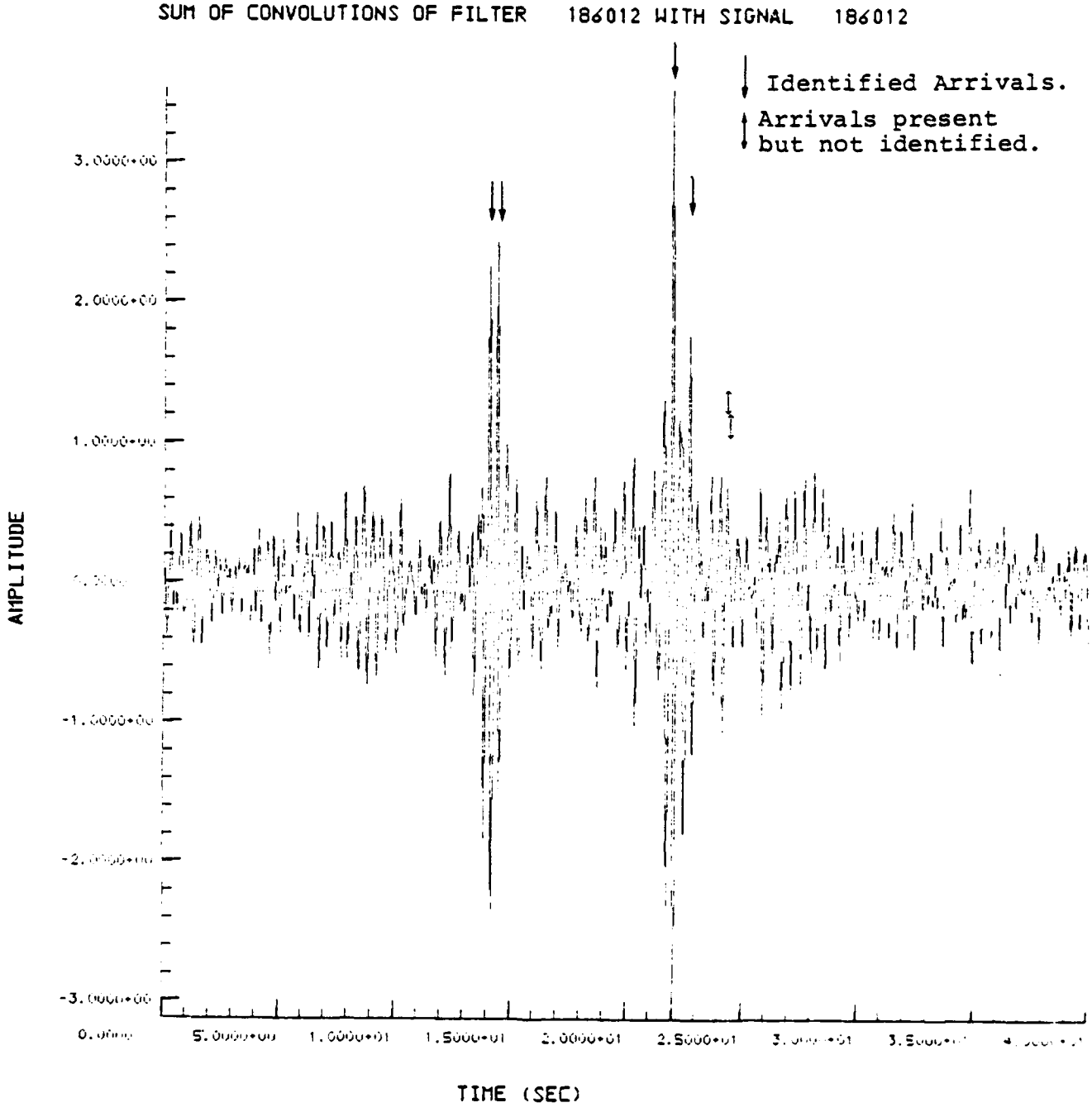

Figure 4. The summation of the cross-correlation functions for ANMO. The four identifiable arrivals are indicated by arrows. Also indicated are the arrivals that are actually present but not identified.

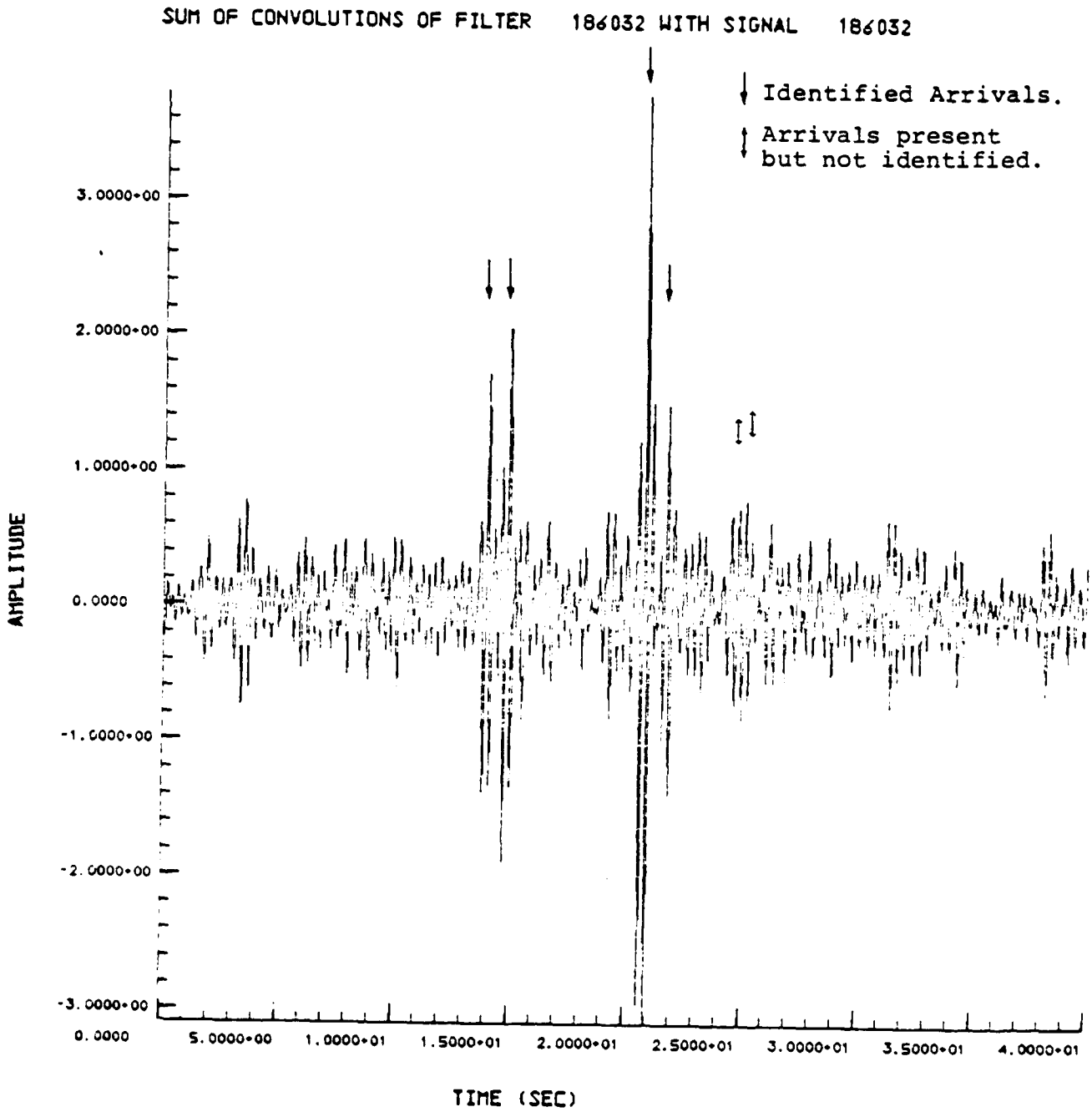

Figure 5. The cross-correlation function for MAIO is shown in the same form as that in the previous figure.

The correlation observed between the station travel time residuals and heat flow was the same as that reported by Cleary and Hales (1966). More travel time observations per station and a larger number of stations were included in the present study, however. In general, negative residuals and low heat flow values were found to characterize shield regions throughout the world (e.g., the Canadian, Fennoscandian, Asian, Indian, Australian and Antarctic shields). In particular, seismic stations located on the Russian and Siberian Platforms are consistently characterized by fairly large negative (e.g., $\sim$ -1 second) travel time residuals while all reported heat flow measurements in these regions are lower than the world average (i.e., < 1.8 cal/cm^2-sec). Positive residuals and higher than normal heat flow, on the other hand, typified continental areas which have been uplifted since the late Tertiary (e.g., regions in the vicinity of the U. S. Cordillera, Caucasus, Dinarics, Carpathians and the Tibetan Plateau).

Magnitude bias, as defined by North (1977), is taken as the mean difference between a station m_b and the average m_b of a large network of stations. Some 400,000 individual station estimates of m_b, as reported in the ISC bulletins, were studied for global variations. No magnitude data, however, were available from stations within the U.S.S.R.

A fairly consistent pattern in the regional variation of magnitude bias and travel time residuals emerged in this study. Results for the contiguous United States, India, the Baltic Shield and the Canadian Shield indicated that, with few exceptions, negative travel time residuals correlate with positive magnitude bias. Put another way, seismically fast stations report high magnitude estimates. Seismically slow stations, on the other hand, rather consistently report low magnitude estimates. A negative magnitude bias, such as that observed in the western United States, is attributed to the

presence of zones of high attenuation in the earth's upper mantle as evidenced on the surface by the prevalence of high heat flow and positive travel time residuals.

The pattern of magnitude bias and travel time residuals for several stations located in southeast Africa was observed to be opposite that for either the United States or India. The African observations are shown in Figure 6. Instead of being of opposite sign, the magnitude biases and travel time residuals are both negative. The reason for this particular pattern remains unclear. Heat flow measurements in this part of Africa, which is quite removed from the rift system further to the north, are all lower than the world average. In addition, Molnar and Oliver (1969) found that there was efficient propagation of the S_n phase throughout this region, and thus, by implication, no anomalously high attenuating upper mantle.

While no magnitude data are available from seismic stations within the U.S.S.R., the prevalence of negative travel time residuals, low values of heat flow, high P_n velocities and large crustal thicknesses all suggest positive magnitude biases. For instance, the travel time residual observed at the station located at Semipalatinsk in Eastern Kazakhstan is -0.81 seconds, a value typical of many of the other stations located on either the Russian or Siberian Platforms. If this region is analogous to the Interior Lowlands of the central United States, then travel time residuals on the order of -0.5 to -1.0 seconds could imply positive magnitude biases of 0.2 to 0.3 m_b units. However, the observed scatter in both the travel-time residual and magnitude bias data, as well as the anomalous pattern observed in Africa, all suggest caution in extrapolating results to Eurasia based on other regions.

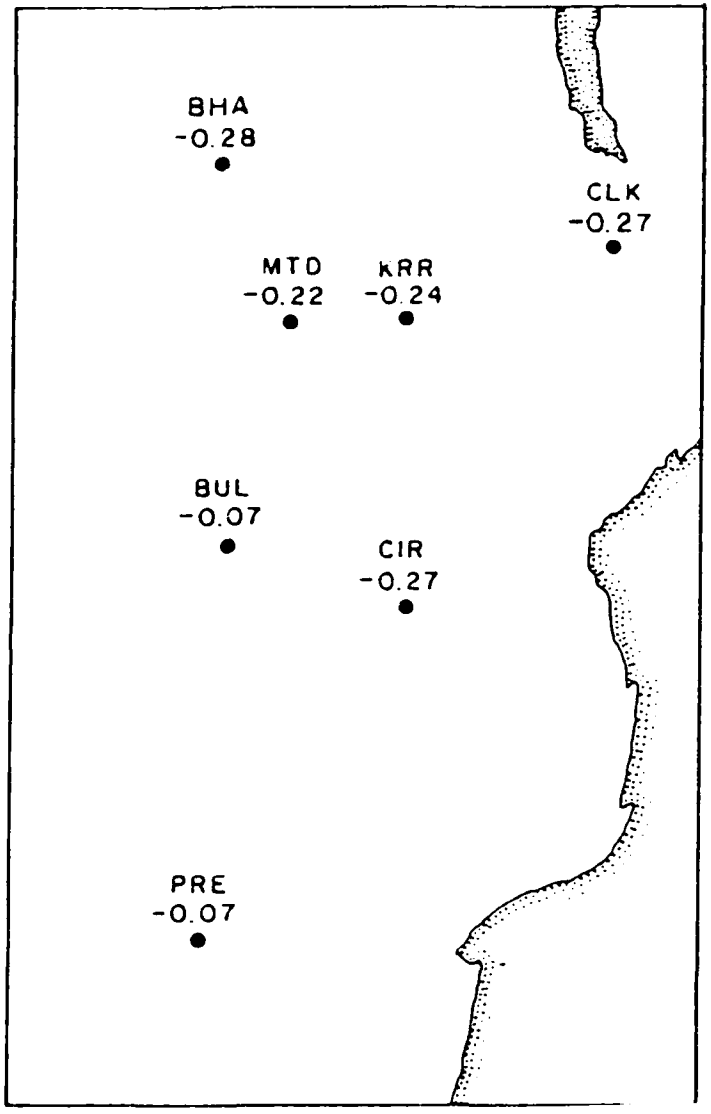

MEAN MAGNITUDE RESIDUALS

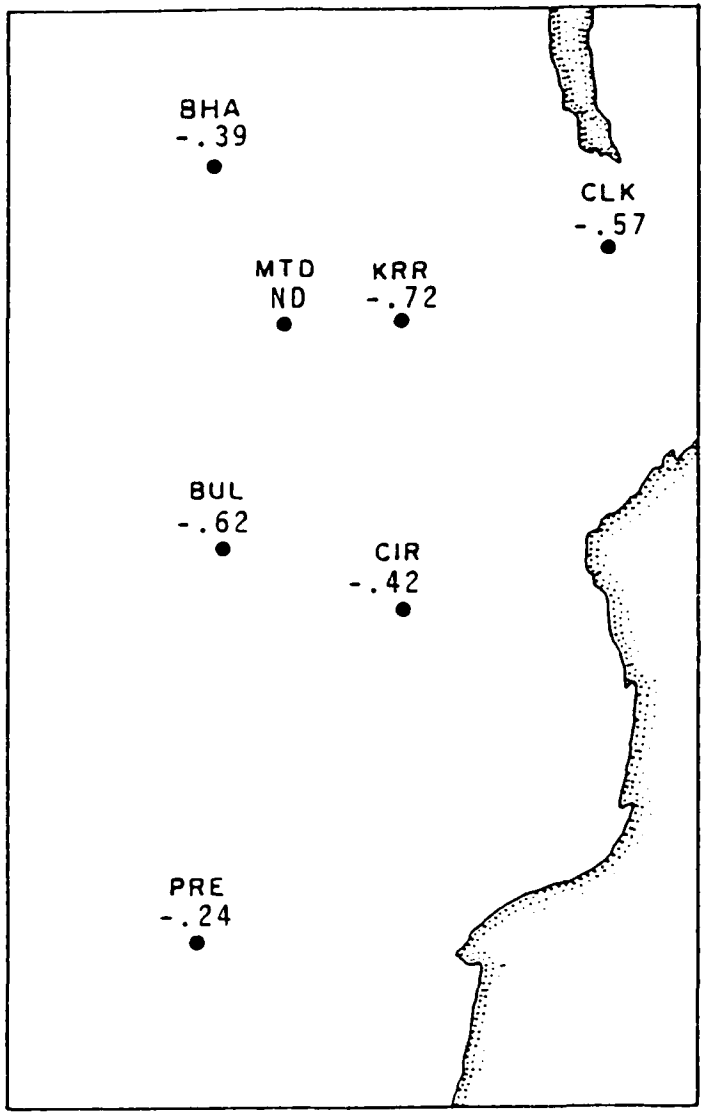

MEAN TRAVEL-TIME RESIDUALS

Figure 6. Mean travel time and magnitude residuals for stations in East Africa.

III. SOURCE STUDIES

3.1 FINITE DIFFERENCE EXPLOSION MODELING

One-, two- and three-dimensional finite difference programs are used to model the seismic source to determine the effect of parameters that are inaccessible to analytical models. The results of some three-dimensional modeling of earthquakes are presented in Section 3.3. We also modeled our small scale explosion experiments in grout blocks in both one and two dimensions. These results are described in Chapter IV.

A fundamental part of our research effort is the use of our one-dimensional (spherically symmetric) finite difference program, SKIPPER, to model explosions in different geological environments. During the last few months of the contract, we made some significant improvements in this code. We will discuss these changes and point out their effect on the source functions for PILEDRIVER (granite), SALMON (salt), and Rainier Mesa Tuff. These are representative of the ranges of materials we expect to encounter.

The important modeling changes are: (1) implementation of better equations-of-state for the cavity gases to replace the constant γ ideal gas treatment; (2) improvements which make the treatment of overburden pressure consistent with the equations-of-state; and (3) development of an improved effective stress law to model the effect of water saturation in rocks.

All of the listed model improvements play a role in calculating the source function for PILEDRIVER in NTS granite. Of particular significance for this material is the effective stress law. Our new effective stress law has no free parameters for a material with negligible air-filled voids. We relate the change in air-filled porosity directly to the

effective stress and assume that below some elastic pressure, P_e, the effective stress is the mean stress. As the voids are crushed, the effective stress reduces to zero smoothly at the crush pressure. For PILEDRIVER, a material with negligible air-filled porosity, we assumed that a small amount of voids were present and created a crush curve. However, this crush curve was not used in computing the material pressure but was used only for the effective stress computations to give a smooth transition between regions. The results do not depend much on P_e but are quite dependent on P_c, the pressure at which the air-filled porosity is irreversibly removed.

Figures 7 and 8 show calculated velocity profiles compared to the measured velocity at two recording stations (Perret, 1968). Peak velocities are in good agreement with the data. The cavity radii for these calculations also match the measured cavity.

Figure 9 shows the computed reduced velocity potential for five source functions. Calculation 310 was done before the recent improvements were implemented. Calculations 410, 407, 411 differ only in the specification of P_e which is 2.0, 1.0, 0.5 kbar, respectively.

These show that the higher the crush pressure, the lower the static level and the more peaked the spectrum. These relationships are reasonable since a higher P_c implies a higher strength, therefore a smaller cavity and smaller static limit. The peaking of the spectrum is a function of the amount of tensile cracking. Since a higher strength implies more cracking, the results are consistent with intuition. Either 407 or 411 is acceptable based on near-field data, cavity size, peak velocity, stress, etc. The cavity radius is too small for 410 and a bit too large for the older calculation, 310.

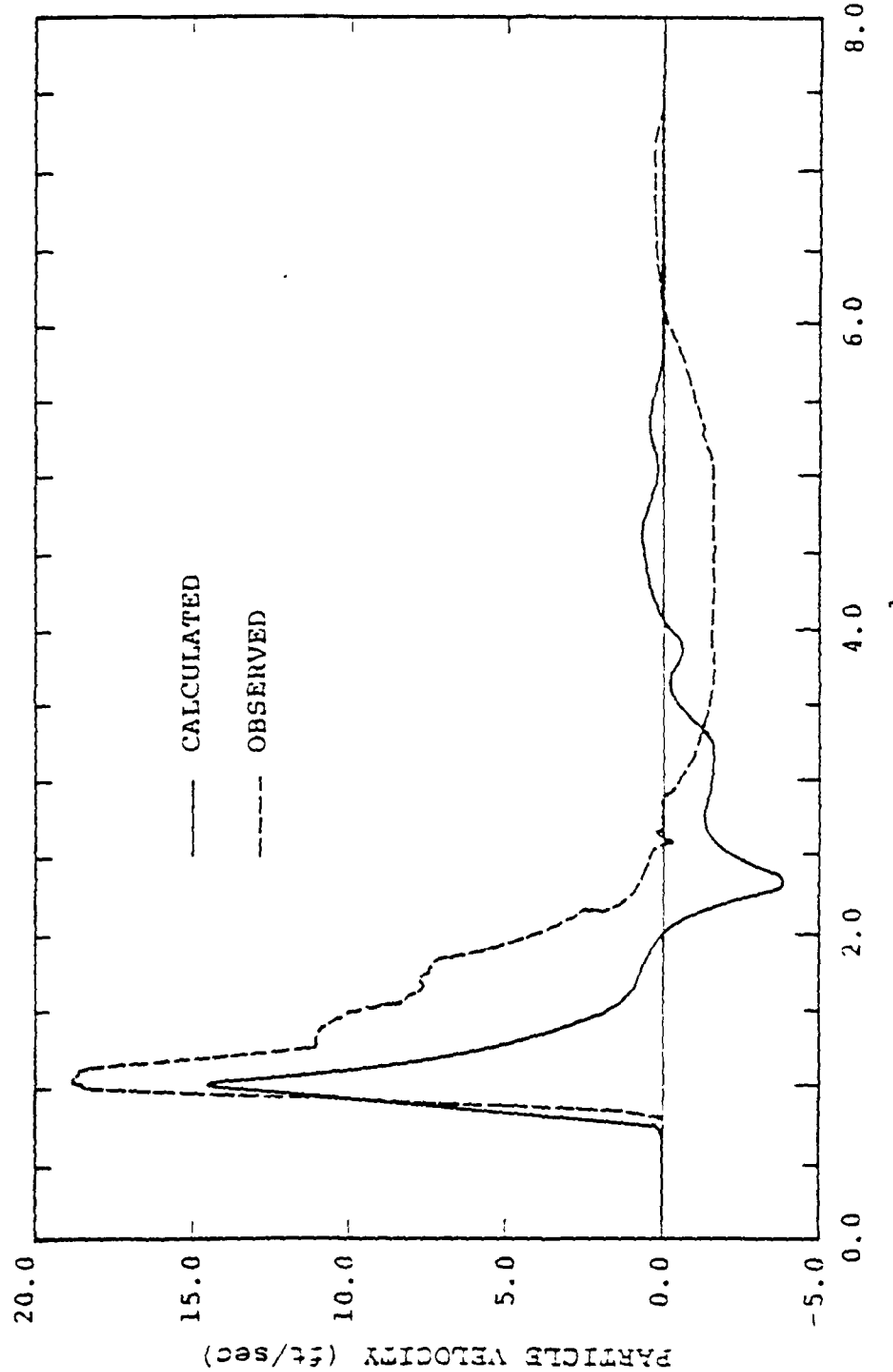

Figure 7. Particle velocity versus time at a range of 1543 feet for PILEDRIVER (61 KT) calculation 411.

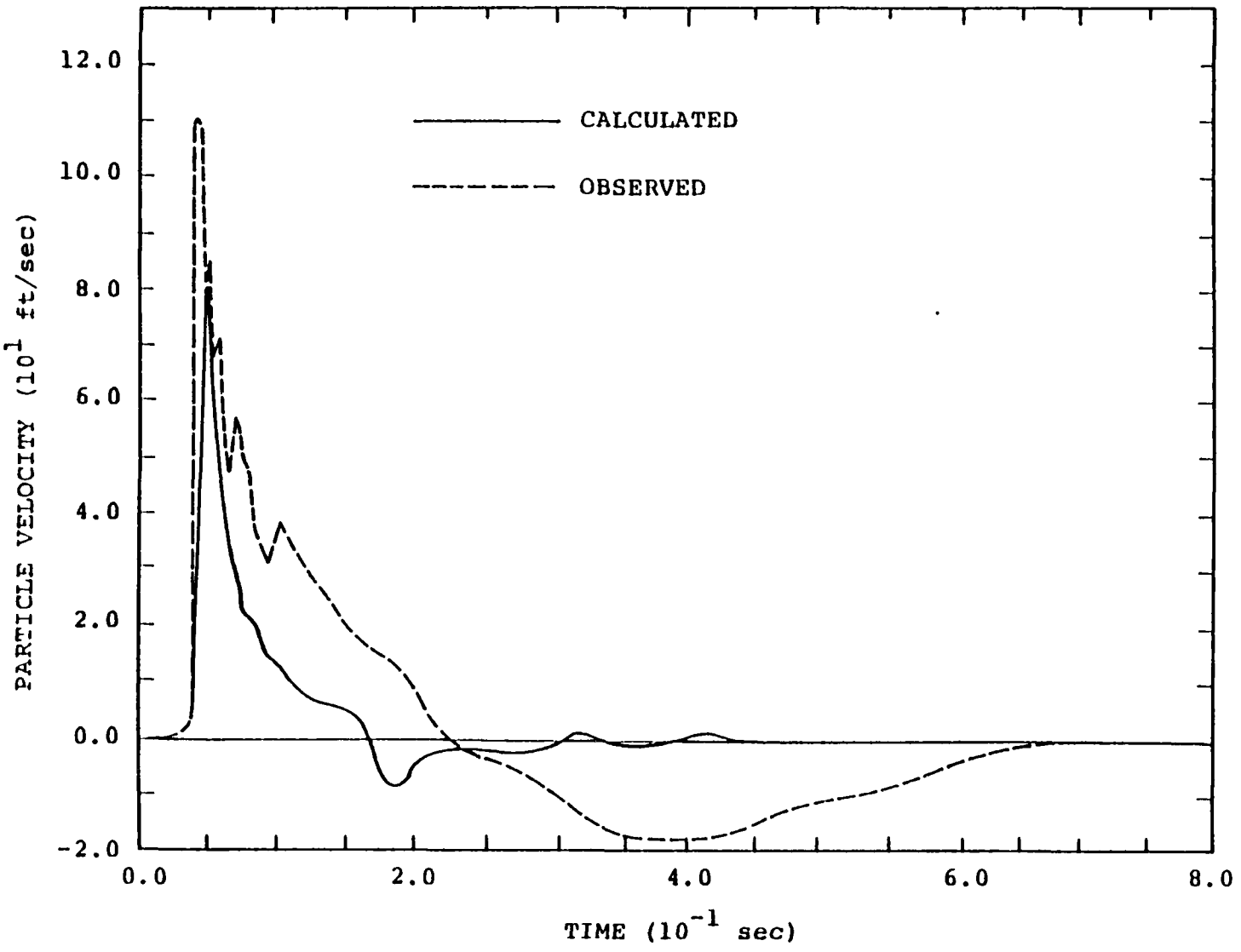

Figure 8. Particle velocity versus time at a range of 668 feet for PILEDRIVER (61 KT) calculation 411.

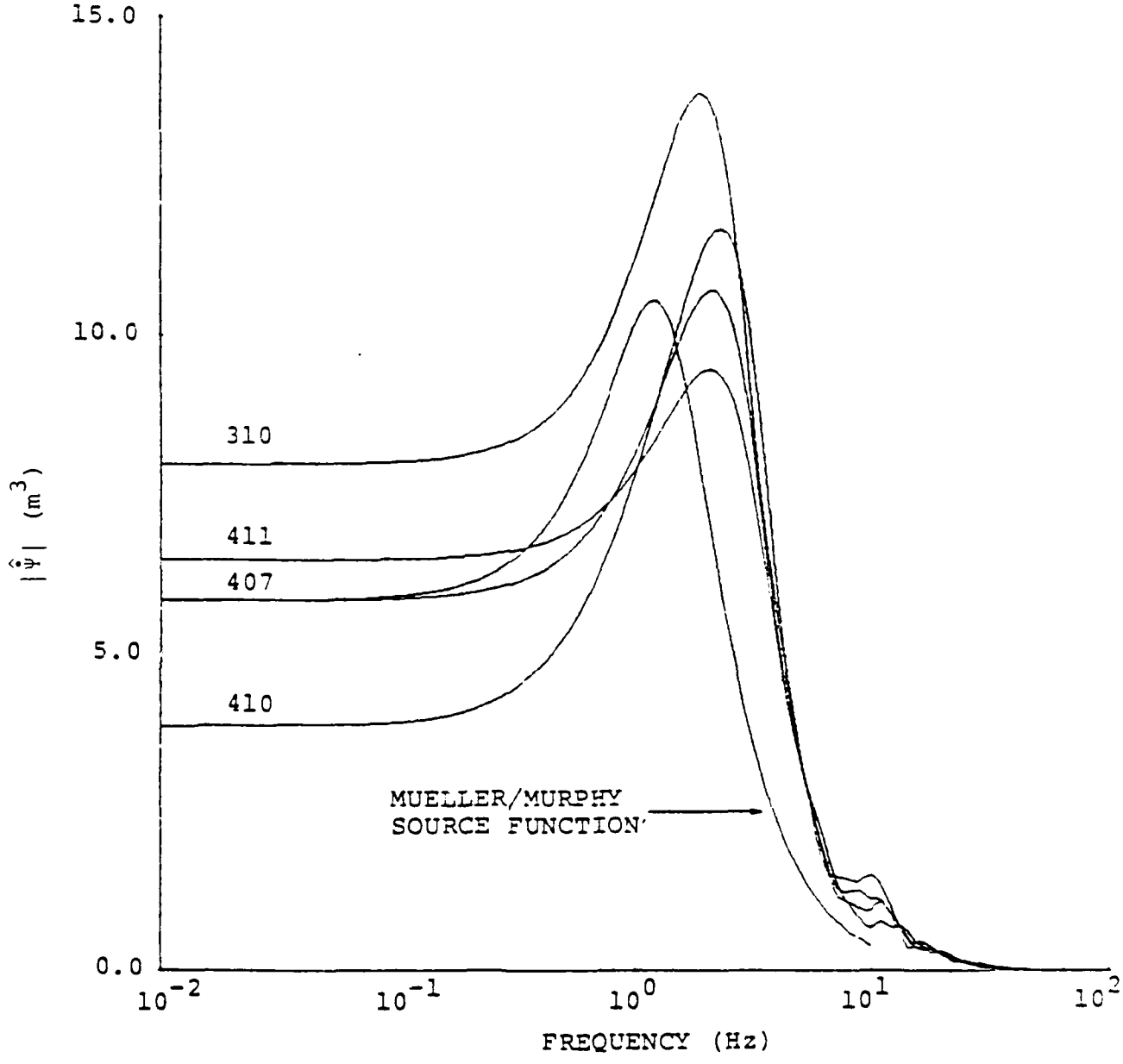

Figure 9. Equivalent source functions for PILEDRIVER calculations. The frequency axis is scaled to 61 kt, the amplitude axis to 0.02 kt. Calculations 410, 407 and 411 show the effect of decreasing P_c. Also shown is the Mueller/Murphy source function scaled to the PILEDRIVER yield and depth.

There are two major modeling differences between 310 and the more recent calculations. The newer calculations have considerably better treatment of the hydrostatic overburden and of the cavity gases. In the older calculations, the scaler overburden pressure was simply added to the pressure obtained from the granite equation-of-state. For the newer calculations, the ambient rock was compressed initially in the code in order to recover the overburden pressure directly from the equation-of-state.

Also, the newer calculations have a far better equation-of-state for the cavity. Until recently, we placed the device energy in a rock sphere having a mass of 70 metric tons per kiloton of device yield and calculated the pressure using an ideal gas equation-of-state with a constant γ of 1.4. We are now using the quartz (S_iO_2) equation-of-state to describe the cavity gases. This equation-of-state, developed by Pyatt and Baker (1978), models the rock behavior from gas pressures of many megabars down to pressures of several bars including the known phase changes.

Also shown in Figure 9 is the Mueller/Murphy source function (Mueller and Murphy, 1971) scaled to the PILEDRIVER yield and depth. This source function is based on a fit to the SHOAL data and gives a reasonable approximation to the PILEDRIVER data (Murphy, 1977), though it should be kept in mind that the measured source functions for PILEDRIVER vary over an order of magnitude. The main difference between the Mueller/Murphy source function and those computed is that the latter peak at higher frequencies.

We have been attempting to compile the measured source function for the SALMON explosion in salt. The basic difficulty is that the calculated RDP for a salt failure envelope as measured by triaxial loading in the laboratory (Pratt, 1978; Heard, et al., 1975) is significantly smaller than the

measured RDP (see Murphy, 1977). If a lower failure envelope is used to raise the calculated RDP, the calculated cavity radius becomes too large when compared with drillback measurements in the SALMON cavity.

The results obtained with one-dimensional calculations of SALMON are summarized in Figure 10. Calculation 252 uses constant γ ideal gas treatment for the cavity and has been reported previously by Bache, Cherry and Mason (1976c). The rest of the calculations used cavity equation-of-state for salt derived using the EIONX equation-of-state (Pyatt, 1966). EIONX is a simple mathematic model which incorporates many of the important features of the more complicated Saha equation models. The new overburden pressure treatment was also used for these calculations. No effective stress law was used for the dry salt dome.

Also shown in Figure 10 is the Mueller/Murphy source function for SALMON (Mueller and Murphy, 1971). Since this source function is based on a fit to the SALMON near-field observations, it is shown as a convenient representation for the observed data.

Calculation 408 used the lowest possible failure surface which we could justify (based on the uniaxial measurements of Heard, et al., 1975). The calculated RDP of 7.8 m^3 for a yield of 0.02 kt was still considerably lower than the measured value of 11 m^3, scaled to this yield. Yet the calculated cavity radius was significaltly higher than 2.8 m, the measured value scaled to 20 tons yield. Calculation 414 represents our best guess for a failure envelope, based on the available triaxial data, in particular the data from Terra Tek, Incorporated (Pratt, 1978) and gives a reasonable cavity radius, peak stresses and velocities. However, the calculated RDP was more than a factor of two low.

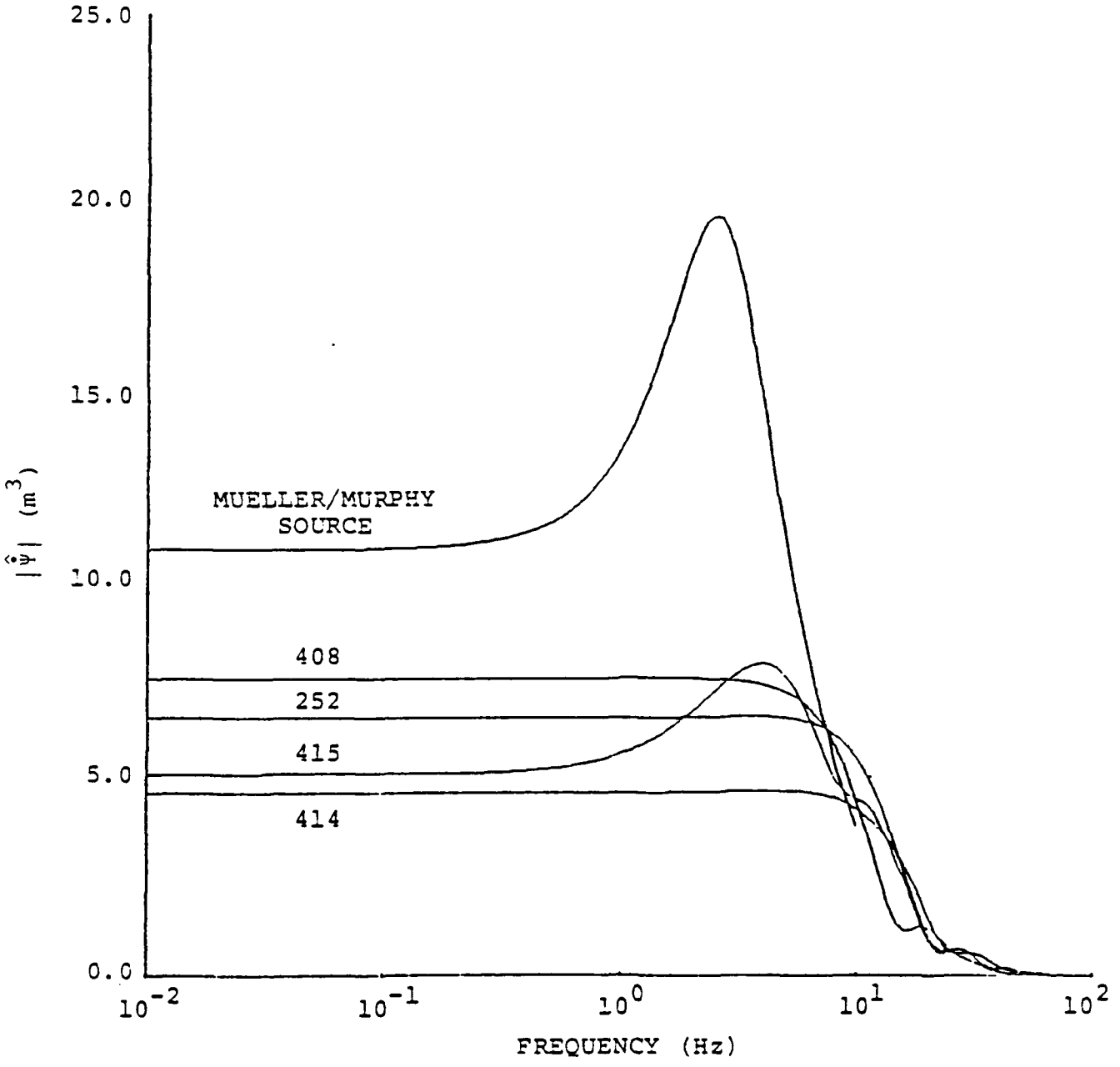

Figure 10. Equivalent source functions for SALMON calculations. The frequency axis is scaled to 5.3 kt, the amplitude axis to 0.02 kt.

We are attempting to calculate the event in two dimensions to study the influence of in situ stresses on the RDP. First, we are assuming that this stress field, due to the overburden, has been arrived at by elastic processes, i.e., in uniaxial strain. However, it is equally likely that the in situ stress field is the result of inelastic processes such as plastic flow. This will also be investigated. If in situ stress proves not to be the explanation of our low calculated RDP, we plan to include viscoelastic effects in the constructive model.

The saturated tuffs of Rainier Mesa are unique at NTS in that they have been characterized by an enormous number of laboratory measurements of material properties data. Although the variation in material properties from event to event is considerable, we have been able in the last few years to compile a series of "average" Area 12 tunnel tuff material properties data which tend to be valid for the more recent nuclear events. A series of SKIPPER calculations were done for these average tuff properties which look at the effects of initial cavity size and of the new effective stress law on source spectra.

We were able to investigate the effect of initial cavity size through the use of the CHEST 24 tuff chemical equilibrium equation-of-state which was developed by Laird (1976) and which accurately models the rock behavior in pressure regimes from tens of megabars down to a few tenths of a bar. This tabular equation-of-state couples an elaborate chemical equilibrium treatment with steam tables and bulk modulus data and was used to describe the tuff both inside and outside of the cavity.

Figure 11 shows source spectra for the tuff calculations. Calculation 127 from the Bache, et al. (1975) study used a smaller overburden pressure causing the spectral peak

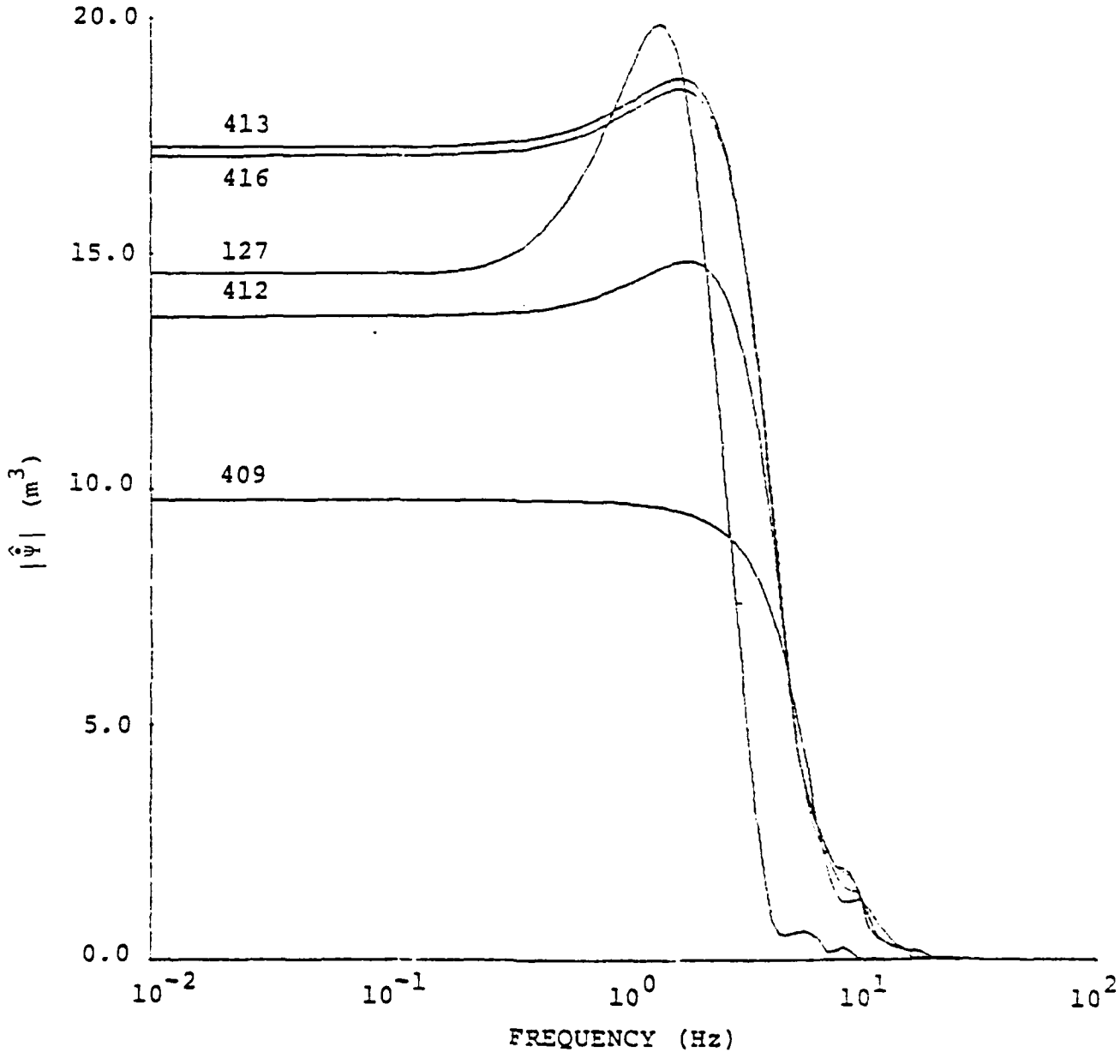

Figure 11. Equivalent source functions for Area 12 tuff. The frequency axis is scaled to 10 kt, the amplitude axis to 0.02 kt. All calculations but 127 (from Bache, et al., 1975) have identical material properties. Calculation 409 (no effective stress law) and 412 (with new effective stress law) have 70 ton/kt initial cavities. Calculations 412, 416 and 413, respectively, show the effect of smaller initial cavity size.

to be at a lower frequency. This calculation, using the old "relaxation" effective stress law, gave a cavity radius of 6.12 meters at the 20 ton yield. This is far greater than the 3.72 to 4.41 meter range for the measured cavity radii. Calculation 412 used the new effective stress law and the new overburden pressure treatment. It gave a cavity radius of 4.30 meters, well within the data range. Calculation 409 had no effective stress law, but otherwise had the same modeling and data as 412. The calculated cavity radius of 3.875 meters was well within the band of measured data.

A comparison of 127, 409 and 412 indicates that the old effective stress law results in more peaked spectra than is seen for the newer effective stress law. For no effective stress law (calculation 409), the spectra is not peaked at all. Calculation 412 with the new effective stress law is in better agreement with free field data.

Calculations 412, 416 and 413 have identical modeling, except for the size of the initial source. For 412, the device yield was placed in an initial cavity with radius equivalent to 70 metric tons/kt of yield, for 416 in 20.7 tons/kt, and for 413 in 8.75 tons/kt. The results for calculations 416 and 413 differ only slightly. They both show a cavity radius slightly larger than the measured values and gave approximately 25 percent greater cavity volume, Ψ_∞, peak spectra, and volume inside the elastic radius than did calculation 412. A careful analysis was made of these rather surprising results. It was noted that the calculated melt for the 70 ton/kt initial cavity extended no further than the initial Lagrangian boundary of the cavity. For the smaller initial cavities, the melt radius (which we call the final cavity radius) extended considerably further. The analysis indicated that, for the 70 ton/kt initial cavity (412), the energy density input into the cavity cells was just sufficient

to vaporize these cells. For the 20.7 ton/kt cavity (416), far more energy was input into the smaller cavity than needed to vaporize the mass present. However, the extra energy did not vaporize further cells. Since the energy required to vaporize the rock is wasted energy that could otherwise go into driving the shock wave, the smaller initial cavity drives a stronger shock wave and, therefore, gives a larger final cavity and RDP. The very small initial cavity (8.75 tons/kt, calculation 413) has a sufficiently high energy density to vaporize rock out almost to the same radius as for calculation 416. Thus, the results are quite similar.

The question that arises is, which calculational procedure is correct? Clearly, hydrodynamic codes do not take into account some basic physical processes such as thermal conductivity or flow of vaporized water through the rock mass. Thus, it becomes difficult to compute both the correct vaporization radius and the melt radius using these codes alone (equilibrium procedures have been developed which take the late-time code output and determine the true melt by mixing the reserve energy of the cavity with rock mass outside). Further study is needed in order to resolve this problem. Meanwhile, we will continue to use the 70 ton/kt rock gas model for all calculations. For the above calculations, this means using 412 which is in better agreement with the measured cavity radius data. Any small under-estimate of the source spectra which may be inherent in this procedure is likely to occur in source calculations in all materials.

Summary

We have added the following features to our nonlinear constitutive models:

1. A new effective stress law which scales with device yield.

2. An improved treatment of overburden pressure which is consistent with our equations-of-state.

3. Better cavity equations-of-state for granite, salt and tuff.

Source calculations made with these improved models lead to the following conclusions:

1. We are unable to calculate the SALMON RDP in one dimension with our present models using laboratory data for the failure envelope. The calculations give the measured cavity radius but too small an RDP.

2. We can calculate the PILEDRIVER RDP with these models and obtain reasonable agreement with near-field velocity data and with the measured cavity radius.

3. Using the new effective stress law, we can calculate an RDP for average NTS Area 12 tuff material properties without any free parameters and obtain good agreement with measured cavity radius. We were unable to obtain good agreement with cavity radius data in our earlier studies.

3.2 TRANSMITTING BOUNDARY CONDITIONS FOR FINITE DIFFERENCE CALCULATIONS

Finite difference methods possess wide flexibility in the specification of boundary conditions, constitutive properties, and model geometries. A severe limitation, however, is the spatial finiteness of the computational grid, which results in the generation of large, nonphysical reflections at the edges of the grid. This necessitates extending the grid to a considerable distance from the region in which rupture is to be modeled, in order that these reflections not influence the simulation of faulting. This excess grid increases computing costs and, as a result, greatly reduces the feasible mesh refinement in the rupture zone.

We have recently implemented a transmitting boundary condition for finite difference codes which effectively eliminates the spurious reflections associated with the edges of the grid. The method is based on a parabolic approximation to the wave equation given by Engquist and Majda (1977) and Clayton and Engquist (1977). Employment of the transmitting boundary dramatically reduces the computation time associated with a given mesh refinement.

Tests of the boundary condition have been performed in two dimensions, for both SH and P-SV problems. The test calculations verify the accuracy of the method. The results for an SH problem are summarized in Figure 12. A quarterspace, represented by a 20 by 20 zone grid, was subjected to a line source (a step function of time). The contours are percent error in displacement of the numerical solution relative to the analytic solution for a line source in a quarterspace. At the wavefront, the finite difference method smooths the (square root) singularity in the analytic solution, as expected. The wavefront is transmitted without generating any noticeable reflected wave, and the residual errors after transmission of the wavefront are very small -- less than one percent for most of the grid. P-SV problems give similar results, with somewhat larger residual errors.

The plane transmitting boundary appears entirely satisfactory, and its implementation in three-dimensional codes is straightforward. The extension to the curved boundaries occurring in axisymmetric problems is more difficult and some analytical reformulation is required.

3.3 THREE-DIMENSIONAL FINITE DIFFERENCE EARTHQUAKE MODELING ON THE ILLIAC COMPUTER

Three-dimensional numerical simulations of earthquake faulting have been done on the ILLIAC computer using the finite

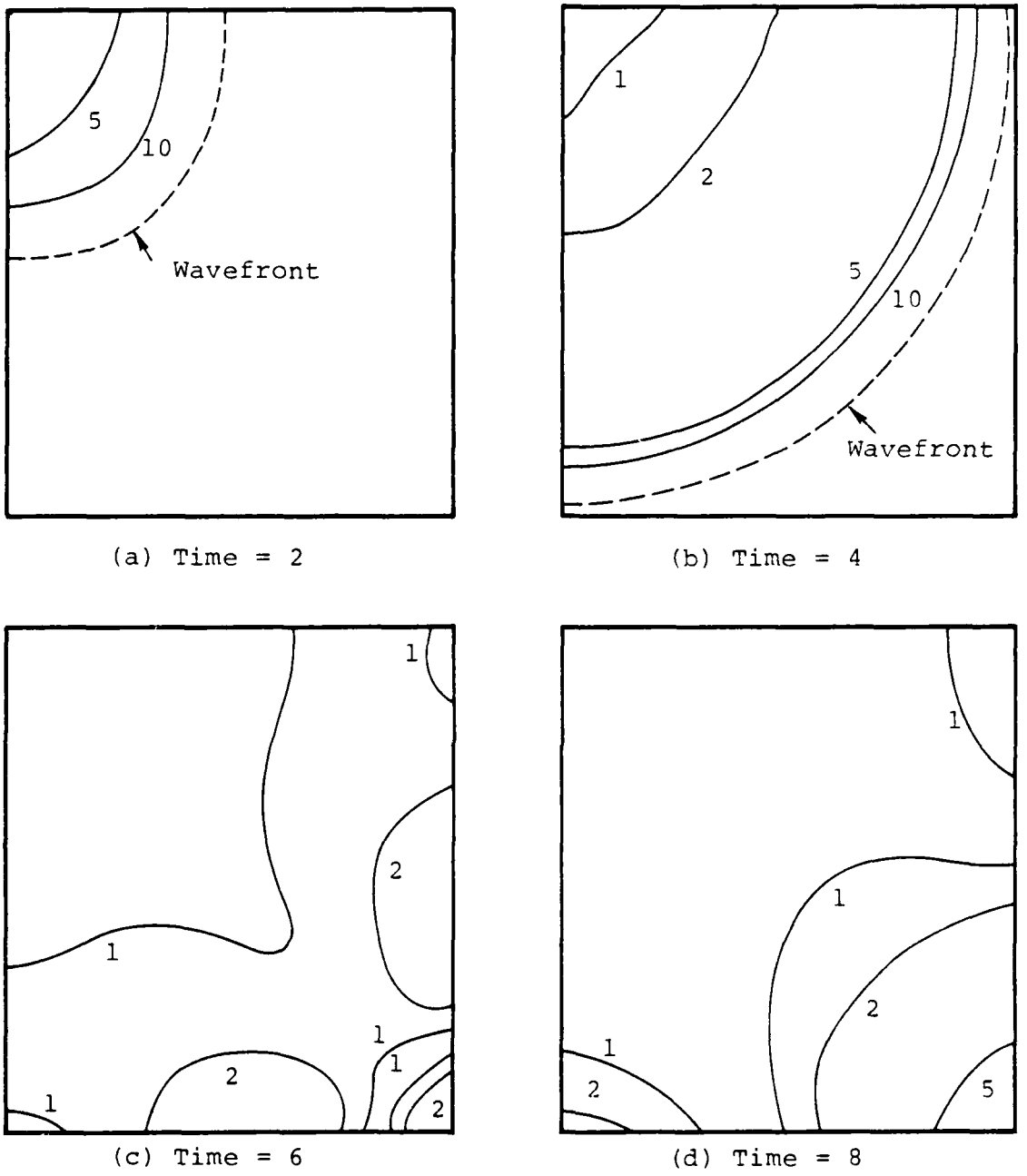

Figure 12. Anti-plane strain response of a quarterspace excited by a line source, showing the effect of a transmitting boundary condition. The transmitting boundaries are located on the bottom and right surfaces, and Dirichlet conditions exist on the top and left surfaces. The dashed line shows the wavefront. Contours of percent error (numerical relative to analytic) are shown at four instants in time.

difference program TRES. The computational method employed admits nonlinear material behavior in the neighborhood of the fault zone, and elastoplastic material response consistent with a von Mises yield criterion is currently available in the program.

A square fault plane (see Figure 13) was studied to assess the effects of plastic yielding in the fault plane. To facilitate comparison to existing analytic models and to previous numerical work, the fault was assumed to be embedded in a homogeneous, unbounded medium. The rupture was assumed to grow symmetrically with a fixed rupture velocity of 0.9 times the shear wave speed, until reaching the boundary of the fault surface. The following parameters were employed for each of two calculations:

P wave velocity	α = 5.93 km/sec
S wave velocity	β = 3.42 km/sec
Density	ρ = 2.74 gm/cm^3
Rupture velocity	v_r = 3.08 km/sec
Stress drop	$\Delta\sigma$ = 180 bars
Fault dimensions	2a × 2a = 3 km × 3 km.

The first calculation was for a linearly elastic constitutive relation. The second calculation was for an elastoplastic constitutive model, in which plastic yielding was permitted in the medium within 0.2 km of the slip plane. In the elastoplastic case, the entire fault zone was presumed to lie initially on the yield surface, so that any increase in shear stress would lead to yielding. In both cases, the medium was represented by cubic finite difference zones 0.1 km on a side. The numerical grid was large enough that no reflections from the exterior grid boundary returned to the fault zone during the calculation.

Our first objective was to verify that the finite difference program properly approximates the fault dynamics.

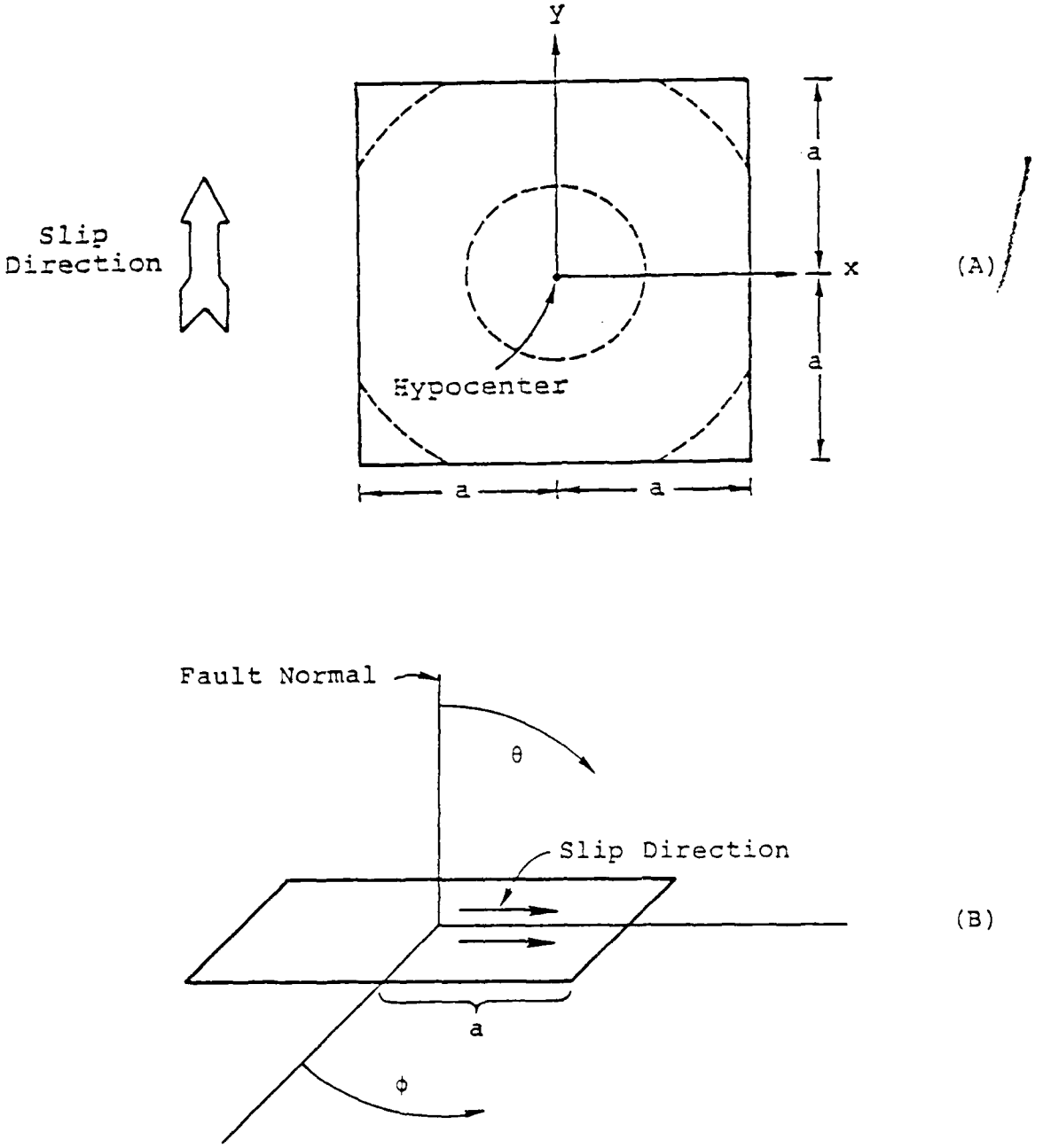

Figure 13. (A) The fault configuration for the finite difference simulation, and (B) the coordinate system for describing the radiated field.

For the elastic case, we have compared the initial portion of the fault slip obtained numerically to the analytic solution for a circular fault which expands at constant rupture velocity without stopping. Figure 14 shows the slip obtained at several points in the fault plane. The solid curves are the finite difference solution; the dashed curves are the analytic solution. The vertical bars indicate the arrival times of edge effects due to stopping of the rupture at its outer edge in the numerical simulation. The two solutions are in good agreement at each point, prior to the arrival of the edge effects. These edge effects then propagate inward toward the focus at the P wave speed, eventually stopping the slip.

Our second objective was to evaluate the effects of anelastic material response in the fault zone. Figure 15 shows the slip velocity obtained at several points in the fault plane. The elastic case is shown as solid lines, the elasto-plastic case as dashed lines. The initial part of the fault slip function is nearly identical for the two cases. This suggests that relaxation of the dynamic stress concentration at the crack edge, via plastic yield, has negligible influence on the initial fault motion.

The stopping phase was slightly modified when yield was permitted. Plastic strains outside the fault edge allowed somewhat greater fault displacements to occur than in the elastic case. The resultant average slip was approximately 11 percent greater than for the elastic case.

3.4 ANALYTIC CONTINUATION OF THE ELASTIC FIELD FROM A COMPLEX SOURCE IN A HALFSPACE

An important problem in nuclear explosion and earthquake seismology is the development of a capability for linking detailed numerical source calculations with efficient analytical techniques for propagating elastic waves in layered

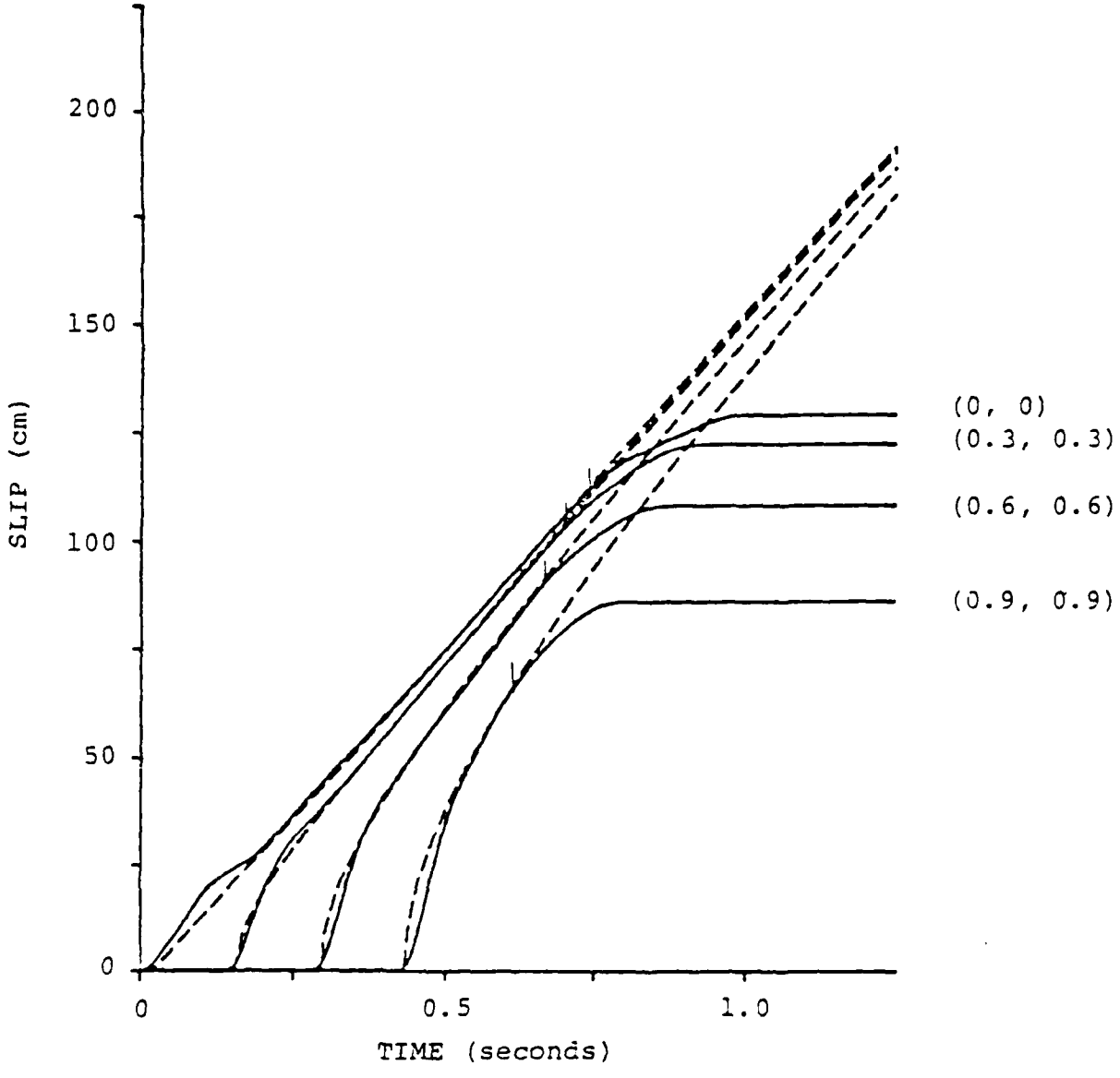

Figure 14. Relative displacement on the fault for the elastic case. The dashed curves are Kostrov's analytic solution; the solid curves are the finite difference results. x,y coordinates in kilometers are given in parenthesis. Vertical lines indicate the arrival times of edge effects due to fault finiteness.

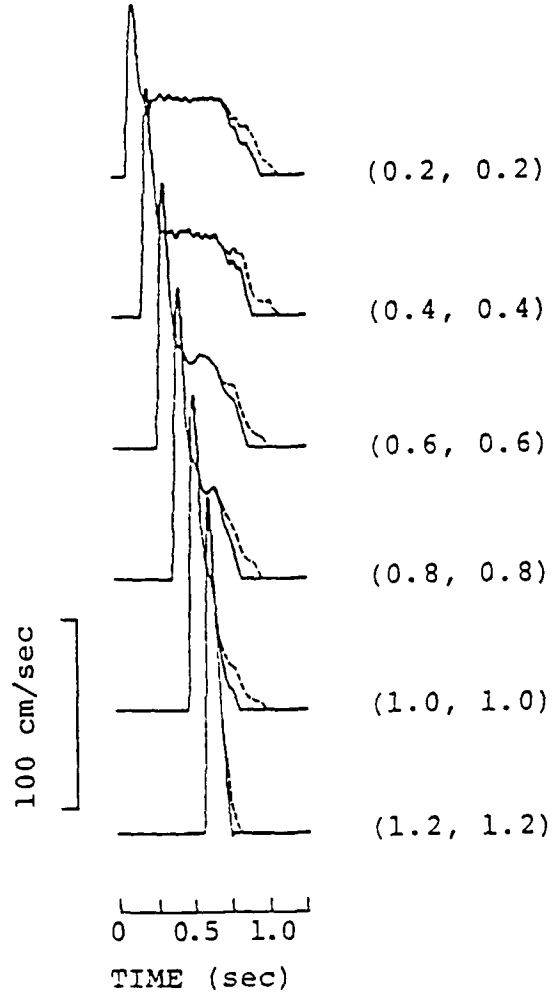

Figure 15. Slip velocity in the fault plane. Solid lines are the elastic case, dashed lines the elasto-plastic case. x,y coordinates in kilometers are shown in parenthesis.

media. If the source is in a homogeneous wholespace, techniques employing an expansion of the out-going waves in spherical harmonics work very well and have been employed to study earthquakes (Bache, et al., 1976) and complex nuclear explosions (Cherry, et al., 1975a, 1976; Bache and Masso, 1978). However, these techniques are not rigorously valid when a material boundary is present in the source region. Bache, et al. (1977) introduced some ad hoc approximations and applied the wholespace technique to study near surface explosions in a halfspace. Even though this worked fairly well for the case studied, it has some serious drawbacks and better methods are needed.

In this section, we outline a method for analytically continuing the output of a finite difference simulation of a source in a layered halfspace. The source calculations may include arbitrary nonlinearity in a portion of the grid. It is also necessary that the waves be computed out into the region where the material response is linearly elastic. The specific case discussed here is the computation of body waves and surface waves in a layered earth model from an axisymmetric source. The basic approaches used for body wave and surface wave calculations are similar, but details of the procedure differ for the two types of wave phenomena.

The mathematical basis of our approach is the elastodynamic integral representation given by Burridge and Knopoff (1964). This is a rigorous expression for the displacement in an elastic medium in terms of a surface integral over a (non-physical) boundary Σ which entirely encloses the source volume (including all inelastic regions). Two elements are required to form this integral solution. First, we must have the time histories of the displacement vector $\underline{U}(\underline{x}_o, t)$ and the stress vector $\underline{T}(\underline{x}_o, t)$ on Σ. These are obtained from the finite difference source calculation. Second, the Green's

tensor $\underset{\approx}{g}(\underline{x}, \underline{x}_o; t - t_o)$ and its spatial derivatives (for the appropriate elastic medium) must be evaluated for the prospective receiver point $\underline{x}$, for all $\underline{x}_o$ on Σ. The elastic medium used to compute $\underset{\sim}{U}(\underline{x}_o, t)$ and $\underset{\sim}{\tau}(\underline{x}_o, t)$ must be the same as that used to compute $\underset{\approx}{g}(\underline{x}, \underline{x}_o; t - t_o)$.

The general form of the integral representation (assuming isotropy) is

$$\underline{U}(\underline{x},t) = \int dt_o \int_\Sigma dS_o [\underline{g}(\underline{x}, \underline{x}_o; t - t_o) \cdot \underline{\tau}(\underline{x}_o, t_o)$$

$$- \underline{g}\, \nabla_o(\underline{x}, \underline{x}_o; t - t_o) : \underline{\underline{M}}(\underline{x}_o, t_o)] \quad (2)$$

where

$$\underline{\underline{M}}(\underline{x}_o, t_o) \equiv \lambda \underline{\underline{I}}\, \hat{n} \cdot \underline{U}(\underline{x}_o, t_o) + \mu[\hat{n}\, \underline{U}(\underline{x}_o, t_o)$$

$$+ \underline{U}(\underline{x}_o, t_o)\, \hat{n}] .$$

$\underline{x}$ and t are receiver positions and time,

λ and μ are elastic constants,

$\hat{n}$ is the normal to Σ, directed into the source volume

$\underline{U}$ is the displacement vector,

$\underline{\tau}$ is the stress vector on Σ,

$\underline{g}$ is the Green's tensor solution,

$\underline{\underline{I}}$ is the identity tensor.

If we assume a geometry as shown in Figure 16, the volume to which the representation theorem is applied is the entire elastic halfspace except for the cylinder which contains the complex source. Since the motion must tend to zero at infinite distances and if we choose a Green's function

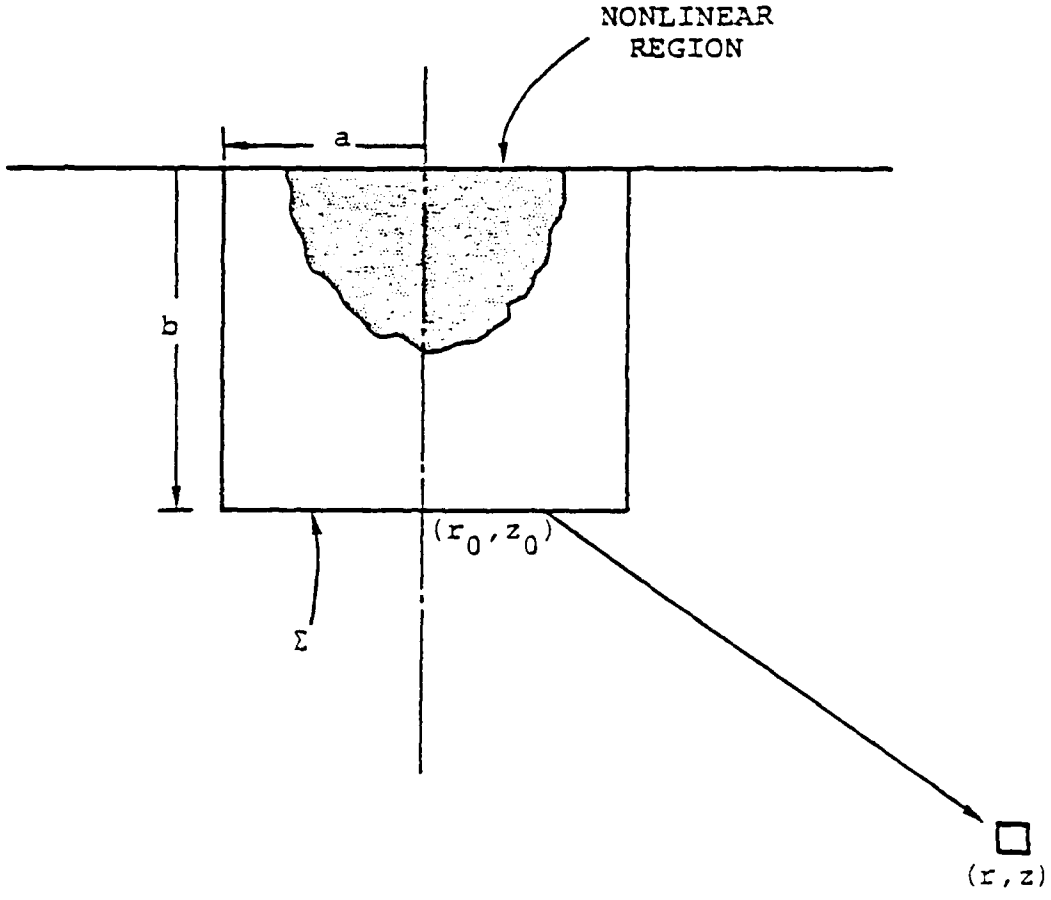

Figure 16. The source-receiver geometry is shown for the axially symmetric case. The monitoring surface Σ is a cylinder of radius a and height b.

response which satisfies the free surface boundary condition, then we can express the motion anywhere in the halfspace as a function of monitored displacements and stresses on the cylinder boundary surrounding the source.

The procedure to be taken can be summarized by the following steps:

1. The source region response is computed using numerical methods. The calculations must be carried out to a region where the response is essentially elastic.

2. Displacements and stresses are monitored on a cylindrical boundary enclosing the nonlinear region of the source calculation.

3. The impulse responses (Green's functions) are computed for point sources located on the edge of the source cylinder. The nature of the impulse responses depends upon the type of wave phenomena of interest (body or surface waves).

4. The motion at the receiver is calculated by applying the integral representation theorem. For the case of an axisymmetric source, some of the integration can often be performed analytically. In general, a numerical integration is necessary.

Application of the integral representation theorem to ground motion synthesis is not new. The theoretical considerations used here are well understood. The mathematical development applying the procedure to body wave and surface wave calculations has been completed. The differences in the nature of the impulse responses for body waves and surface wave motion require separate procedures in practice.

The major problem to be solved is the determination of the numerical tolerances of the procedure. Programs have been written for application of the method to both types of wave phenomena and are being tested with simple problems with known solutions. Results of these problems should determine what specific numerical procedures will be necessary to apply the method to more complex problems on a routine basis.

IV. SMALL SCALE EXPERIMENTS TO SIMULATE UNDERGROUND EXPLOSIONS

4.1 INTRODUCTION

Laboratory experiments were conducted to model underground explosions. Two types of experiments were carried out. First we overburied the charge in order to measure the direct (free-field) P wave radiated by the explosion. We call this class of experiments free-field since the seismic radiation is uncontaminated by the pP event. In the second type of experiment the charge was detonated near a free surface and the direct P wave is contaminated by pP. We call this class of experiments underburied. It includes as a subset depths of burial which produce craters at the free surface.

The research project involved three phases:

1. The experiments were conducted and the ground motion data were collected.

2. Constitutive models were constructed for the material and the experiments were modeled using one and two dimensional finite difference techniques.

3. Using the computational results as a guide, the experimental data were analyzed.

Detailed results from the experiments and their analysis are given by Cherry, et al. (1977).

4.2 THE LABORATORY MODEL

Free-field and underburied cratering explosions were modeled in the laboratory on a small scale by embedding one-fourth gram spheres of the high explosive, PETN, in concrete cylinders of 120 cm diameter. The bottom end of the cylinders represented the ground surface and the seismic coupling of the charge was determined by measuring the displacement

of a point on the top surface directly above the charge. The thickness of the cylinders varied between 33 and 60 cm. The vertical distance between charges and sensors was constant (30.5 cm) for all the experiments. The distance between the charges and the bottom free surface was varied to simulate different depths of burial. The dimensions of the cylinder were selected such that all surfaces except the bottom surface were well beyond the inelastic region surrounding the charge. The top surface, where sensors were located, was always outside the inelastic region surrounding the explosive.

The experimental configuration is shown in Figure 17. Each cylinder was used for three shots fired separately with charges spaced in a triangular array. The vertices were at wide enough separation to assure that the inelastic regions for separate shots did not overlap. The gauges were also located at the vertices of a triangle with each gauge directly above a charge.

The recorded displacement time histories for five events are shown in Figure 18. These are representative of the entire suite of ten explosions. In Figure 19 the records from tests 4 and 8 are superimposed to demonstrate the remarkable consistency of the peak motions.

4.3 NUMERICAL MODELING OF EXPERIMENTS

The one-dimensional Lagrangian finite difference program SKIPPER was used to model the free-field data. The results are plotted in Figure 20 compared to all the free-field experimental data. Two free-field calculations are presented in the figure: one in which tension failure was permitted only if $\bar{P} \leq 0$, that is the hydrodynamic component of stress, is tensile, and one in which tension failure could occur for any value of $\bar{P}$. The reduced velocity potential (RDP) transforms

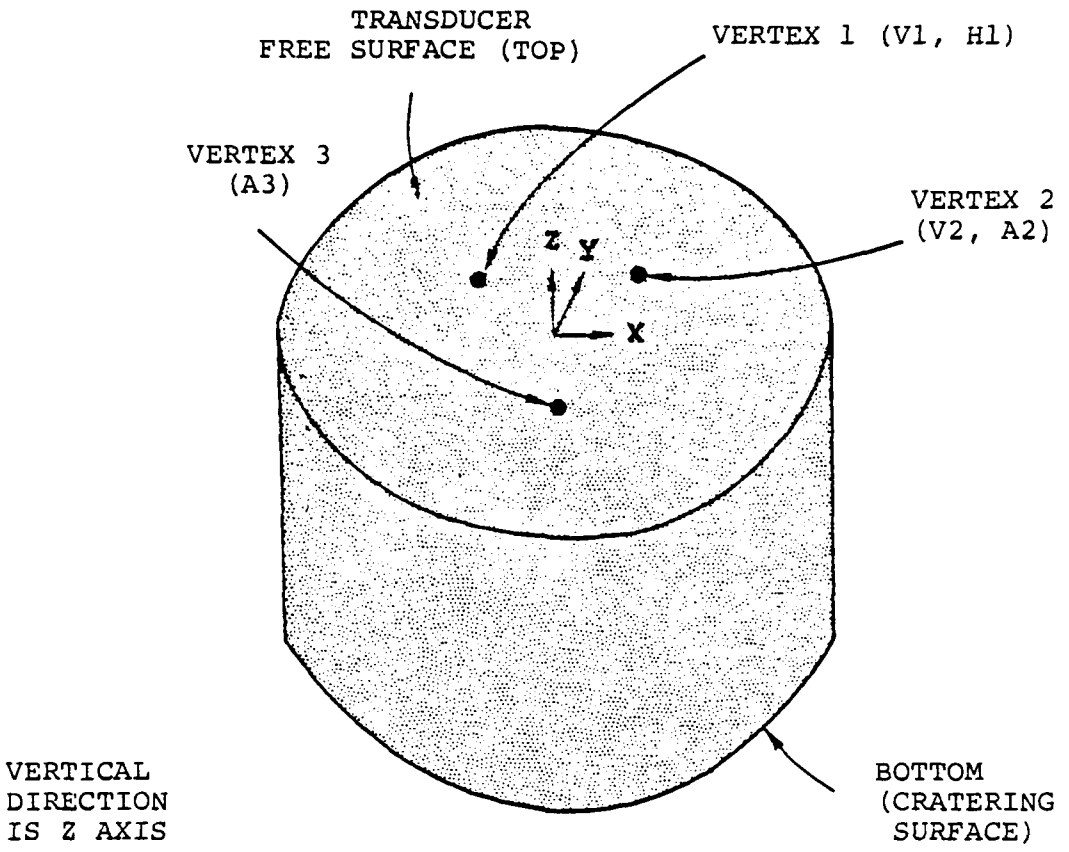

POINT	COORDINATES (X,Y,Z) cm
Vertex 1	(-15.2, 8.7, 0)
Vertex 2	(15.2, 8.7, 0)
Vertex 3	(0, -17.6, 0)
V1, Vertical Displacement Gauge	(-14.0, 8.7, 0)
H1, Horizontal Displacement Gauge	(-16.5, 8.7, -0.5) Sensitive Axis ∥x
V2, Vertical Displacement Gauge	(14.0, 8.7, 0)
A2, Vertical Accelerometer	(16.5, 8.7,0)
A3, Vertical Accelerometer	(0, -17.6, 0)
Charge 1	(-15.2, 8.7, -31)
Charge 2	(15.2, 8.7, -31)
Charge 3	(0, -17.6, -31)
Cylinder Bottom	(X, Y, -33 or -37 or -60)

Figure 17. Schematic of the laboratory model. The diameter of the cylinder was 122 cm.

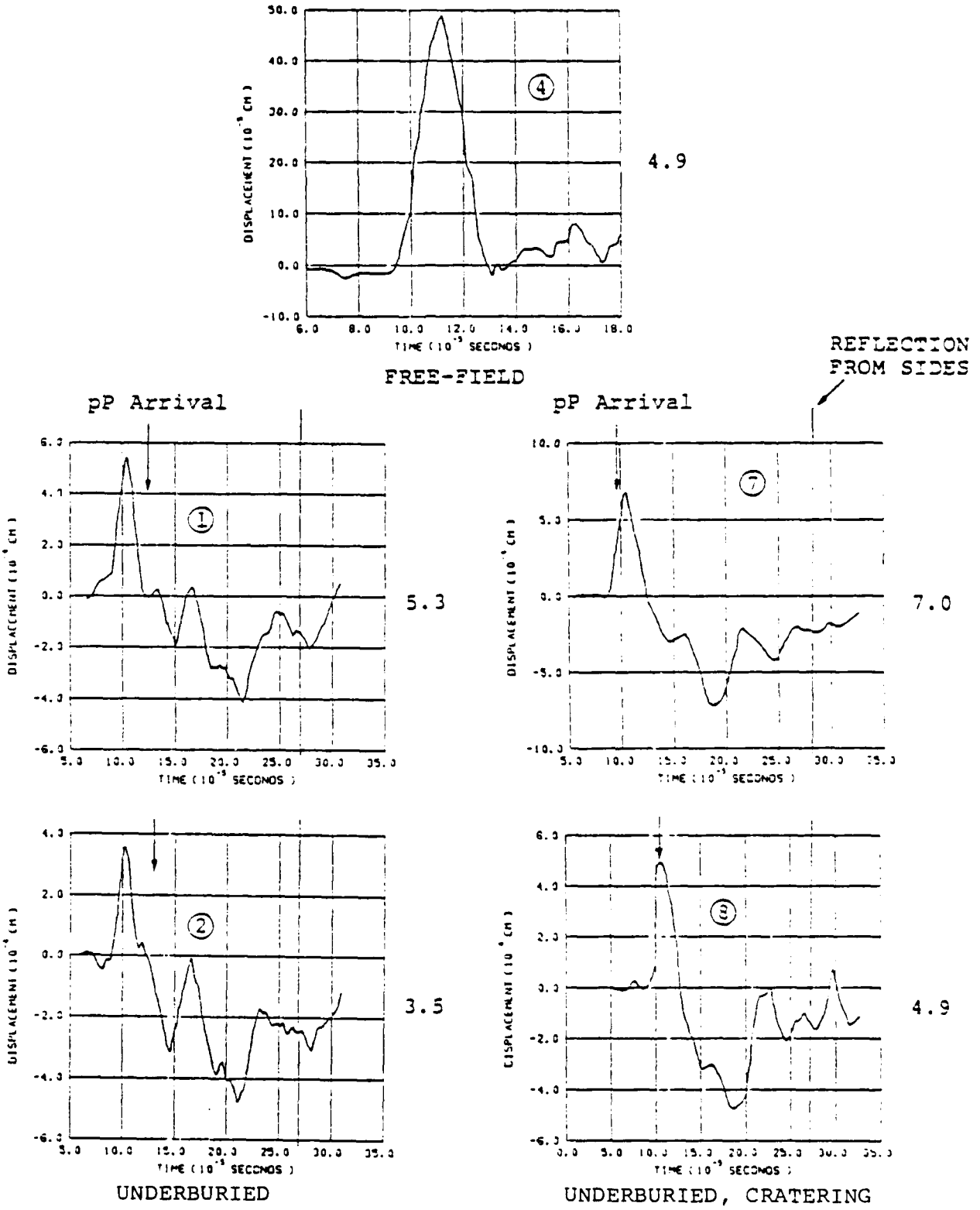

Figure 18. The displacement-time histories are plotted for the five experiments to be further analyzed. The test identifier is noted on each plot. At the right are the amplitudes of the peak displacement in microns. On the plots for the underburied experiments we show the expected arrival times (from elastic theory) of the free surface $_{p}P$ phase and the unwanted reflections from sides of the cylinder.

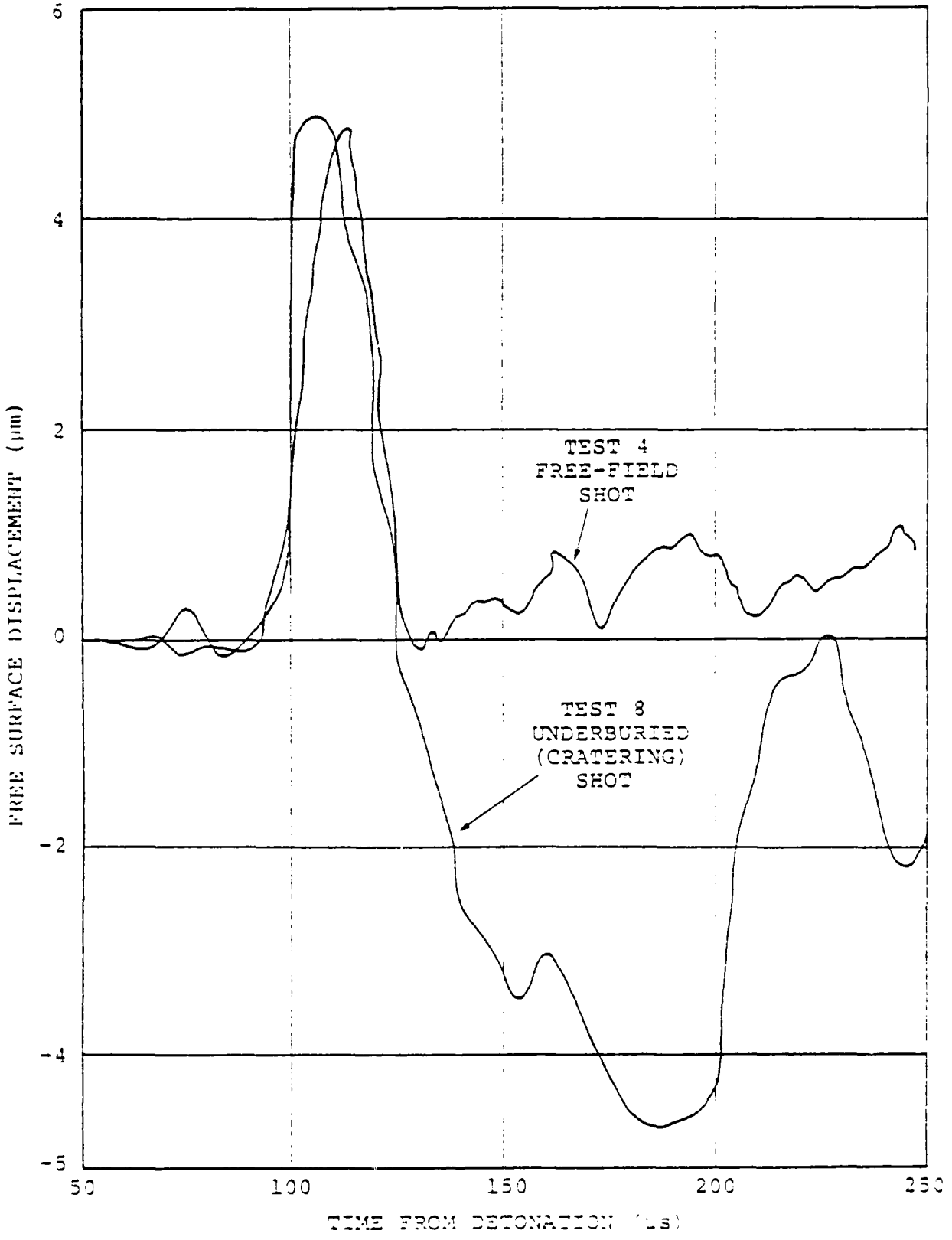

Figure 19. Comparison of typical records for displacement from free-field and underburied (cratering) shots.

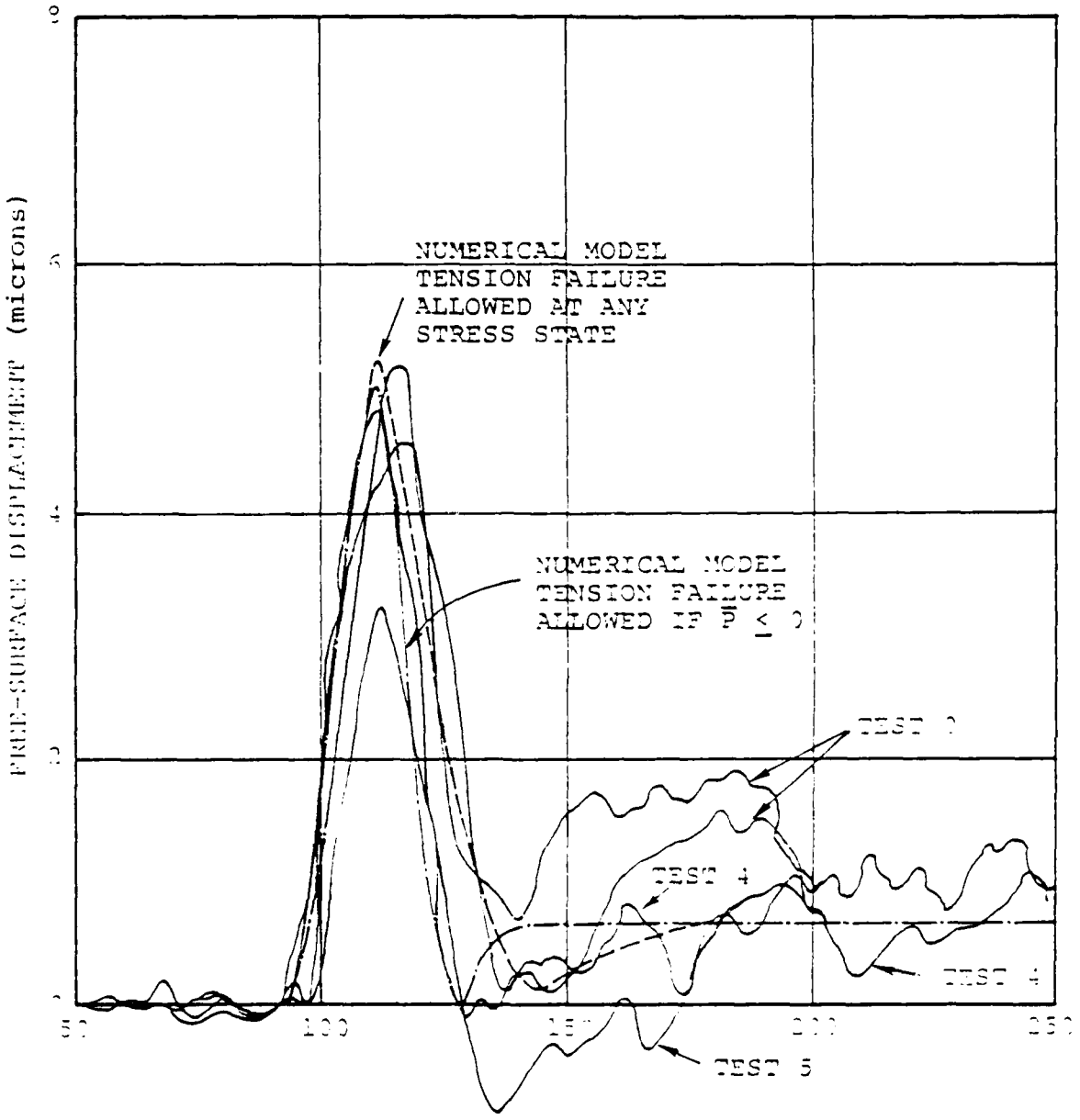

Figure 20. Comparison of measured and numerically simulated displacements.

for the two calculations are shown in Figure 21 compared to the RVP from Test 4.

We see from these two figures that agreement between simulation and data is excellent when $\bar{P}$ is not restricted. However, when this model is used in a two-dimensional program to simulate the experiments with the charge buried 6.5 cm below the free surface, the pP arrival is not present. The absence of pP is due to tension fractures which surround the cavity and which remain open at late time.

Figures 22 and 23 compare simulations and data for Test 1 and Test 8, respectively, with $\bar{P} \leq 0$ included in the tension fracture model. The pP event is now a distinct arrival in Test 1 and the overall agreement between the simulation results and the data is quite acceptable.

All underburied shots have two events in common:

1. The direct P wave,
2. A large, low frequency arrival opposite (negative) in phase to the direct P wave.

The pP phase is depth of burial dependent and is absent in the cratering experiment.

The long period negative motion can be explained as an elastic effect due to near-field reflections from the free surface. The negative motion thus does not propagate to teleseismic distances. To demonstrate this, we did the following experiment. Using the reduced velocity potential from the free-field source (Figure 21) as a source time function, the seismic waves were propagated as though the medium were linearly elastic. The elastic propagation was done both numerically and analytically to eliminate the possibility of program errors. The numerical calculations were done with a finite element code. The analytic program is a generalized ray program which is capable of propagating the entire (near-field and far-field) seismic wave field (Barker, 1976).

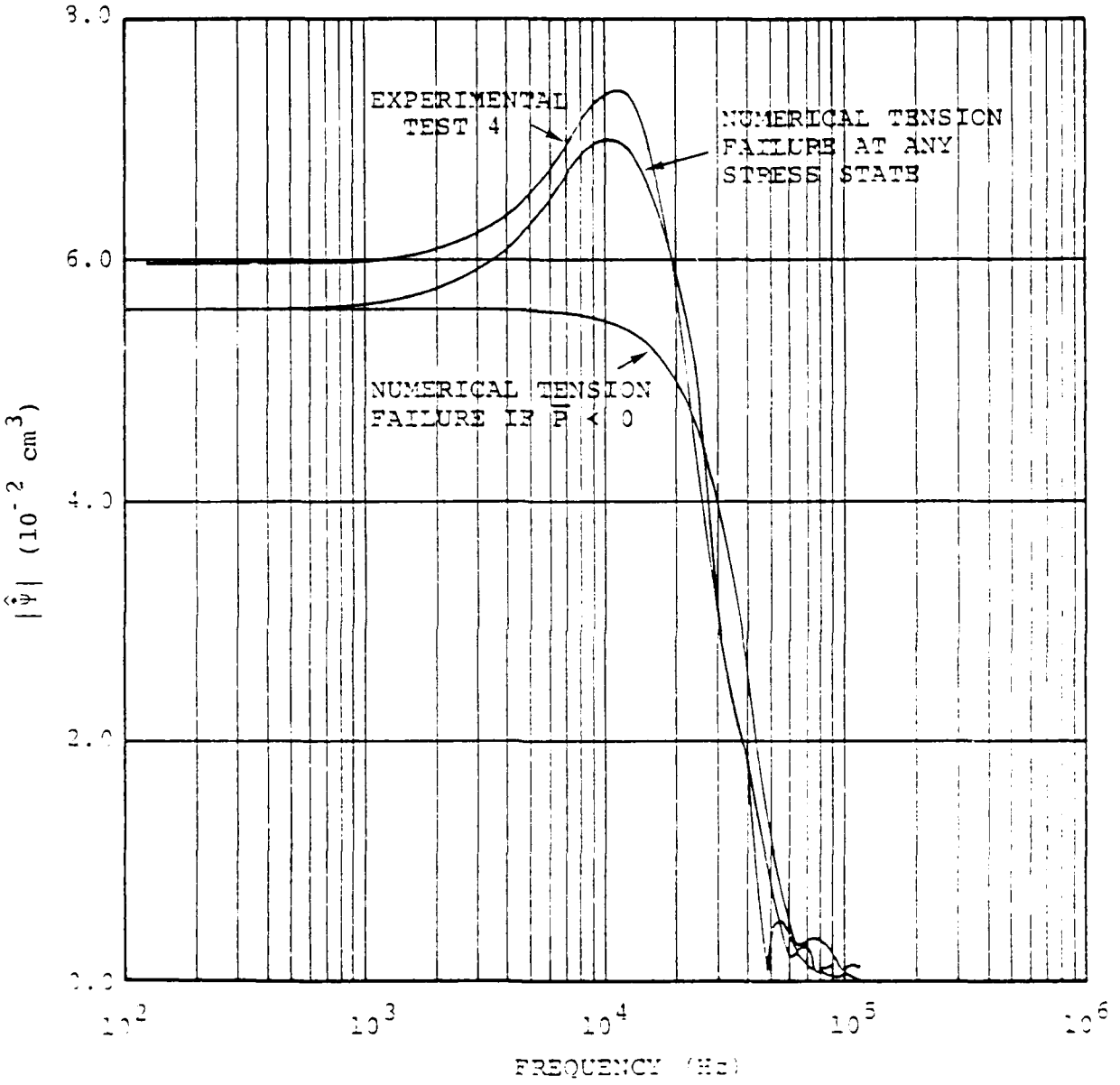

Figure 21. Comparison of experimental and numerically simulated source functions expressed as RVP transforms.

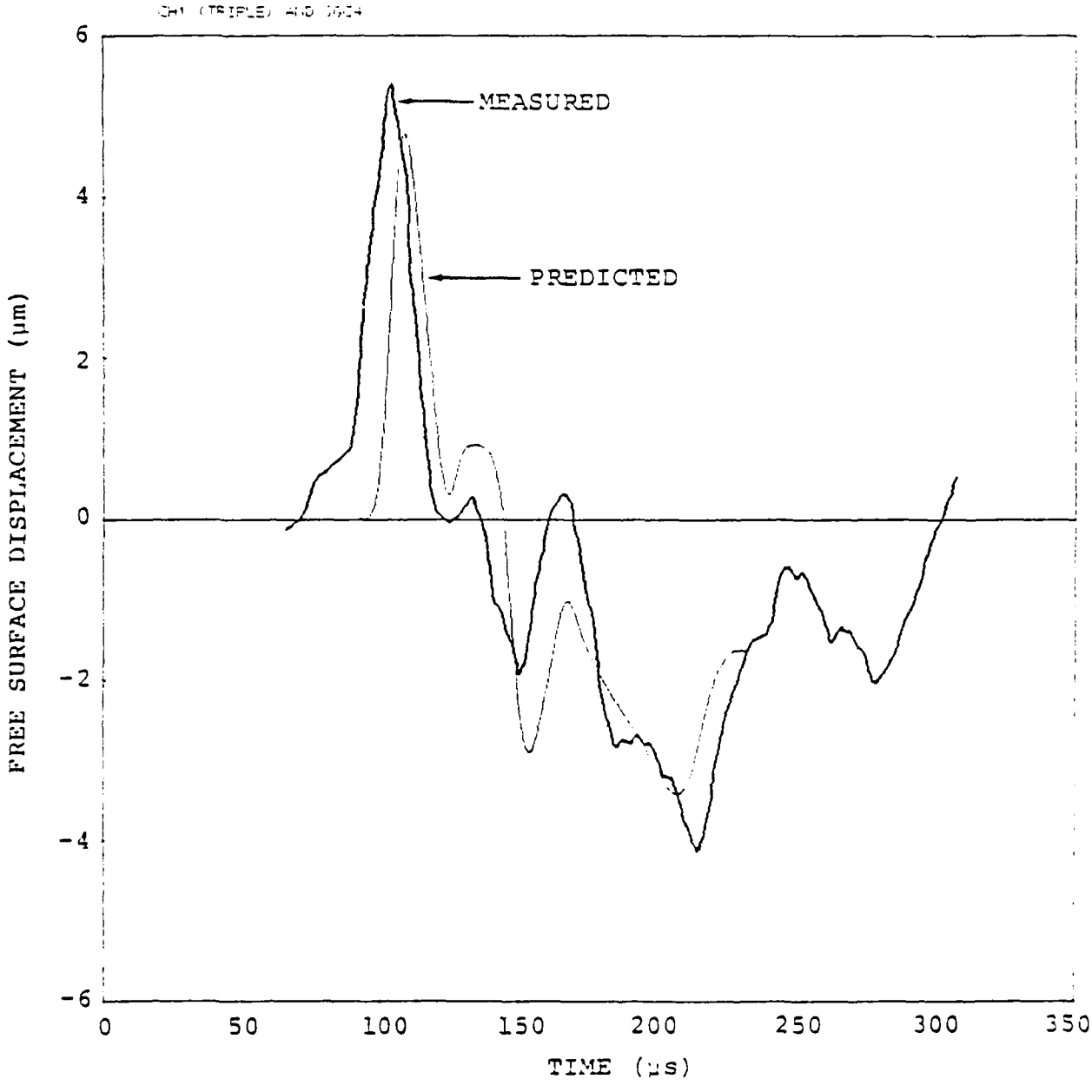

Figure 22. Comparison of measured and predicted displacements for Test 1. The depth of burial was 6.5 cm. The gauge was located 30.5 cm below the charge.

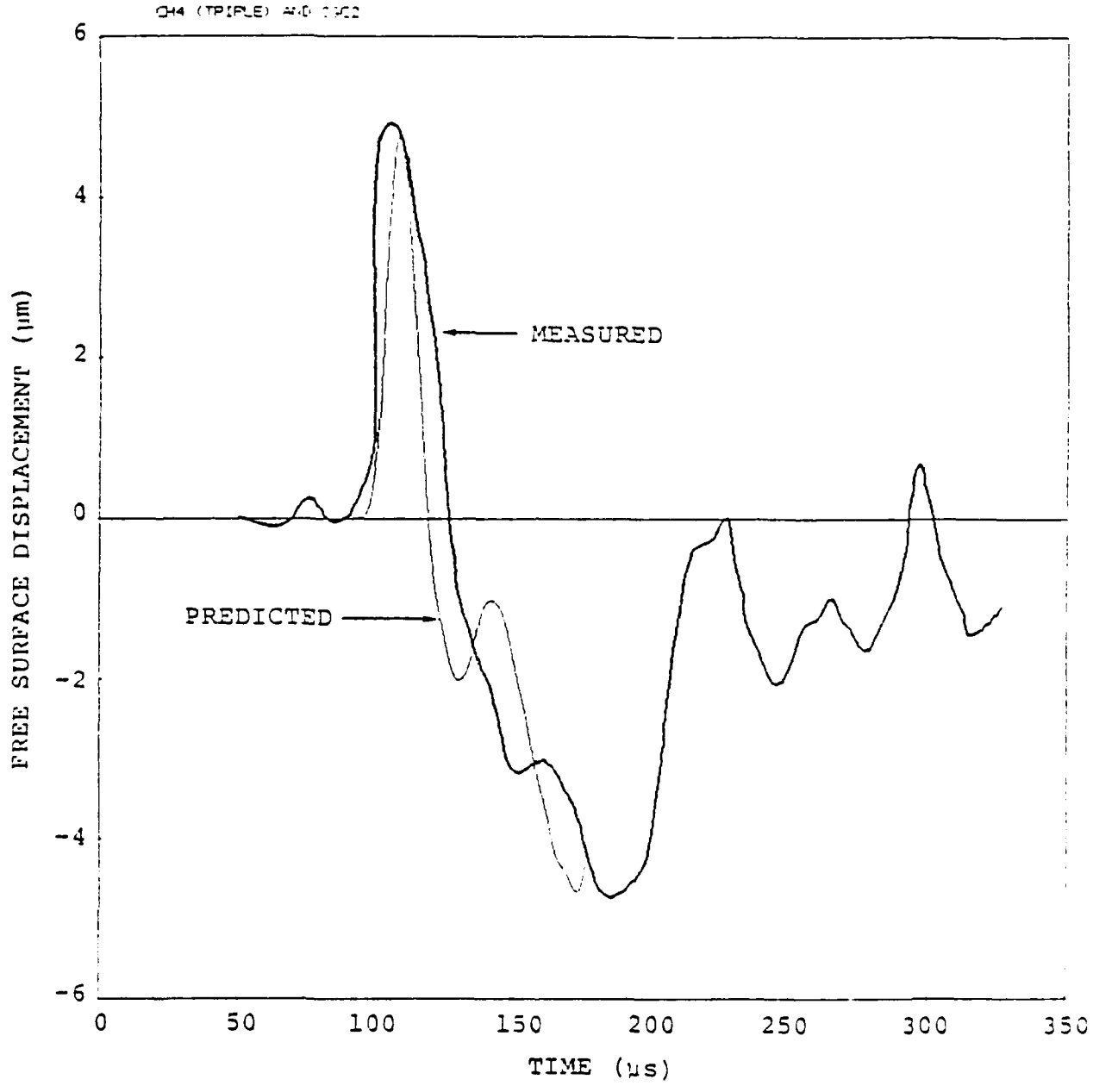

Figure 23. Comparison of measured and predicted displacements from the cratering shot (Test 8). The depth of burial was 1.75 cm and the crater radius was approximately 8.5 cm. The gauge was located 30.5 cm below the charge.

Figure 24 shows the comparison between the vertical ground motion from the two-dimensional calculation described above with that obtained by propagating the free-field reduced velocity potential elastically. The elastic propagation was done numerically using a finite element code. In this case $\theta = 0$ and the receiver is located on the bottom free surface at a depth of 30 cm. We see that the signals are very much alike. In particular, they both exhibit the long period negative pulse mentioned above. We may therefore conclude that this pulse is due to elastic propagation effects.

In order to understand the elastic propagation effects, we turn to the generalized ray calculations. These calculations allow one to examine separately the contributions of the direct P and reflected pP and pS phases. The impulse response of the medium is first computed. These were convolved with the free-field reduced velocity potential from Figure 21. An example is shown in Figure 25 where the shape of the signal is very much like the data.

To show how the waveform develops and how it propagates to teleseismic distances, we have computed the signal along a teleseismic ray path, $\theta = 20°$, for increasing values of R (Figure 26). For small values of R, the negative pulse is not apparent because the pP-pS time is too short. As this time difference increases, the long period negative pulse becomes prominent. At larger ranges, the pP near-field term becomes small. At teleseismic ranges, the negative pulse is absent and has no effect on measurements of m_b or M_s. These results make clear the importance of using the appropriate Green's function when extrapolating near-source numerical solutions to the far-field.

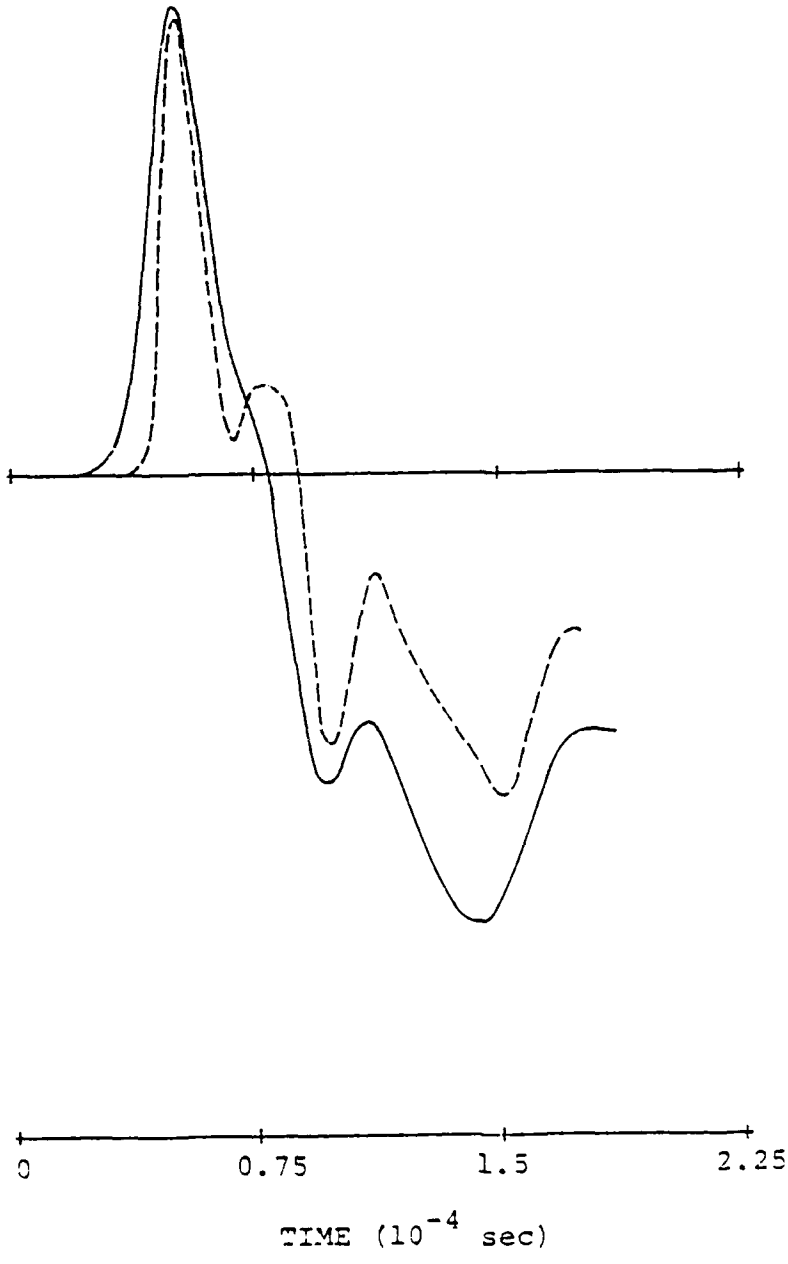

Figure 24. The vertical displacement from the complete two-dimensional calculation (dashed line) is compared with the displacement obtained by elastically propagating the free-field reduced velocity potential (solid line). The elastic propagation was performed numerically using the RVP of Figure 21 as a source.

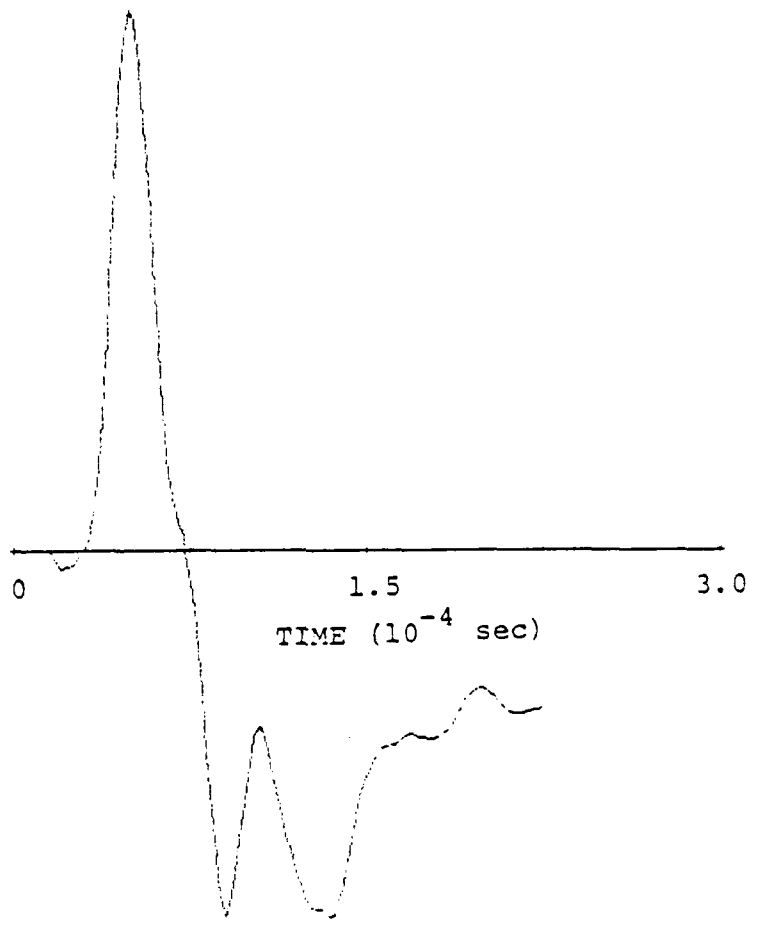

Figure 25. The vertical displacement is shown for θ = 4°, R = 30 cm. The reduced velocity potential is propagated using the analytic generalized ray program.

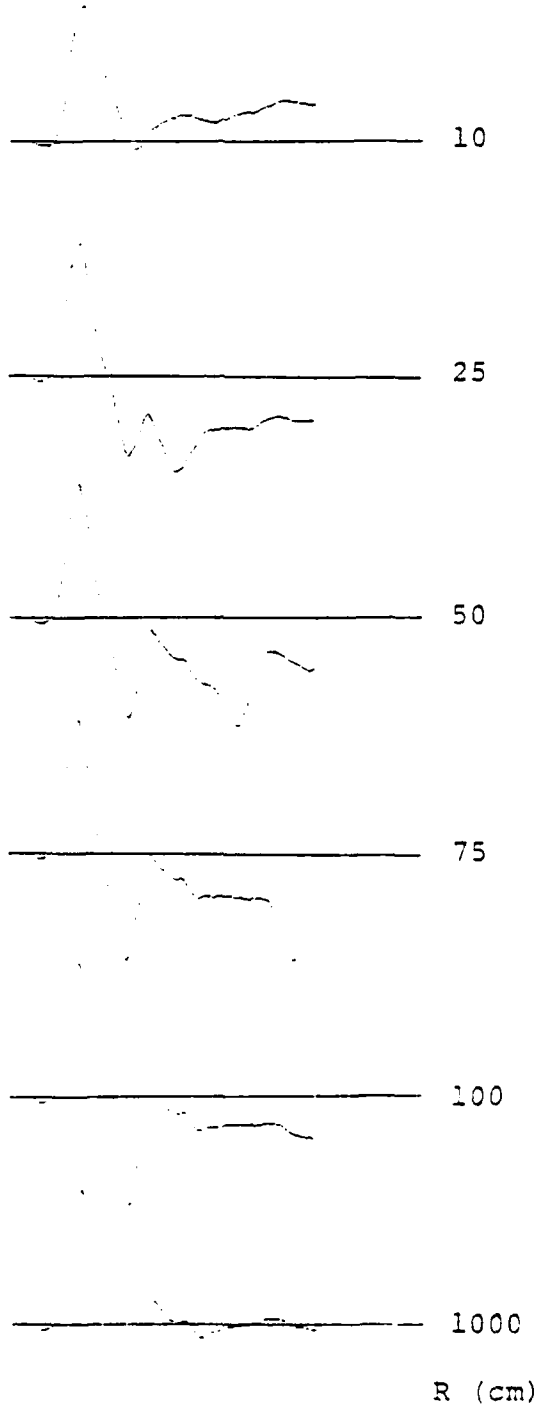

Figure 26. Vertical displacements are shown along the ray $\theta = 20°$. Tick marks are 0.75×10^{-4} sec apart.

4.4 SUMMARY

1. The free-field RVP spectrum for an explosion in concrete was observed to be mildly peaked, with the difference between the spectral peak and Ψ_∞ corresponding to 0.09 magnitude units.

2. We were able to obtain an excellent match to the free-field data by using published data for the material properties of concrete, our own measurements of P velocity and unconfined compressive strength and published data for PETN.

3. The large, long period negative pulse was observed on all underburied shots in both the laboratory data and the numerical simulation, whether or not spall and/or cratering occurred at the free surface. Our explanation of this pulse is that it is a near-field wave produced by a spherical P wave reflecting from a plane impedance contrast. It should not propagate to the far-field.

4. We were able to obtain an acceptable match to the underburied shot data only after modifying the tension failure model. This modification somewhat degraded the match to the free-field data.

5. The calculational results indicate that tension failure is required to produce a peaked spectrum. However, the distinct pP arrival observed in the data suggest that these features either do not remain open or else fill with water. It would be interesting to section the concrete blocks and observe the degree of fractures produced in each experiment.

6. Sufficient data from each calculation has been saved in order to analytically continue the close-in ground motion to the far-field. Rigorous analytic continuation algorithms for sources in a halfspace are being developed at S^3. They will be used to determine the effect of depth of burial on teleseismic ground motion using the data obtained under this contract.

7. The laboratory modeling work should be extended to include multiple charge, decoupling and asymmetrical cavity studies.

V. SURFACE WAVE STUDIES

5.1 CRUSTAL STRUCTURES INFERRED FROM RAYLEIGH WAVE SIGNATURES OF EXPLOSIONS

In a paper appearing in the October issue of BSSA, "Crustal Structures Inferred from Rayleigh Wave-Signatures of NTS Explosions," Bache, Rodi and Harkrider presented an improved method for determining plane-layered earth models that accurately represent the important features controlling the amplitude and waveform of the Rayleigh waves propagated along particular paths. Since dispersion data provide valuable information about earth structure, it is desirable to develop effective inversion techniques for interpreting them. Further, the better our models account for path effects, the more confidently we can relate the amplitudes of Rayleigh waves to source parameters, source structure and dissipation effects.

We briefly summarize the main features of the crustal structure determination. A large number of recordings of NTS explosions at two WWSSN stations (ALQ and TUC) were collected and the waveforms were found to be quite consistent. Some examples are shown in Figure 27. For one event in each of the three different test areas the records were digitized and analyzed to determine the phase and group velocities. For the phase velocities we used a straightforward unwrapping of the phase spectrum of the entire seismogram plotted in Figure 27 and no special windowing was found to be necessary. The group velocities were determined by a more sophisticated approach relying on the Hilbert transform envelope of the narrow-band filtered seismogram. The two sets of data are shown in Figure 28. They are entirely consistent and vary little from event to event.

Using an average phase and group velocity fit to the data at each station, a linear inversion was done to determine the earth structure of the two paths. The results are shown

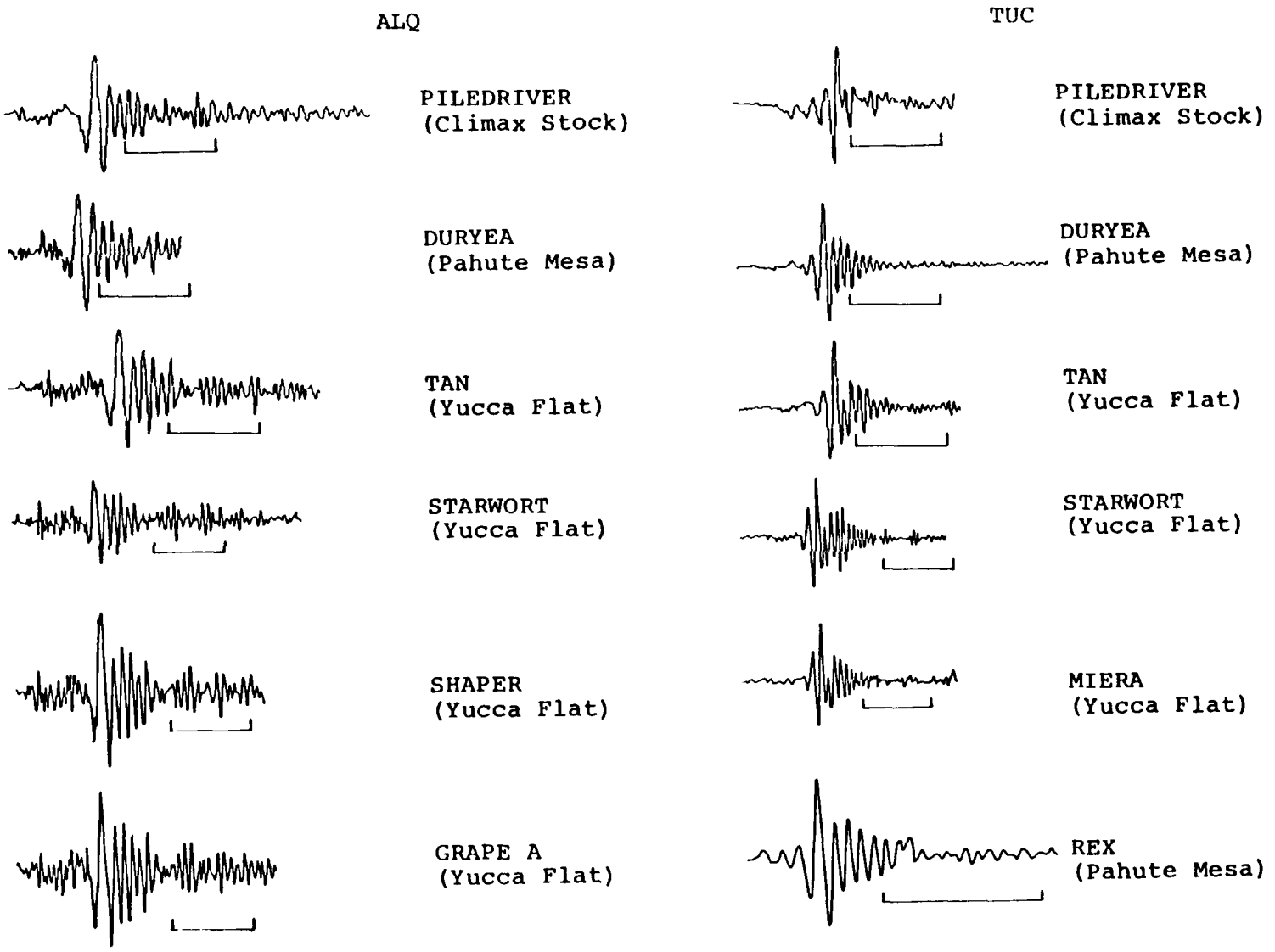

Figure 27. Typical seismograms are shown for six events recorded at each station. The first three events in each column are plotted from hand-digitized data while the others are tracings from the film records. All seismograms are not on the same time scale - one minute is indicated on each record.

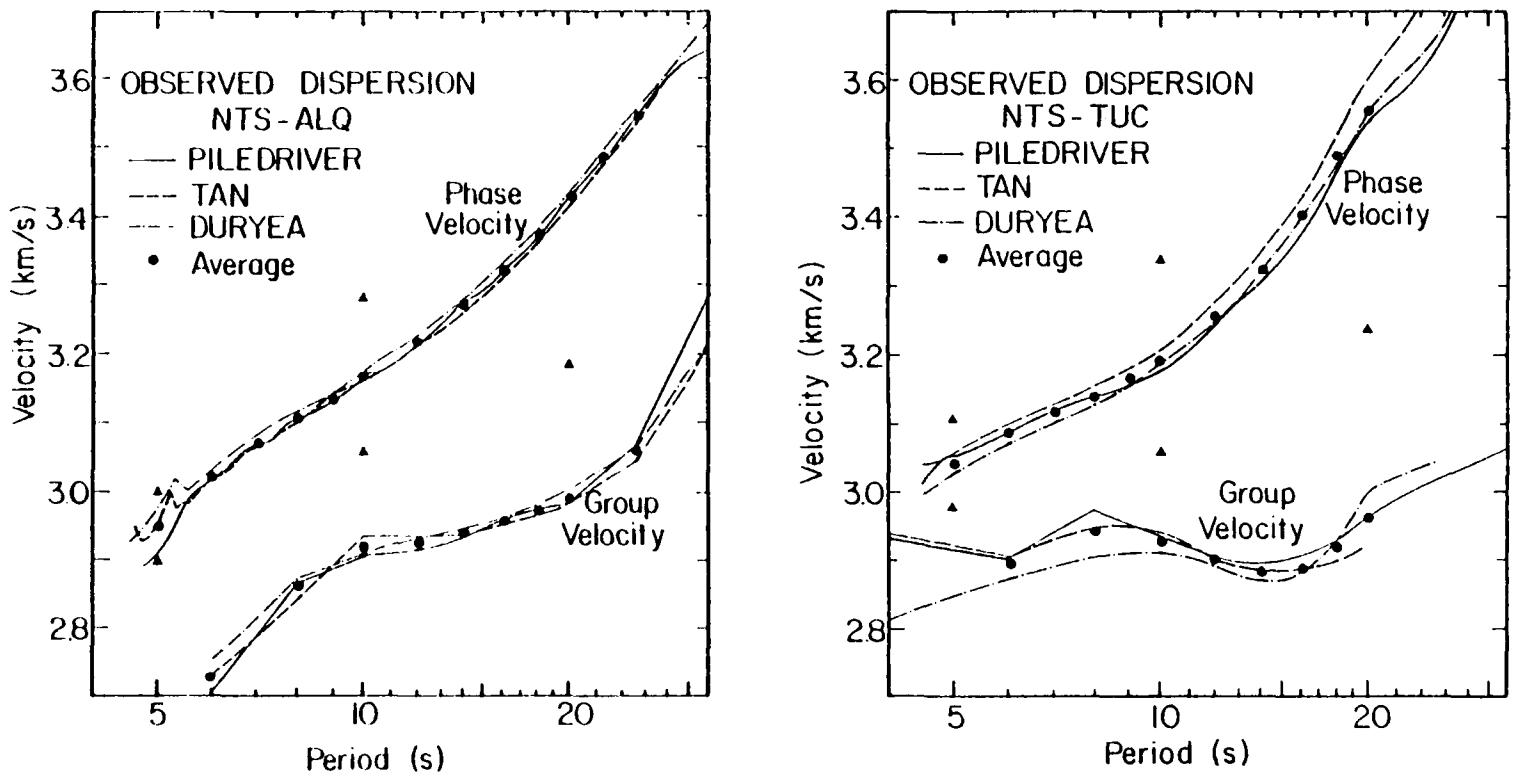

Figure 28. The observed phase and group velocities are shown for three events at NTS to ALQ (left) and TUC (right). The lines denote the values determined from each event, while the closed circles are the average values used in the inversion. The closed triangles are the phase velocities implied by adding plus and minus 2π to the phase spectrum of each seismogram.

in Figures 29 and 30. The models found agreed with the dispersion data with a maximum error of 0.01 km/sec. Further, these models are consistent with other available information on these paths, including that from refraction studies. The main difference between the two models is that the NTS-TUC path has a crustal thickness of 31 km while the average crustal thickness for NTS-ALQ is 42 km.

To compute synthetic seismograms, we must address the fact that conventional surface wave theories (e.g., Harkrider, 1964) cannot be used in a consistent way when events in close proximity occur in different source materials, as is common at NTS. Therefore, we construct, albeit in a somewhat ad hoc way, a theory in which two structures are used to model the source-receiver travel path. The amplitude excitation is computed in a source structure and the dispersion is computed in a separate path structure. A transmission coefficient accounts for passage of Rayleigh waves between the two.

As a test of the models, synthetic seismograms were computed and are compared to the observations in Figure 31. The two are found to be in remarkable agreement. Thus, our models quite accurately account for the propagation of surface waves along these paths. Within the resolving power of the data and the restrictions imposed by the assumption of plane layers, the crustal structures in the regions sampled by the two paths must then closely resemble our models.

In the next section we describe the results from a study in which we use these crustal models to account for path effects and then infer the characteristics of the explosion source.

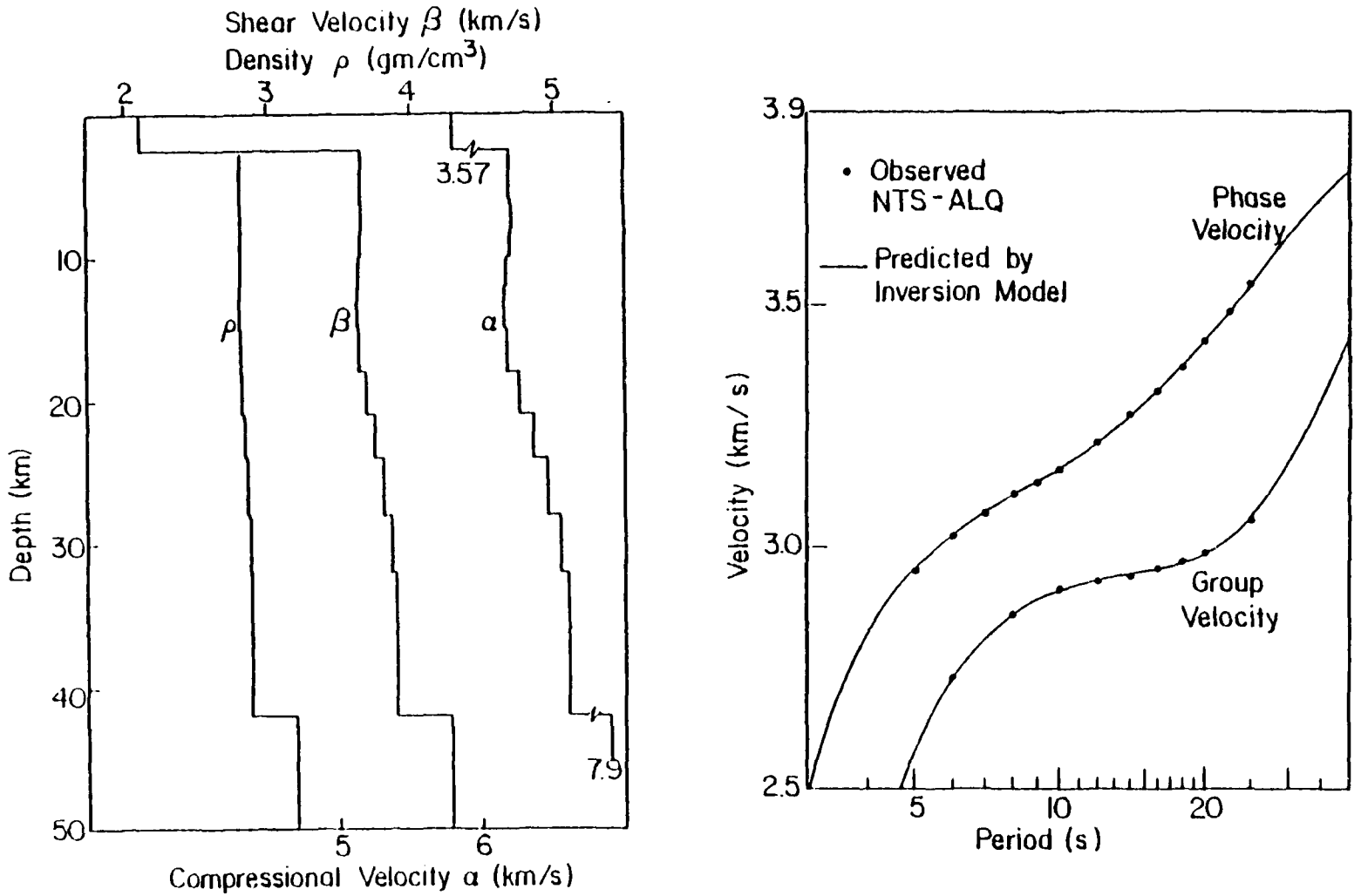

Figure 29. The inversion model (left) for the NTS-ALQ path is shown together with a comparison of its predicted dispersion with the observed NTS-ALQ dispersion.

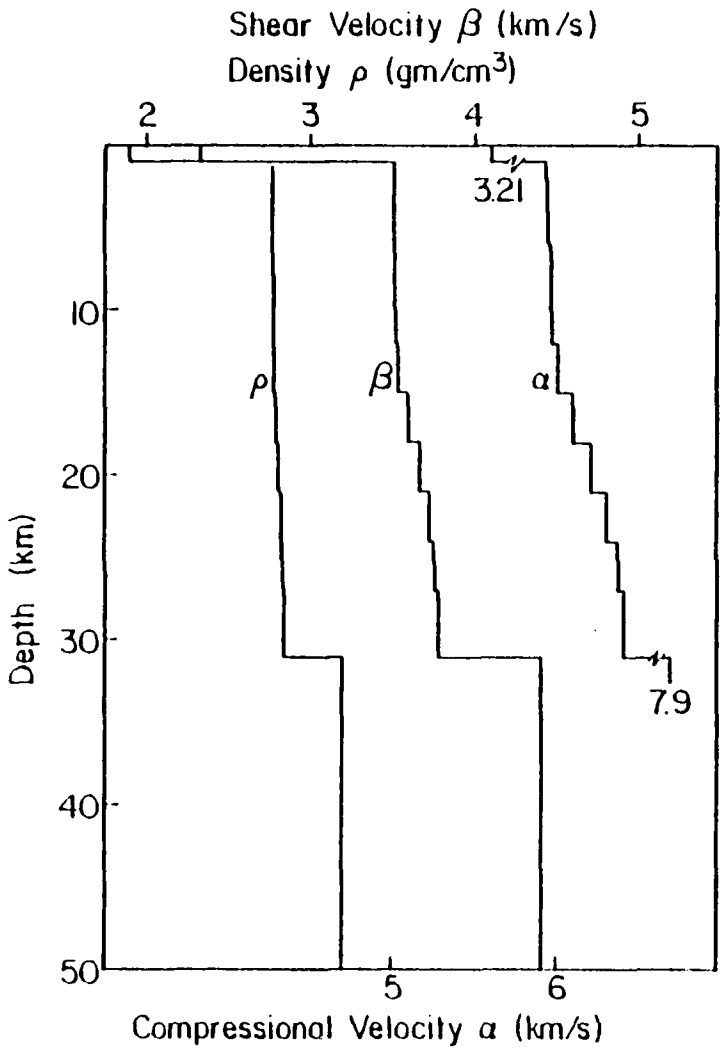

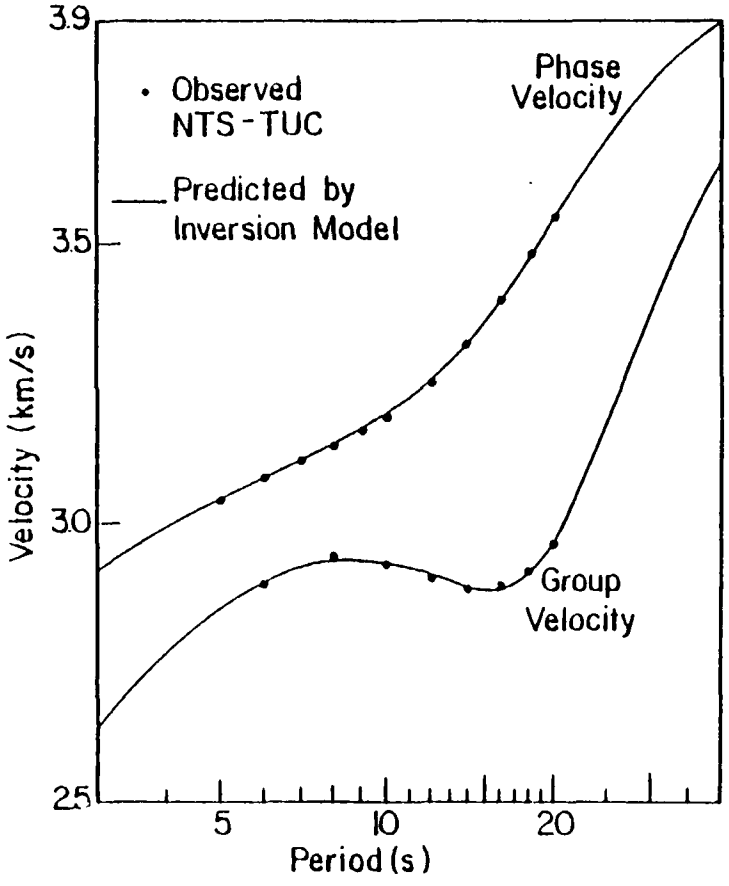

Figure 30. The inversion model (left) for the NTS-TUC path is shown together with a comparison of its predicted dispersion with the observed NTS-TUC dispersion.

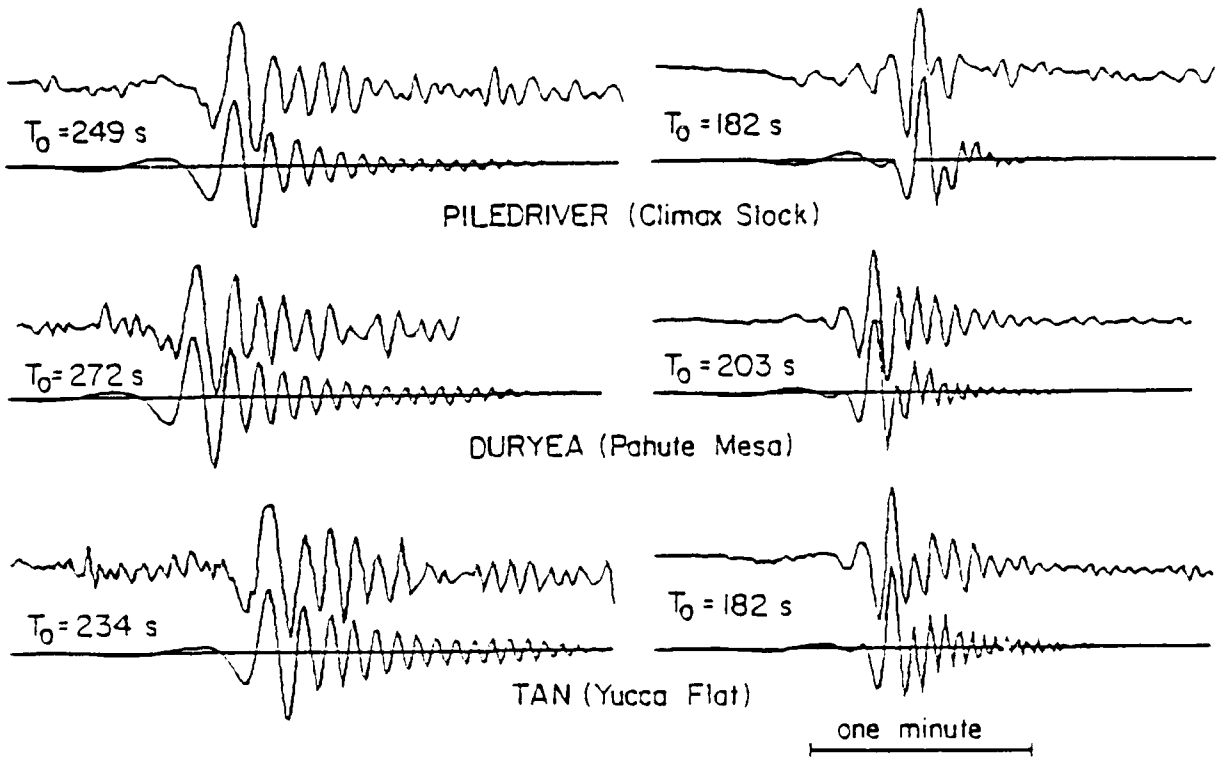

Figure 31. Theoretical and observed seismograms are compared at ALQ (left) and TUC for events in three test areas at NTS. A bar indicating one minute is shown. In each pair the observed (top) and theoretical records start at the same time with respect to the explosion detonation and this time is indicated as T_o.

5.2 SOURCE AMPLITUDES OF NTS EXPLOSIONS INFERRED FROM RAYLEIGH WAVES AT ALBUQUERQUE AND TUCSON

5.2.1 Introduction

Commonly used methods for estimating the yield of foreign underground nuclear explosion rely on the use of empirical relations between body (m_b) and surface (M_s) wave magnitudes and yield. The difficulty with empirical relationships is that they can be systematically in error when applied to events outside the empirical data base. This problem is widely recognized and, as a result, there is considerable interest in developing a clear understanding of the important parameters that control the seismic signatures of underground explosions.

In a paper by Bache, Rodi and Harkrider (1978) we describe a study of NTS explosions in which we attempted to model in great detail the recorded Rayleigh waves at two WWSSN stations: Albuquerque, New Mexico (ALQ) and Tucson, Arizona (TUC). We find that our synthetic waveforms are in excellent agreement with the observations. This suggests that most of the important contributing factors are properly represented by our models.

The main objectives of the work which is summarized here were to use the comparison of synthetic and observed Rayleigh waves to infer the long period amplitude of the NTS explosion source and to explore the potential influence of supposed source complexities, particularly surface spallation and related phenomena. In pursuing these objectives we address the following questions:

- How accurately can the Rayleigh wave signature of NTS explosions be modeled with plane-layered elastic models for the travel path?
- Is a spherically symmetric point source adequate for modeling the source?

- What is the effect of surface spallation on the Rayleigh wave?
- What is the effect of tectonic strain release on the Rayleigh wave?
- What is the source amplitude and how does it depend on source material, source depth and yield?
- How much scatter is to be expected for events in relatively homogeneous regions (e.g., below the water table at Yucca Flat) and what are the main causes of this scatter?

We chose to use data from stations ALQ and TUC because the data was conveniently available and because these stations are at an excellent range (700 to 950 km) for studying NTS explosions. They are close enough to record many of the smaller yield events, while being at a range where the trace is dominated by the fundamental mode Rayleigh wave. The first step in our analysis of the ALQ and TUC data was to determine the crustal structure along the two paths and this work was reported by Bache, Rodi and Harkrider (1978) and summarized in Section 5.1.

5.2.2 Outline of the Analysis

The results of the surface wave inversion gave reasons to believe that we could quite accurately account for the path effects for NTS explosions observed at ALQ and TUC and thus determine the characteristics of the source. This is our primary objective. In outline form, our work includes the following:

A. A spherically symmetric source represented by a reduced displacement potential is assumed. Then for each of the test areas studied (Yucca Flat, Pahute Mesa and PILEDRIVER), the Rayleigh wave amplitude is directly proportional to the static value of the reduced displacement potential (Ψ_∞). Comparing theoretical and observed seismograms, a Ψ_∞ is determined from each station for each event and the values are scaled to a common yield. The important results are as follows:

- At ALQ the mean values of the Ψ_∞ scaled to 0.02 KT are 9.1 m^3 for the seventeen Yucca Flat events, 6.6 m^3 for the seven Pahute Mesa events and 3.9 for PILEDRIVER.* Only events below the water table with yields from 40 to 200 KT were studied. The standard deviation for each population is about 40 percent of the mean.

- The Ψ_∞ inferred from the TUC records are consistently 1.5 times larger than from ALQ.

- For similar materials the Rayleigh waves are proportional to $\mu_s \Psi_\infty$, where μ_s is the average shear modulus in the source region. Variations in μ_s and errors in the official yield are two sources of random scatter in the Ψ_∞ in a particular area.

- Random effects can plausibly account for at most half the scatter in the inferred source levels for each population. The remainder of the scatter appears to be due to real differences among the source levels of the different events in each population.

- The slope of the log Ψ_∞-log yield curve (comparable to M_S-log yield) cannot be determined with confidence for the rather narrow yield range represented in our data.

B. The Ψ_∞ values from this analysis of Rayleigh waves are compared to estimates of Ψ_∞ made by other methods; for example, for close-in methods, from far-field body and surface waves or from theoretical considerations. Our values are within the range expected from this other work except for PILEDRIVER where our value is low.

C. The assumption that the source is spherically symmetric is clearly an oversimplification. Using results obtained by Toksoz and Kehrer (1972), we correct our solution for the effect of a double-couple component in the source. We find that the double-couple has virtually no effect on the

*We use the notation Ψ_∞ for both the absolute value for a given event and for values scaled by the cube-root of the yield to 0.02 KT. When there is any possibility of confusion about what kind of value is meant, we use the notation $\Psi_\infty^{0.02}$ to indicate the common yield value.

waveform, but simply scales the amplitude. If the values given by Toksoz and Kehrer are typical, some 15 to 20 percent of the discrepancy between the ALQ and TUC solutions for the Yucca Flat and Pahute Mesa Ψ_∞ is due to the double-couple. The mean $\Psi_\infty^{0.02}$ values at ALQ are reduced from 9.1 and 6.6 to 8.1 and 4.3 for these two areas. For PILEDRIVER, Toksoz and Kehrer predict a much larger effect on the Rayleigh waves at these two stations. Their solution actually increases the discrepancy between the values obtained at the two stations, though it is quite sensitive to small errors in the double-couple orientation. Further, the double-couple contribution so dominates the solution that the $\Psi_\infty^{0.02}$ required to match the data at ALQ is reduced to about 1.0.

D. The impulse delivered by the impact of the large mass of spalled material returning to the free surface has been supposed to have some significant effect on the Rayleigh wave signature of explosions (e.g., Viecelli, 1973). Using estimates for the spall impulse given by Viecelli (1973) and somewhat larger estimates given by Sobel (1978), we compute expected Rayleigh waves at ALQ and TUC to determine its effect. We find it to be quite small. It seems implausible to suppose that the spall impulse could change the Rayleigh wave amplitude by more than 5 to 10 percent.

E. A spall-related phenomenon that may be much more significant is the associated loss of energy from the waves traveling upward from the source. We explore the potential effect by simply deleting a portion of the up-going waves from the solution. A more appropriate filter may be frequency-dependent, having its primary effect on the short periods, but at present we have no results to support this conjecture. The events at Yucca Flat are quite insensitive to the suppression of the up-going waves. The effect at Pahute Mesa is much larger with suppression of half the up-going waves leading to a decrease of about 25 percent in the amplitude. PILEDRIVER is extremely sensitive to the amount of up-going waves suppressed and this is a very important parameter for events in granite. If we suppose that 50 percent of the up-going wave is lost to spallation or scattering, the Rayleigh wave amplitude is reduced by about 40 percent. Suppression of 25 percent of the up-going waves caused a decrease of about 20 percent in the amplitude.

F. We carefully examine the factors that control the amplitude of the synthetic seismograms to determine why the source level inferred from the TUC observations is about 1.5 times larger than that inferred from the ALQ observations. A partial explanation is provided by the presence of asymmetries at the source, particularly the double-couple (C), but a substantial amount remains. There are four main features of the theoretical calculation that are examined closely; the dispersion, the model for the source region, the transition between the local source structure and average path structure and the anelastic attentuation (Q) for the two paths. Rather than from any one factor, the differences in the source estimates seem to be due to contributions from each of these. Errors in the dispersion and attenuation are small, but tend in the right direction. The main source of error is probably associated with the failure of plane-layered models to precisely represent the complex real earth. We recommend that the answers from the two stations be averaged, but give more weight to those from ALQ. A better definition of the true source amplitude would probably be achieved by carrying out the same analysis for more stations and averaging the results.

5.2.3 Summary of Results

In our analysis we divided the explosions into three groups (Yucca Flat, Pahute Mesa and PILEDRIVER) separated geographically and by the average material properties at the source. Using plane-layered earth models, synthetic seismograms were computed that give excellent agreement with the observed waveforms. For the source we used four different models that were combined in various ways. These are:

- A spherically symmetric point source given by a reduced displacement potential.
- A reduced displacement potential source with a portion of the up-going waves suppressed.
- A downward impulse representing the impact of the spalled material.
- A double-couple.

The source quantity most directly related to explosion yield is the static level of the reduced displacement potential (Ψ_∞).* We first estimate this quantity assuming the source is spherically symmetric, then correct these estimates for other effects. Our best estimates for the mean Ψ_∞ in m^3 scaled to 0.02 kt in each area are as follows:

	Yucca Flat	Pahute Mesa	PILEDRIVER
1. Assume spherical symmetry	10.5	8.1	4.7
2. Correct for observed double-couple	8.3	4.8	1.4
3. Correct for spallation#	11.4	10.0	5.9
4. Simultaneously correct for spallation and double-couple	9.1	5.8	1.8 2.7†

Throughout the report, values are determined separately for the two stations ALQ and TUC. The "best" estimates given above were determined by averaging the two with the ALQ values given double weight.

The values given represent mean values and individual events can deviate substantially from these. The corrections for the double-couple and spallation contributions are again based on mean values, but these effects must vary widely from

*The relationship between Ψ_∞ and yield is dependent on the local material properties and is a subject for separate discussion (e.g., Cherry, et al., 1975b).

#The spall impact makes little contribution. The main event is the suppression of up-going waves from the source. This estimate is based on suppression of 75 percent of these waves.

†25 percent of the up-going waves from both the explosion and double-couple are suppressed. For Yucca Flat and Pahute Mesa, the suppression is only applied to the explosion waves.

event to event. In fact, variation in these effects is likely to be responsible for a large portion of what we have called "real" source level variations; that is, variations that cannot be attributed to random errors in our modeling procedure. The effect of the double-couple can be reduced by averaging values for many azimuths, while the spallation effects are not likely to depend on azimuth.

5.2.4 Conclusions

Our most important conclusion is that available techniques are capable of modeling surface wave signatures of underground explosions in considerable detail. The amplitude of the source can thus be inferred from a comparison of synthetic and observed seismograms. Applied to foreign explosions, this would lead to yield estimates that are independent of the estimates from empirical M_s-yield curves.

The uncertainties in yield estimates from the matching of synthetic and observed records may be summarized as follows:

1. Different estimates would be obtained from different stations. After correcting for radiation pattern effects, taking Love waves into account, these would be averaged and a statistical estimate of the uncertainty would result.

2. Neither the velocity nor Q models will ever be determined with ideal accuracy. We can estimate the errors associated with uncertainties in these models and the models themselves should improve with time if the effort is made.

3. The most important uncertainties are associated with the source itself. First, there is the relationship between the source amplitude and the explosion yield. However, the most that can ever be determined with seismic methods is the source amplitude. Second, there are the uncertainties associated with the selection of the appropriate model for the spallation process and, particularly, the loss of energy from the up-going waves. More research will help resolve these questions. Also, we point out that there is no reason to suppose

foreign and U. S. explosions would be much different as far as this aspect of the physics is concerned. If we select a particular model for this process (for example, assuming that 25 percent of the up-going waves are suppressed) and interpret U. S. and foreign events with this assumption, our source amplitude estimates will be consistent.

VI. BODY WAVE STUDIES

6.1 ANALYSIS OF DECOUPLED EXPLOSION CALCULATIONS BY APPLIED THEORY, INCORPORATED

Two axisymmetric ground motion calculations were carried out by Applied Theory, Incorporated (ATI) to simulate decoupled explosions in mined cavities in salt. Results from these calculations were provided to Systems, Science and Software (S^3) for analysis to determine the character of the teleseismic signatures of these decoupled explosions.

The ATI calculations were in a homogeneous wholespace and were carried into the elastic regime where the divergence and curl of the displacement field were monitored. From these quantities an equivalent elastic source representation was computed for each of the two calculations. In the first case, the mined cavity was spherical and the equivalent elastic source is a center of dilatation. In the second calculation the cavity was an ellipsoid of revolution. In this case, the equivalent elastic source includes higher order terms representing the departure from spherical symmetry.

The method for determining the equivalent elastic source is based on an expansion of the displacement field in spherical harmonics. The source is then described by a series of multipole coefficients. An advantage of this representation is that the near- and far-field terms and the P and S waves are conveniently separated. Also, the long period asymptotic behavior of the coefficients can be bounded.

While the time domain coefficients are exact, apart from numerical error, there is some ambiguity in the Fourier transformed coefficients at long periods. This arises from the fact that the calculations are carried out for only a few tenths of a second while our primary interest is in the character of the solution at periods of 1 to 30 seconds. The

ambiguity results from the fact that we cannot be sure the values at the last computed time step are close to the true static solution. This is particularly a problem for the S wave portion of the solution. The best we can do is to attempt to bound the contribution of the long period S waves.

The normalized monopole term for each of the sources is plotted in Figure 32. This is proportional to the reduced velocity potential and represents the spherically symmetric part of the field. In Figure 33 the source function for the spherical cavity is compared to two other estimates of the source function for fully coupled explosions in salt.

The Mueller/Murphy source function (Mueller and Murphy, 1971) is based on a fit to the SALMON data. Therefore, it can be taken to represent our empirical experience in this material. The S^3 source function 255 was computed with one-dimensional finite difference methods for a tamped explosion at a depth of 500 meters and is described by Bache, Cherry and Mason (1976c). It represents computational results for explosions in this material.

As far as the spherically symmetric portion of the field is concerned, we find that the spherical cavity is slightly more decoupled (20 to 25 percent) than the elliptical cavity. The higher order terms increase the radiation from the latter, increasing the decoupling difference between the two. Comparing other estimates for the source function for a tamped explosion in salt, we find decoupling factors ranging from 300 at long period to less than 100 at frequencies greater than 3 Hz.

Using the equivalent elastic source representation, body and surface wave synthetic seismograms were computed for the two sources. While changing interference between the direct P, pP and sP phases can lead to minor variations in m_b and the waveforms, we conclude that radiation pattern

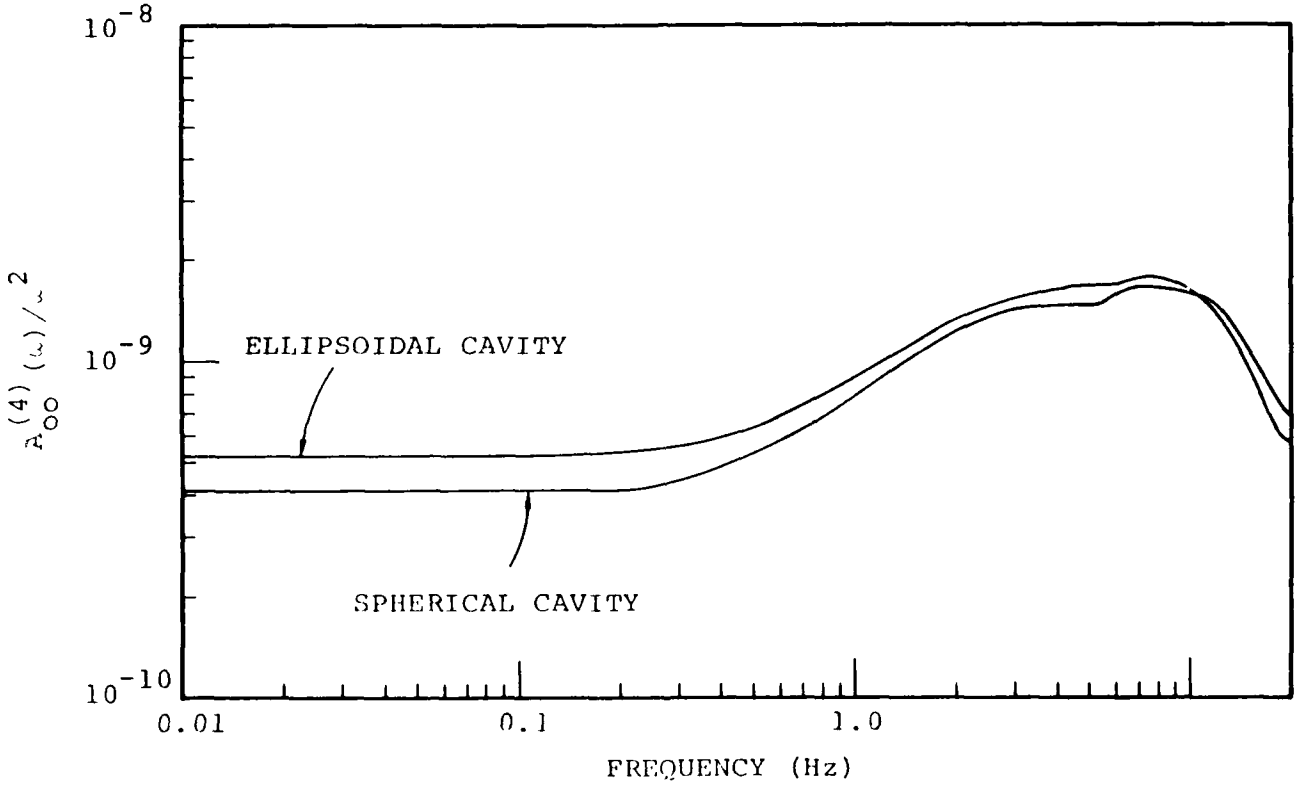

Figure 32. The normalized monopole terms are compared for the two source calculations.

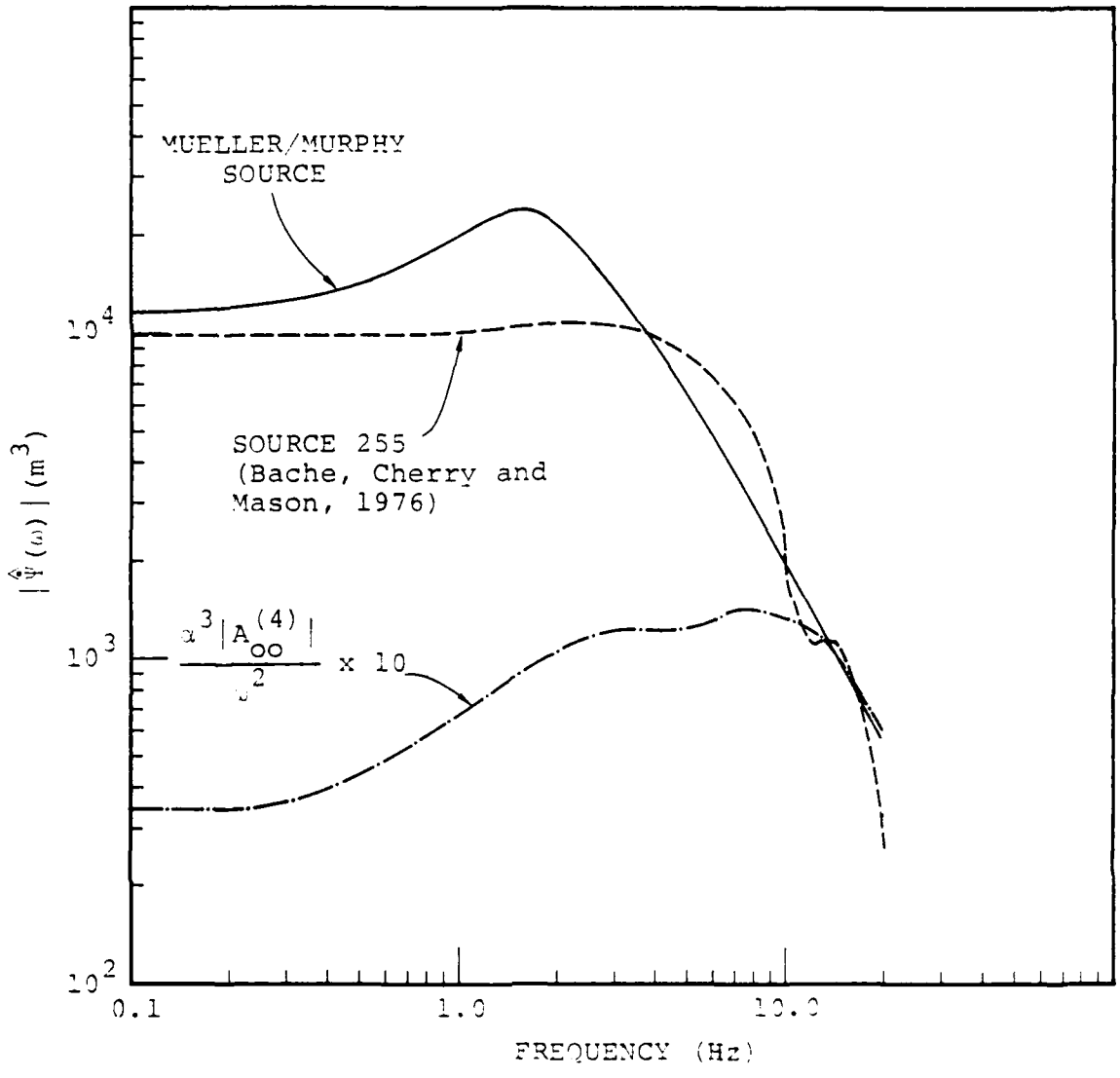

Decoupling Factors

Frequency	Mueller/Murphy Source	Source 255
0.1	325	282
0.5	310	220
1.0	298	151
3.0	114	86
5.0	52	67
10.0	14	16
20.0	9	6

Figure 33. The source function from Figure 32 is compared to two estimates for the source function for a fully coupled explosion in salt. The decoupling factors implied by each of the fully coupled sources are listed for several frequencies

effects are unimportant for short period body waves and m_b. That is, the m_b for the ellipsoidal cavity is not substantially different than that for the spherically symmetric cavity. For surface waves, the results are very much the same. It is true that the ellipsoidal cavity will generate Love waves. However, the Rayleigh wave radiation patterns do not differ substantially from the spherically symmetric case. These conclusions are based on a series of calculations assuming the largest reasonable contribution from the S wave portion of the field and rotating the source to orientations expected to give optimum radiation pattern effects.

6.2 NEAR-FIELD INSTRUMENTATION TO DETERMINE THE EQUIVALENT ELASTIC SOURCE FOR UNDERGROUND NUCLEAR EXPLOSIONS

Our objective is to summarize our thinking about the best way to instrument underground explosions to measure the equivalent elastic source. The ideal situation would allow direct measurement of the reduced displacement potential (RDP). This measured source could then be used in the propagation codes to really pin down the path effects. However, the near-field data collected to date require the application of some theory to deduce the RDP and ambiguity is inevitably introduced.

As we shall explicate more fully below, we believe it is almost impossible to directly measure the RDP, so we can never entirely dispense with the need to resort to some theoretical interpretation. The realistic goal is to achieve a situation in which the interpretation can be done with great confidence.

Let us assume that adequate technology exists to recover the true ground motions. The problem is then to select the best locations for the gauges. The factors that make it difficult to measure the RDP (more properly, to measure a complete radial velocity time history that can be converted

to RDP) arise from the departure of the shot medium from the environment in which the RDP solution is valid; i.e., a homogeneous, isotropic, elastic wholespace. These factors may be divided into the following categories:

1. Elastic effects due to the presence of the free surface.
2. Elastic effects due to the departure from homogeneity.
    a. Elastic reflections from material interfaces.
    b. Material property variations between the explosion and the gauge locations.
3. Inelastic effects.
    a. The gauges must be outside the "elastic radius" which may be difficult to estimate.
    b. Strong signals due to spall closure may contaminate the records.
4. Departure of the source from spherical symmetry.
    a. Asymmetries in the highly stressed region near the source can cause the source to have a substantial quadrupole component.
    b. Tectonic strain release can add a large double-couple component to the source.

We will discuss each of these factors to point out the constraints they place on selection of the gauge locations.

Elastic Free Surface Effects

Computational techniques are now available to compute the exact elastic near-field response for stationary or propagating point sources in layered elastic media. To our knowledge, these techniques have not been applied to see how well they can explain anomalies in the data from past experiments. SALMON seems to be an excellent event to study in this context and we hope to get a chance to look at it.

To demonstrate the free surface effect, we did the problem illustrated in Figure 34. The vertical, horizontal and radial velocities and displacements were computed at twelve stations for a center of dilatation explosion source in a halfspace. The geometry and elastic properties of the material are close to those for PILEDRIVER. The source time history is that given by Bache, et al. (1975) for PILEDRIVER. The details of this source function will be discussed under "Inelastic Effects".

In Figures 35 through 37 the computed halfspace ground motions are compared to the same motions when the free surface is ignored. There are three arrivals on each record, P, pP and pS and these are indicated by arrows at the geometric arrival time for the peak velocity. The near-field terms have a large contribution and cannot be ignored. Perhaps the most important near-field effect is that the free surface reflection coefficients are frequency-dependent; the shape of the pP and pS wavelets can differ substantially from that of P.

For this example the source time duration is long compared to the delay time for the surface reflected phases and the phasing between arrivals is smoothed. If the source were scaled to a different yield, the pulse shapes would be somewhat different. However, the trends would be unchanged. This is illustrated by the examples shown in Figure 38. For the nearly vertical ray the calculations were repeated with the source yield scaled to be 27 times smaller. With the higher frequency source the individual phase arrivals are more easily distinguished on the records.

The radial velocities in Figure 37 can be integrated to determine the apparent RDP that would be found if the influence of the free surface were ignored. The RDP and its derivative, the RVP (reduced velocity potential), are compared to the RDP and RVP for the spherically symmetric source in Figure 39. The format of the plots is changed to permit

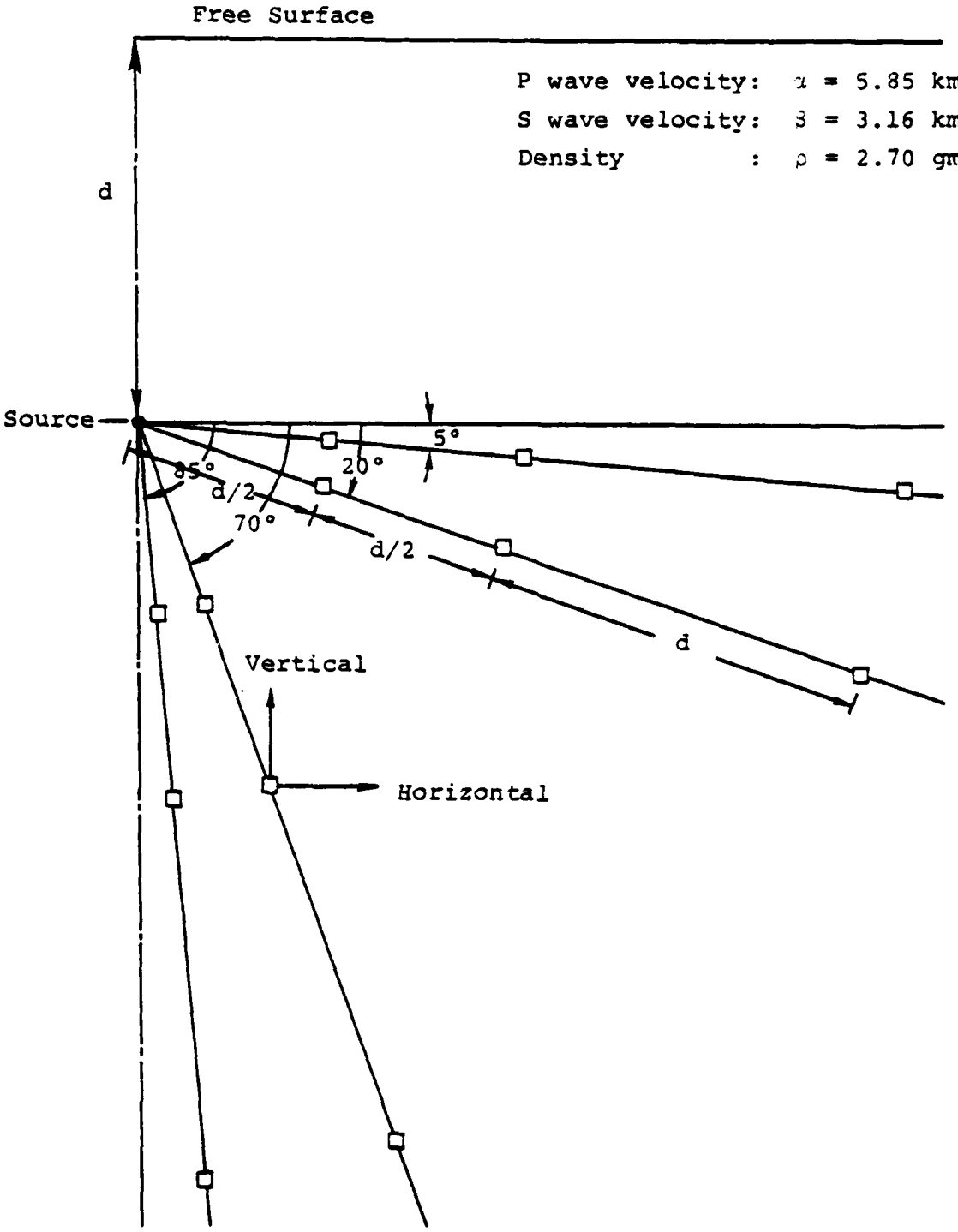

Figure 34. The geometry for the calculations of Figures 35-39 is illustrated schematically. Vertical, horizontal and radial velocities and displacements were computed at the twelve stations shown. The stations were at three ranges along four radial lines from the source. The source RDP is appropriate for PILEDRIVER and the depth d = 450 meters.

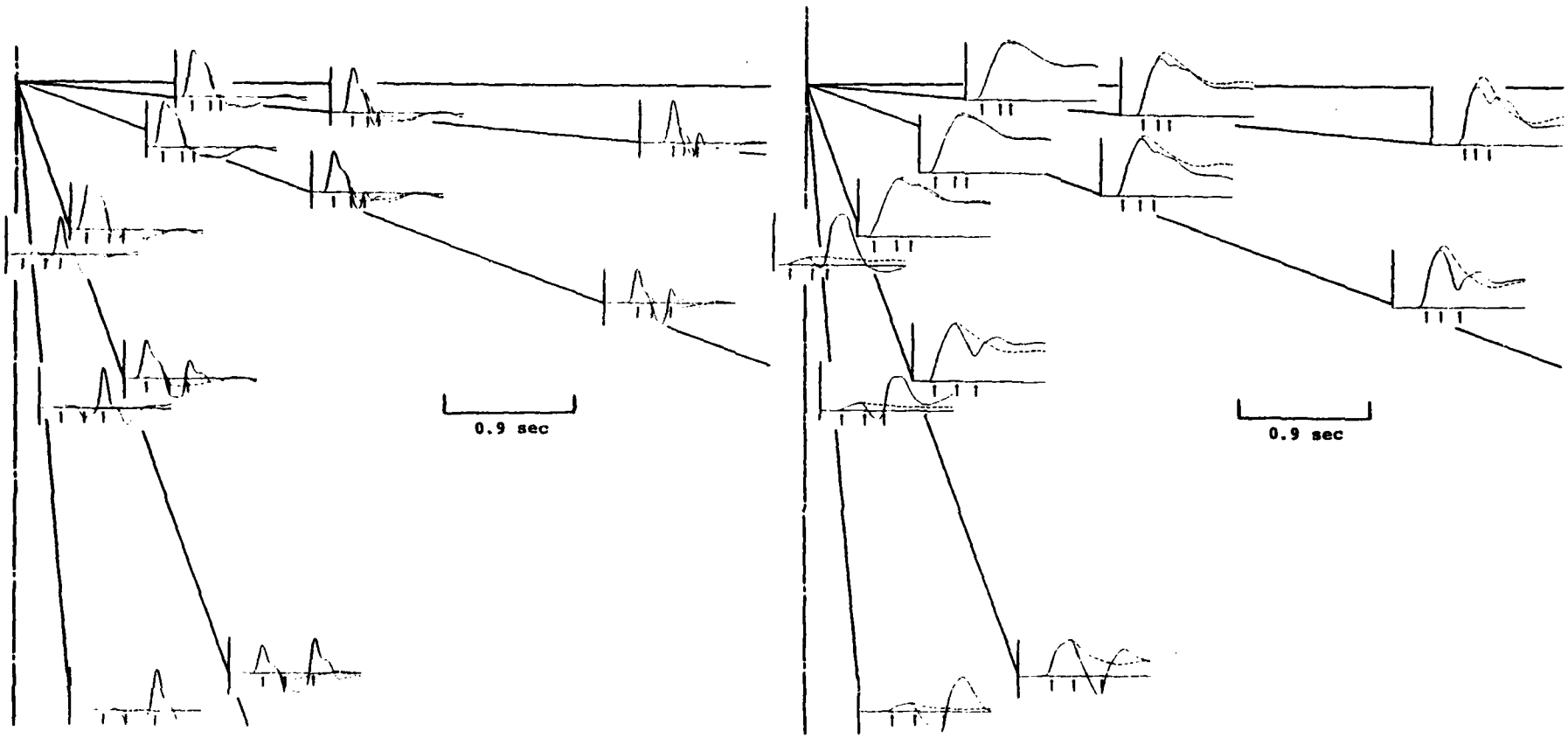

VELOCITY

DISPLACEMENT

Figure 35. Horizontal ground motions are plotted. The wholespace solution is the dashed line. The arrival times for the P, pP and pS phases are indicated by arrows at the geometric arrival time for the peak velocity.

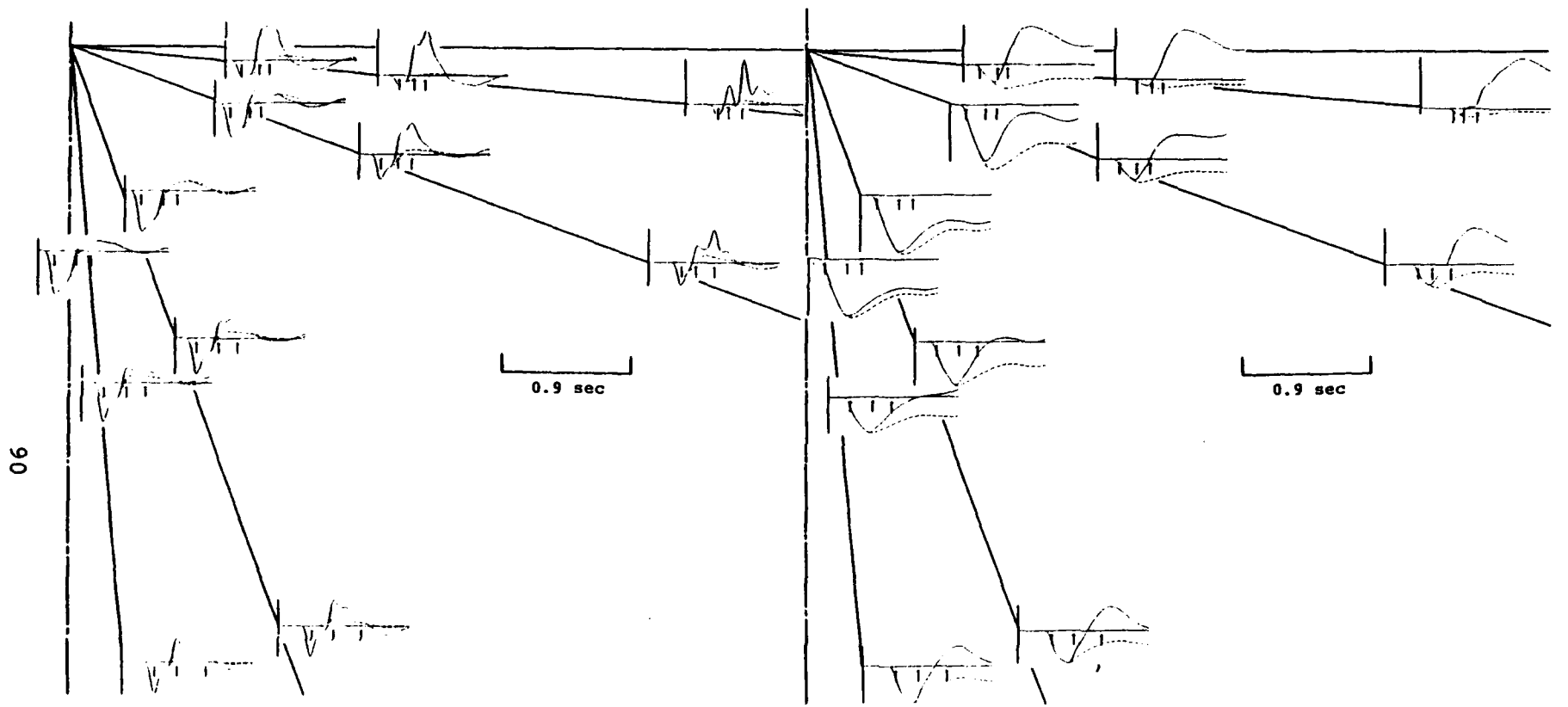

VELOCITY DISPLACEMENT

Figure 36. Vertical ground motions are plotted.

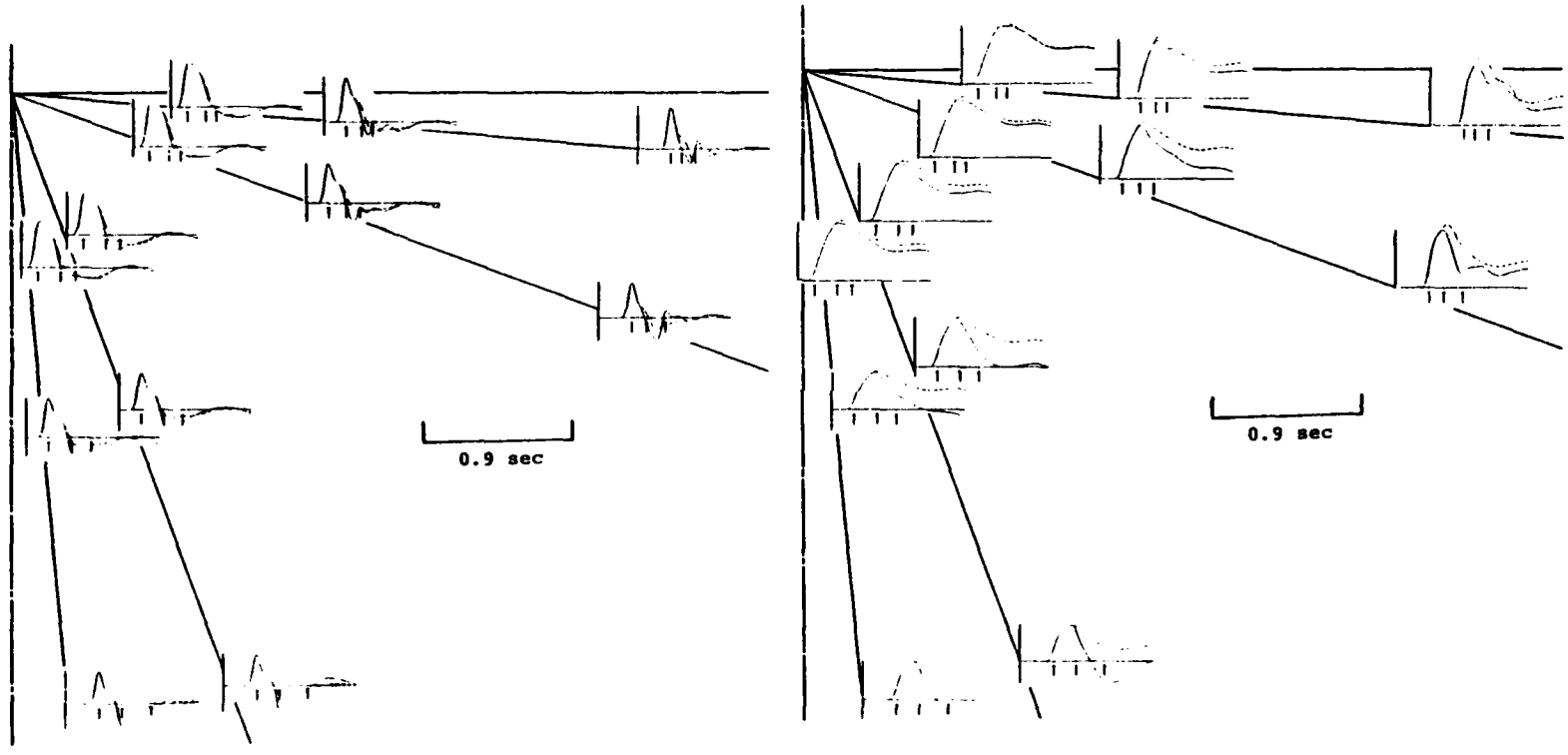

VELOCITY DISPLACEMENT

Figure 37. Radial ground motions are plotted.

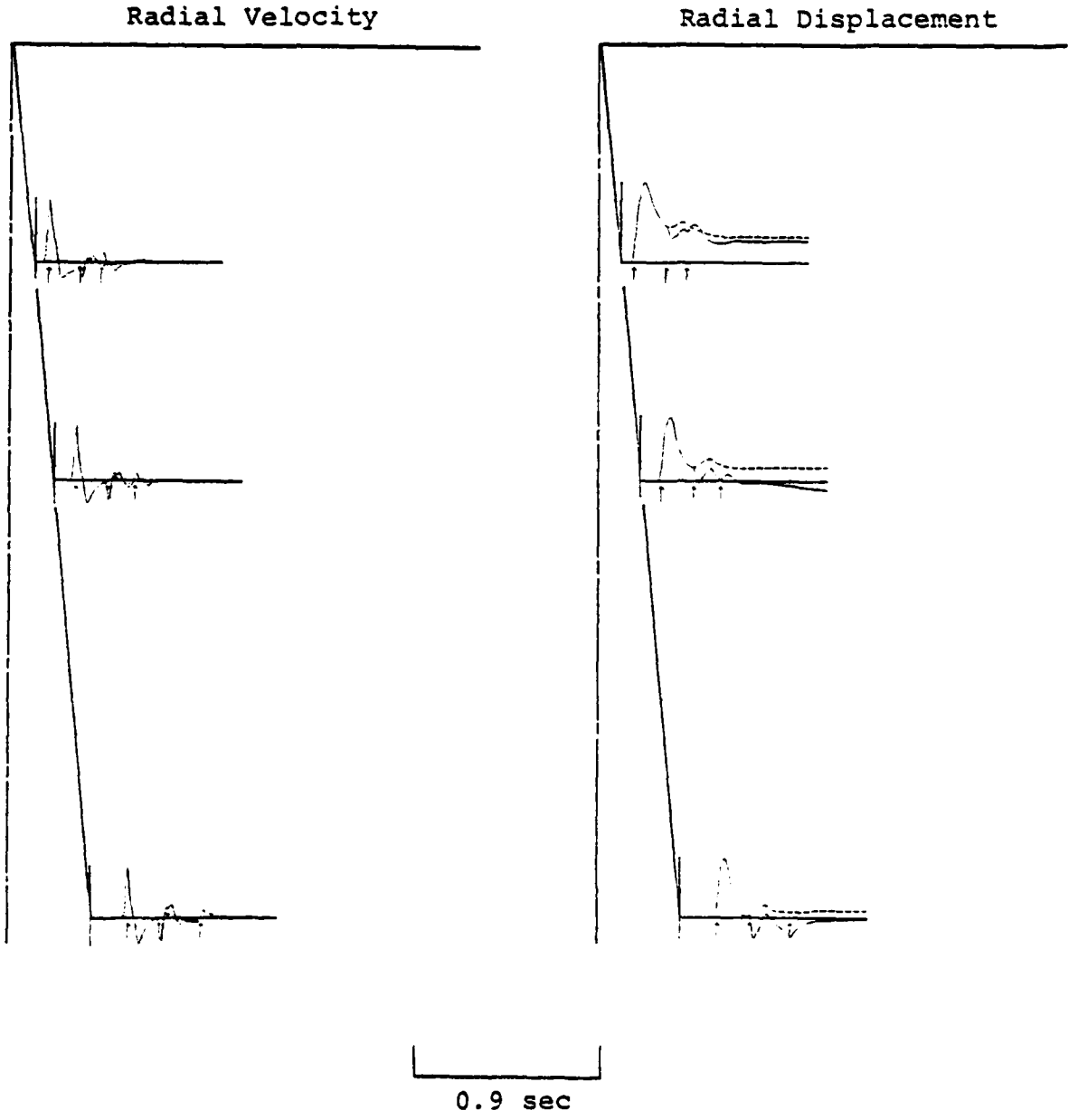

Figure 38. The radial velocity and displacement along the nearly vertical ray for a source with the yield a factor of 27 smaller than that used for Figures 35 through 37.

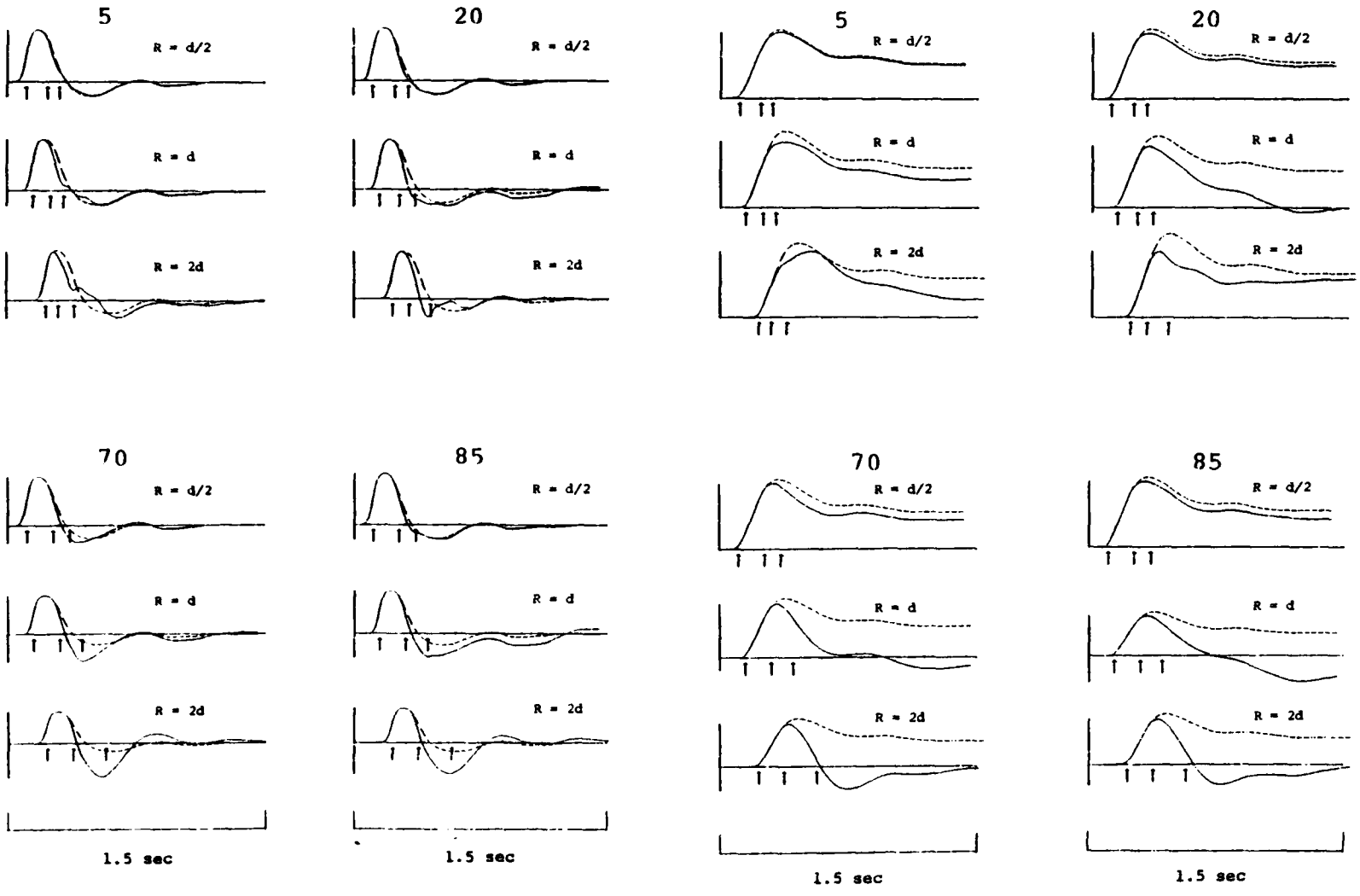

Figure 39. Reduced velocity potential (left) and reduced displacement potential computed from the velocity records of Figure 37.

longer time histories to appear. The plots are again arranged along four rays at three ranges. The takeoff angle in the sense indicated in Figure 34 is shown with each set of three plots.

The comparisons in Figures 35 through 37 clearly indicate that radial measurements along the horizontal and as close as possible to the shot point are good for minimizing the contribution of the free surface phases. The reason is, of course, that the particle motion of the free surface reflected phases is most nearly vertical at such locations.

Vertical gauges directly below the shot and at close range are not too badly affected by the free surface contribution. Here we are taking advantage of the much longer travel path for the reflected waves. However, at greater ranges below the shot the free surface effects become quite prominant, especially at the longer periods.

Elastic Effects Due to Material Inhomogeneity

While the free surface is the most important elastic reflector, we must also be concerned about elastic reflections from other material interfaces. Some time ago (Bache, et al., 1976a) we estimated the effect of the free surface and the near-surface weathered layers on the motions at two of the best PILEDRIVER gauges. The geometry for these calculations is shown in Figure 40. The same source used in the halfspace calculations of Figures 35 through 37 was used.

In Figure 41 the radial displacement and velocity for the layered halfspace are compared to the wholespace ground motions. Comparing to the records from stations at about the same range in Figure 37, we see that the layering has only a minor effect. This is largely due to the source duration being long compared to the differential phase arrival times from the various layers. For a higher frequency signal the

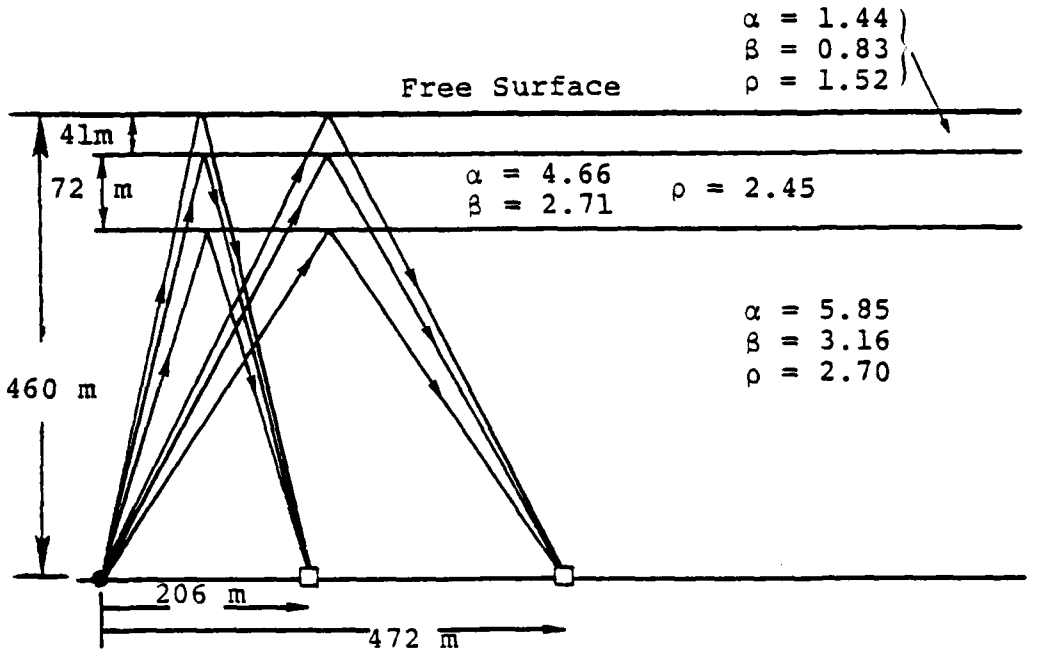

Figure 40. The geometry for the calculations of Figure 41 is illustrated schematically. For computational convenience, the stations were actually located 10 meters below the horizontal line. A total of 43 rays were computed for each seismogram. These are the rays shown with all possible P-S and S-P conversions included. Internal reflections were not included but numerical tests showed these to be small.

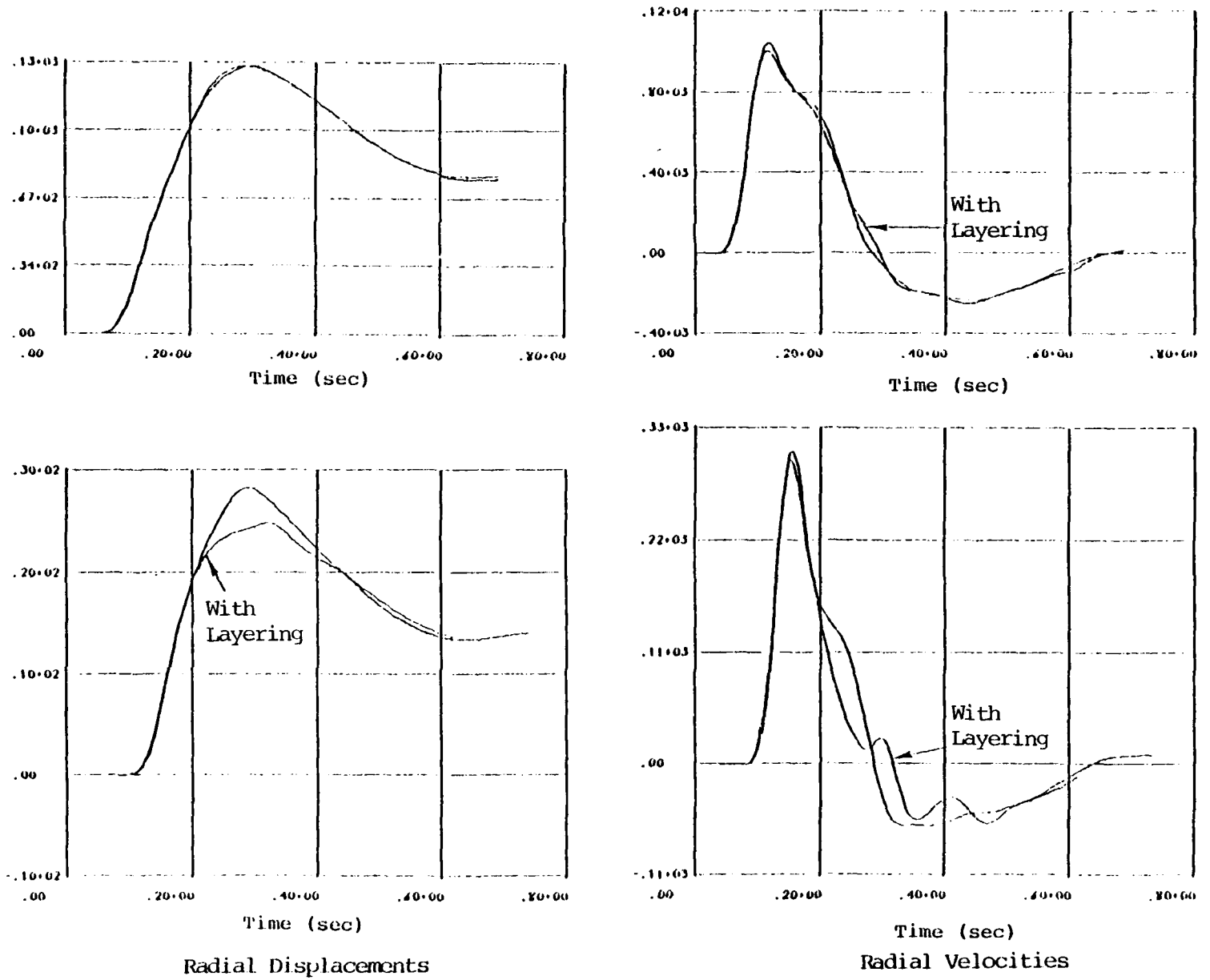

Figure 41. The radial displacements (c.n) and velocities (cm/sec) for an elastic source in a wholespace are compared to those for the same sources in the geometry of Figure 40.

separate arrivals would be apparent. For example, Murphy (1978) convincingly identifies an arrival from the salt-anhydrite interface on one of the SALMON accelerograms. The period of this arrival is about 0.01 seconds.

Before leaving this subject, we should point out that the calculations we have done have been in plane-layered media. However, it is possible to relax this restriction and handle non-planar layers if necessary.

The second subject listed under this category was the effect of material property variations between the source and the gauge locations. By this we mean gradual changes not identified with any material interface. The most likely situation would be the presence of some ambiguity in the elastic P wave velocity which is used to derive the RDP from the recorded velocity history. As long as the range of uncertainty is not too large, the effect is not great and is restricted to the higher frequencies. Murphy (1978, Figures 3-9) gives an example of an RDP calculated with two different velocities. His results are reproduced as Figure 42. Note that the static value is independent of velocity ($\Psi_\infty = R^2 U_\infty$).

Inelastic Effects

To compute an accurate RDP it is necessary that the ground motions be measured outside the elastic radius. Correcting for inelastic material behavior would be very difficult. The PILEDRIVER source calculation used in the elastic calculations described above provides a useful example of the effect of inelasticity.

The elastic radius for the PILEDRIVER calculation is about 650 meters. This is controlled by the maximum radius at which tension cracks open in the prefractured material model used in the calculation. The computed peak radial stress at this range is only about 450 bars. The maximum

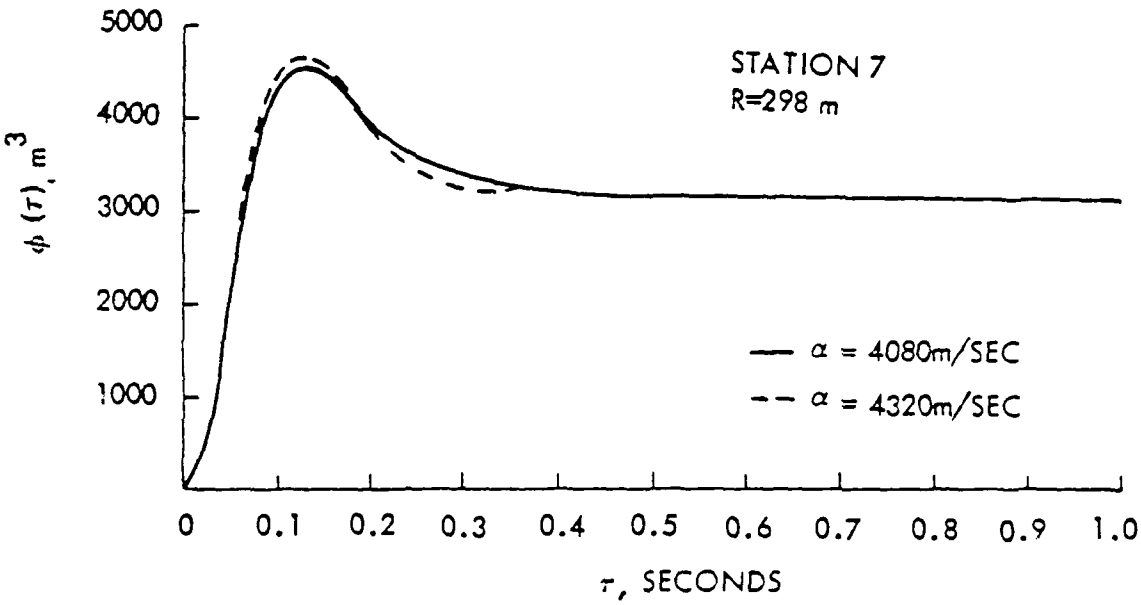

Figure 42. Observed gnome reduced displacement potential, station 7.

radius for material yielding, which occurs at stresses of several kbars, is much smaller, perhaps only a few hundred meters.

In Figure 43 we compare the computed and measured radial velocity time histories at ranges of 204 and 472 meters. The computed velocities were monitored in the inelastic regime in the one-dimensional source calculation. In Figure 41 are plotted the wholespace velocity histories computed elastically at the same ranges from the RDP. Comparing the computed wholespace velocities in Figure 41 and 43, we can see the theoretical effect of the inelasticity. For example, the peak velocity in the inelastic regime is about 580 m/sec at 472 meters. The RDP source has a peak velocity of about 300 m/sec which is only half as large. At the range of 201 m the inelastic peak velocity/RDP peak velocity ratio is about 3350/1030. As might be expected, the displacements in the inelastic regime in the calculation are much larger. This example suggests that RDP's computed from measured velocities inside the elastic radius would probably over-estimate the true RDP.

The second subject listed under this category was the effect of signals arising from spall closure. To our knowledge, signals due to this phenomena have not been identified on records at depth. It would be very interesting to see them.

Stress waves arising from spall closure should mainly affect the vertical component records. This is a reason for preferring to measure the ground motions parallel to the surface.

Departure of the Source from Spherical Symmetry

There are two kinds of source asymmetries that we know something about. One is due to asymmetries in the source region and results in a partitioning of the source energy

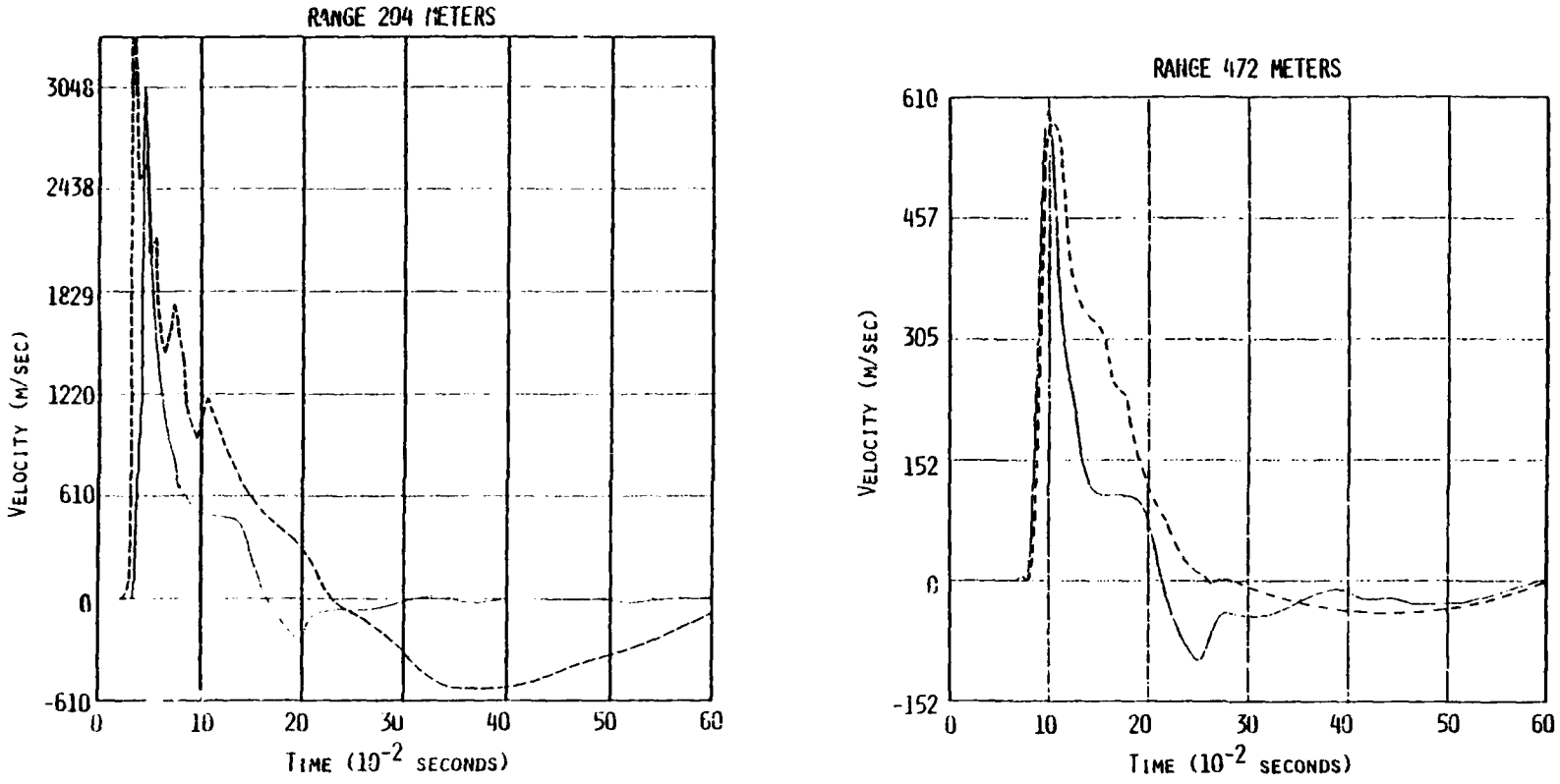

Figure 43. The measured radial velocity time histories (dashed lines) from two PILEDRIVER stations are compared to computed velocities monitored at the appropriate ranges in a one-dimensional source calculation. The computed material response at these ranges is nonlinear due to the opening of tension cracks in the prefractured material model.

between the center of dilatation and higher order terms. The second is due to tectonic strain release and adds to the total source energy. Since we would like to measure the entire equivalent elastic source, the extent to which these asymmetric components are present is an important question. However, just as important is the ability to separate the constituent parts of the composite source since they scale differently. There seems to be no real good way to do this except by collecting a lot of data offering good azimuthal coverage and then interpreting these data with a good theory.

Summary and Conclusions

- The most important requirement for measuring the RDP is probably that the gauges be outside the elastic radius. It is not easy to estimate the elastic radius preshot, and we would have to rely on calculations to do so. Proof that the gauges did record elastic motions is that the same RDP is recorded at different ranges along the same ray.

- Radial component gauges at shot depths are advantageous because they minimize the contribution of free surface reflected phases and spall closure phases which are expected to be larger on the vertical.

- There is an inherent conflict between the requirement to increase the source-receiver range to be certain to be outside the elastic radius and the desire to be closer to the source to minimize the propagation effects.

- Gauges vertically below the event may be attractive because the free surface effects may be accounted for relatively easily. However, the gauges would have to be very deep to be elastic and to include different ranges to verify the RDP.

- A key parameter is the ratio of elastic radius to shot depth. The advantages of the elastic radius being less than the depth include the following:

  a. Radial gauges could be placed along the horizontal at ranges less than the depth. In this case particle motion is mostly vertical for the reflected waves.

b. Spallation would be minimized.

c. The ratio of the source pulse duration to the lag time between phase arrivals would probably be smaller than in our examples, allowing more confident identification of separate phases.

- There is excellent gauge location we have not yet mentioned that is attractive if the shot is greatly overburied. If the material response directly above the shot is elastic and almost no spallation occurs, the RDP can be determined from a ground zero gauge. This is how we recovered the RDP in our grout block experiments (Cherry, et al., 1977). However, we would have to deal with the fact that the material properties are generally quite variable between source and surface.

- In order to account for any source asymmetries that might be present, it is necessary to have an adequate sample of the radiation pattern. The data must be interpreted with a theory that accounts for this possibility. It is necessary to record all three components of motion.

Recommendations

- The experiment should be greatly overburied, but still have a large enough yield to be well recorded teleseismically. The greater the scaled depth, the greater the possibility that the amplitude of pP could be estimated from the teleseismic body waves which would help in the interpretation. Also, spallation can be reduced or eliminated by increasing the scaled depth.

- Attempts should be made to site the event in as nearly homogeneous a material as possible.

- Preshot calculations should be made to estimate the elastic radius.

- Gauges should be placed at several ranges outside the estimated elastic radius on several radial lines at shot depth. Three components of motion should be recorded.

- The data should be analyzed with exact near-field propagation codes and theories capable of representing non-spherically symmetric source components should be used.

- The analysis should take into account the far-field body and surface wave data.

REFERENCES

Archambeau, C. G., D. G. Harkrider and D. V. Helmberger (1974), "Studies of Multiple Seismic Events," California Institute of Technology, Final Report prepared for U. S. Arms Control and Disarmament Agency.

Bache, T. C. and J. F. Masso (1978), "Analysis of Two Decoupled Explosion Simulations," Systems, Science and Software Topical Report submitted to ARPA/VSC, SSS-R-78-3627, April.

Bache, T. C., W. L. Rodi and D. G. Harkrider (1978), "Crustal Structures Inferred from Rayleigh Wave Signatures of NTS Explosions," BSSA, 68, 1399-1413.

Bache, T. C., J. F. Masso and B. F. Mason (1977), "Theoretical Body and Surface Wave Amplitudes for Twelve Numerically Simulated Cratering Explosions," Systems, Science and Software Technical Report, SSS-R-77-3119, January.

T. C. Bache, T. G. Barker, J. T. Cherry, N. Rimer and J. M. Savino (1976a), "Explosion Source Modeling, Seismic Waveform Analysis and Yield Verification Research," Systems, Science and Software Quarterly Technical Report submitted to ARPA/VSC, SSS-R-76-2924, May.

Bache, T. C., J. T. Cherry, D. G. Lambert, J. F. Masso and J. M. Savino (1976b), "A Deterministic Methodology for Discriminating Between Earthquake and Underground Nuclear Explosions," Systems, Science and Software Final Technical Report submitted to ARPA/AFOSR, SSS-R-76-2925, July.

Bache, T. C., J. T. Cherry and B. F. Mason (1976c), "The Dependence of Body Wave Magnitude on Yield for Underground Explosions in Salt," Systems, Science and Software Technical Report, SSS-R-77-3119, January.

Bache, T. C., J. T. Cherry, N. Rimer, J. M. Savino, T. R. Blake, T. G. Barker and D. G. Lambert (1975), "An Explanation of the Relative Amplitudes Generated by Explosions in Different Test Areas at NTS," Systems, Science and Software Final Report to the Defense Nuclear Agency, DNA 3958F, October.

Barker, T. B. (1976), "Calculation of the Effects of Layered Geology on Near-Field Ground Motions Using a Hybrid Finite Difference/Linear Elastic Code for the NYS MIGHTY EPIC Event," Systems, Science and Software Topical Report submitted to the Defense Nuclear Agency, SSS-R-76-2914, May.

Burridge, R. and L. Knopoff (1964), "Body Force Equivalent for Seismic Dislocation," BSSA, 54, 1875-1888.

Cherry, J. T., T. G. Barker, S. M. Day and P. L. Coleman (1977), "Seismic Ground Motion from Free-Field and Underburied Explosive Sources," Systems, Science and Software Final Contract Report submitted to ARPA/VSC, SSS-R-76-3349, July.

Cherry, J. T., T. C. Bache, W. O. Wray and J. F. Masso (1976), "Teleseismic Coupling from the Simultaneous Detonation of an Array of Nuclear Explosions," Systems, Science and Software Technical Report, SSS-R-76-2865, February.

Cherry, J. T., T. C. Bache and W. O. Wray (1975a), "Teleseismic Ground Motion from Multiple Underground Nuclear Explosions," Systems, Science and Software Technical Report submitted to AFOSR, SSS-R-75-2709, September.

Cherry, J. T. N. Rimer and W. O. Wray (1975b), "Seismic Coupling from a Nuclear Explosion: The Dependence of the Reduced Displacement Potential on the Nonlinear Behavior of the Near Source Rock Environment," Systems, Science and Software Technical Report submitted to AFTAC/VSC, SSS-R-76-2742, September.

Clayton, R. and B. Engquist (1977), "Absorbing Boundary Conditions for Acoustic and Elastic Wave Equations," BSSA, 67, 1529-1540.

Cleary, J. and A. L. Hales (1966), "An Analysis of the Travel Times of P Waves to North American Stations in the Distance Range 32 to 100," BSSA, 56, 147-489.

Engquist, B. and A. Majda (1977), "Absorbing Boundary Conditions for Numerical Simulation of Waves," Proc. Natl. Acad. Sci. U.S.A., 74, 1765-1766.

Harkrider, D. G. (1964), "Surface Waves in Multilayered Media I. Rayleigh and Love Waves from Buried Sources in a Multilayered Elastic Half-Space," BSSA, 54, 627-679.

Heard, H. C., E. A. Abey, B. P. Bonner and A. Duba (1975), "Stress-Strain Behavior of Polycrystaline NaCl to 3.2 GPa," Lawrence Livermore Laboratory Report UCRL-51743.

Kostrov, B. V. (1964), "Self-Similar Problems of Propagation of Shear Cracks," J. Appl. Math. Mech., 28, 1077-1087.

Laird, D. H. (1976), "A Chemical Equilibrium Equation of State for Saturated Tuff," Systems, Science and Software Topical Report SSS-R-75-2740.

Lambert, D. G. and T. C. Bache (1977), "Identification of Individual Events in a Multiple Explosion from Teleseismic Short Period Body Wave Recordings," Systems, Science and Software Technical Report, SSS-R-78-3421, October.

Lambert, D. G., T. C. Bache and J. M. Savino (1977), "Simulation and Decomposition of Multiple Explosions," Systems, Science and Software Topical Report submitted to AFTAC/VSC, SSS-R-77-3194, June.

Lee, W. H. K. and S. Uyeda (1965), "Review of Heat Flow Data," in Terrestrial Heat Flow, Geophysical Monograph No. 8, American Geophysical Union.

Molnar, P. and J. Oliver (1969), "Lateral Variations of Attenuation in the Upper Mantle and Discontinuities in the Lithosphere," JGR, 74, 2648-2682.

Mueller, R. A. and J. R. Murphy (1971), "Seismic Characteristics of Underground Nuclear Detonations," BSSA, 61.

Murphy, J. R. (1978), "A Review of Available Free-Field Seismic Data from Underground Nuclear Explosions in Salt and Granite," Computer Sciences Corporation Report CSC-TR-78-0003.

Murphy, J. R. (1977), "Seismic Coupling and Magnitude/Yield Relations for Underground Nuclear Detonations in Salt, Grainite, Tuff/Rhyolite and Shale Emplacement Media," Computer Sciences Corporation Technical Report CSC-TR-77-0004, December.

North, R. G. (1977), "Station Magnitude Bias - Its Determination, Causes and Effects," Technical Note 1977-24 Lincoln Laboratory, M.I.T. ESD-TR-77-85, April.

Perett, W. R. (1968), "Free Field Ground Motions in Granite," Operation Flintlock, Shot PILEDRIVER," DASA POR-4001.

Pratt, H. R. (1978), Private Communication.

Pyatt, K. D. (1966), "Nuclear Explosion Interaction Studies Vol. II, Methods for Analysis of Thermal Phenomena," General Atomic Final Report GA-737, AFWL-TR-66-108.

Pyatt, K. D. and J. C. Baker (1978), Private Communication.

Rodi, W. L., J. M. Savino, T. G. Barker, S. M. Day and T. C. Bache (1978), "Analysis of Explosion Generated Surface Waves in Africa, Results from the Discrimination Experiment and Summary of Current Research," Systems, Science and Software Quarterly Technical Report, SSS-R-78-3653, April.

Savino, J. M., T. C. Bache, J. T. Cherry, K. G. Hamilton, D. G. Lambert and J. F. Masso (1975), "Application of Advanced Methods for Identification and Detection of Nuclear Explosions from the Asian Continent," Systems, Science and Software Semi-Annual Technical Report submitted to AFOSR, SSS-R-76-2792, December.

Savino, J. M. and C. B. Archambeau (1974), "Discrimination of Earthquakes from Single and Multiple Explosions Using Spectrally Defined Event Madnitudes," Trans. Amer. Geophys. Union, EOS (Abstract), 56, 1148.

Sobel, P. A. (1978), "The Effects of Spall on m_b and M_s," Unpublished Teledyne Geotech Report.

Toksoz, M. N. and H. H. Kehrer (1972), "Tectonic Strain Release by Underground Nuclear Explosions and Its Effects on Seismic Discrimination," Geophys. J., 31, 141-161.

Viecelli, J. A. (1973), "Spallation and the Generation of Surface Waves by an Underground Explosion," JGR, 78, 2475-2487.

APPENDIX A

ABSTRACTS OF TECHNICAL REPORTS SUBMITTED TO AFTAC/VSC MAY 1975 - AUGUST 1978

A.1 QUARTERLY REPORTS

- August 1975, "Improved Yield Determination and Event Identification Research," J. T. Cherry, N. Rimer, J. M. Savino and W. O. Wray, SSS-R-75-2696, 28 pages.

A one-dimensional parameter study which identifies the dependence of teleseismic magnitude on near source material properties was carried out. The major results of the material parameter sensitivity study may be summarized as follows: (1) increasing the air-filled porosity greatly reduces seismic coupling; (2) if any parameter describing the yield surface is varied such that the material strength is reduced, seismic coupling may be substantially enhanced; (3) seismic coupling is relatively insensitive to water content; a slight decoupling is observed with increasing water content; (4) increasing the overburden pressure substantially reduces seismic coupling.

The near-field coupling and the equivalent source were computed for the recent underground explosion, MAST, at Pahute Mesa. The next step is to generate synthetic seismograms for this event at recently specified receiver locations. The enhanced computational capabilities for treating realistic earth structures will be exercised in this experiment.

- November 1975, "Improved Yield Determination and Event Identification Research," J. M. Savino, T. C. Bache, T. G. Barker, J. T. Cherry and W. O. Wray, SSS-R-76-2788, 42 pages.

Telesesimic ground motion predictions for the recent Pahute Mesa explosion, MAST, were quite successful in terms

of both amplitude and waveform matching. The predicted short-period body wave amplitudes were within 30 to 50 percent of the observed amplitudes at most of the SDCS stations. In addition, the general character of the first few seconds of the P wavetrains at the various SDCS stations were matched in reasonable detail.

A tension failure model that describes the development of a region of enhanced tension failure (cracking) produced during stress release behind the interacting shock fronts from closely spaced explosions was developed. Calculations for a multiple explosion scenario (three closely spaced explosions detonated simultaneously) were carried out into the elastic region using the two-dimensional CRAM code with the new material failure model included.

- February 1976, "Improved Yield Determination and Event Identification Research," J. M. Savino, SSS-R-76-2870, 64 pages.

Comparison of computed and observed short and long period seismograms for the Pahute Mesa explosion, MAST, were made with respect to amplitude, waveform and travel times. Travel times were closely matched as were the waveforms for surface waves recorded at the SDCS stations. For body waves a number of the SDCS stations are within the triplication range and the waveform match was far from ideal. Still, amplitudes for both body and surface waves were matched to within 50 percent and were much closer in most cases.

- May 1976, "Explosion Source Modeling, Seismic Waveform Prediction and Yield Verification Research," T. C. Bache, T. G. Barker, J. T. Cherry, N. Rimer and J. M. Savino, SSS-R-76-2924, 54 pages.

The theoretically computed and observed amplitudes of both b and d (maximum) body wave phases for KASSERI agree to

well within a factor of two at all of the five SDCS stations. Minor adjustments of the upper mantle model could improve the agreement at all the SDCS sites.

Computations of the effect of material strength on teleseismic body wave amplitudes indicate that the amplitude of the b phase increases with decreasing strength; the rate of increase being more rapid at lower levels of material strength. An additional effect is that the apparent period of the b phase increases rapidly with decreasing strength due to a shift in the corner frequency of the source spectrum.

Further verification of the explosion source modeling code, SKIPPER, was achieved by comparison of free-field ground motion calculations and observations for the PILEDRIVER and GASBUGGY explosions. In the case of PILEDRIVER, the exercise of a recently developed elastic wave propagation code verified that the observed PILEDRIVER RDP was not affected by reflected waves from the free surface or from layer interfaces in the source region.

Excellent free-field ground motion measurements and material properties data are available for the GASBUGGY explosion. The computed RDP, employing these data, agrees quite well with the measured RDP, increasing our confidence in the constitutive modeling of the explosion source and ultimately the teleseismic ground motion predictions based on these source calculations.

- August 1976, "Explosion Yield Verification, Multiple Explosion Scenarios and Three-Dimensional Seismic Modeling Research," D. G. Lambert, C. F. Petersen and J. M. Savino, SSS-R-76-2993, 46 pages.

A procedure for directly inverting teleseismic ground motion data in order to obtain estimates of explosion yields was developed. The particular inversion scheme employes a

a deterministic modeling capability which predicts the teleseismic ground motion from a nuclear explosion. This procedure supplements expected data exchange packages that provide information on the near explosion source environment.

Experiments involving computer simulation and decomposition of multiple explosion scenarios were recently initiated. Application of narrow-band filtering to synthesized multiple event seismograms has yielded accurate determinations of the relative amplitudes and time separations between individual explosions in the multiple explosion event examined.

Preparations are nearing completion for a series of three-dimensional seismic modeling experiments. The intent of these experiments is to measure differences in signals between single and multiple sources and between near surface and deeply buried sources. Theoretical explosion calculations will be compared to the experimental results.

- January 1977, "Seismic Studies for Improved Yield Determination," T. C. Bache, J. M. Savino, M. Baker and P. L. Coleman, SSS-R-77-3108, 80 pages.

The report summarizes the results of the first three months of research on a contract whose main objective is to examine the parameters that affect the seismic signals from underground explosions. Results are presented from research in five areas: (1) theoretical teleseismic magnitudes (M_s and m_b) were determined for a series of nuclear explosion cratering calculations carried out by Applied Theory, Inc.; (2) the relative frequency content of signals from U.S.S.R. and U. S. explosions were studied by comparing the periods of the first few cycles of recordings from several stations at teleseismic ranges; (3) some improved techniques were developed for computing the equivalent point source representation for explosions in highly porous materials; (4) the dependence of body wave magnitude on yield for underground

explosions in salt was studied and compared to that for explosions in granite; (5) small scale experiments were carried out in which underground explosions were modeled by 0.25 gram charges embedded in concrete.

- April 1977, "Seismic Studies for Improved Yield Determination," T. G. Barker, M. Baker, P. Coleman, and D. G. Lambert, SSS-R-77-3191, 48 pages.

The report summarizes the results of the second three months of research on a contract whose main objective is to examine the parameters that effect the seismic signals from underground nuclear explosions. Results were presented on research in five areas: (1) data pertinent to regional bias in m_b and M_s in the United States and central Asia were summarized; (2) signals simulating those from multiple explosions were decomposed and scaled by narrow-band filtering methods; (3) numerical simulations of contained explosions were compared with previous laboratory simulations; (4) laboratory experiments of cratering explosions were completed using 0.25 gram charges embedded in concrete; (5) the primary factors controlling amplitude-yield scaling at regional distances were investigated.

- July 1977, "Seismic Studies for Improved Yield Determination," T. C. Bache, P. L. Goupillaud and B. F. Mason, SSS-R-77-3345, 65 pages.

Results are presented from research conducted during the quarter from April to June 1977. Work in three research areas is discussed:

1. The dependence of observed surface wave amplitudes on explosion yield and the characteristics of the emplacement medium is reviewed. Surface wave data compiled by others are used in conjunction with a new data set consisting of Airy phase amplitudes from the WWSSN stations ALQ and TUC.

2. The theoretical dependence of surface wave amplitude on the important controlling parameters is discussed. Attention is directed to the assumptions of the theoretical models and their consequences.

3. Preliminary results are presented for the development and testing of a deconvolution technique for analyzing short period teleseismic recordings of explosions.

- October 1977, "Seismic Studies of Surface and Body Waves for Improved Yield Determination," T. C. Bache and W. L. Rodi, SSS-R-78-3448, 79 pages.

The majority of the report is devoted to describing the results of two research projects not previously reported. One of these, "Determination of Crustal Structure from Surface Wave Dispersion Data," describes a recently developed method for obtaining crustal structure and gives results from application of this method to two paths in the southwestern United States: Nevada Test Site (NTS) to Albuquerque, New Mexico and NTS to Tucson, Arizona. Phase and group velocities are determined from NTS explosion recordings. These data are used in a formal generalized inversion procedure to determine crustal structures that are also consistent with other available data about the region; e.g., P_n velocities. Theoretical seismograms computed with the new crustal models show remarkable agreement with observations of NTS explosions at the two stations.

The second research study described is entitled, "Small-Scale Laboratory Simulations of Explosion Produced Body Waves - Implications for the teleseismic Signatures of Underground Nuclear Explosions." Small scale laboratory experiments were carried out to measure the ground motions from spherical charges. There were two classes of experiments; one in which the ground motions were free-field and one in which they included a free surface effect. Of the latter, some were quite

shallow and cratered. The most important feature of the experimental data is a large negative pulse that occurs at late-time in the experiments that include free-surface effects. Much of the study is directed toward determining the effect a pulse of this kind would have on the teleseismic body waves from nuclear explosions and m_b-log yield relations. If a late arriving negative pulse like that in the experimental data also occurs in underground nuclear explosions, the effect is to lower the slope of the m_b-log yield relation. This may explain why observed slopes are lower than predicted by theoretical models in which the free surface is represented elastically.

- January 1978, "Station Transfer Functions, Analysis of P-Wave Residuals and Summary of Current Research," J. F. Masso, J. M. Savino and T. C. Bache, SSS-R-78-3559, 80 pages.

Brief summaries of work are given in four topic areas: Source Studies, Data Analysis, Surface Wave Studies and Body Wave Studies.

Also included in the report is a detailed description of a research project not previously reported. This study is entitled, "Worldwide Observations of P-Wave Travel-Time Residuals." A large set of residuals compiled from ISC bulletins by Georges Poupinet of Institute de physique du Globe were compared with other data from the United States. The conclusions are that; (1) large negative residuals correlate with low heat flow and positive magnitude bias, and (2) large positive residuals correlate with high heat flow and negative magnitude bias. The same correlation between heat flow and travel-time residuals holds for stations located on the Russian and Siberian Platforms in the U.S.S.R.

- April 1978, "Analysis of Explosion Generated Surface Waves in Africa, Results from the Discrimination

Experiment and Summary of Current Research," W. L. Rodi, J. M. Savino, T. G. Barker, S. M. Day and T. C. Bache, SSS-R-78-3653, 92 pages.

The majority of the report is devoted to presentation of results not previously reported from four research projects. The first is entitled, "Discrimination Experiment." Digital short- and long-period body and surface wave data for Eurasian events recorded at a global network of stations are being provided for event discrimination. Efforts to date have focused on the application of the VFM (variable frequency magnitude) discriminant to the short period P waves at four stations. Thirteen events have been analyzed and tentative identification has been made.

The second project is entitled, "Analytic Continuation of the Elastic Field from a Complex Source in a Halfspace." We present the mathematical development of a method for linking finite difference numerical source calculations in a halfspace with analytical techniques for propagating elastic waves in layered media.

The third detailed discussion, "Theoretical Computation of Lg," is concerned with the theoretical generation of Lg in a continental earth model. Synthetic seismograms are shown for several ranges and source depths. The fourth topic is, "Analysis of Surface Waves from the French Test Site in the Sahara." For an underground explosion in Algeria surface wave recordings from five stations in or near Africa were analyzed to determine the phase and group dispersion. Using formal linear inversion, these data were inverted to obtain preliminary models for the crust and upper mantle along the five paths. Using these models, synthetic seismograms were computed and were found to be in good agreement with the observations at most of the stations.

- August 1978, "Source Studies, Results from the Discrimination Experiment and Summary of Current Research," J. M. Savino, N. Rimer, H. J. Swanger and T. C. Bache, SSS-R-78-3736, 68 pages.

The majority of the report is devoted to presentation of results not previously reported from three research projects. The first is entitled, "Discrimination Experiment." Digital short and long period body and surface wave data for Eurasian events recorded at a global network of stations are being provided for event discrimination. Efforts to date have focused on the application of the VFM (variable frequency magnitude) discriminant to the short period P waves at eight stations. Twenty-eight events have been analyzed and tentative identification has been made.

The second project is entitled, "Surface Wave Solution for the Elastic Equivalent of a Complex Axisymmetric Source." In our last quarterly report we presented the mathematical development of a method for linking finite difference numerical source calculations with analytical techniques for propagating body waves in layered elastic media. In this report the theory is extended to include the propagation of Rayleigh waves.

The third project is entitled, "Source Calculations." Our one-dimensional constitutive models for the numerical simulation of the explosion source were reviewed to ensure their compatibility with our two-dimensional finite difference programs. Three important improvements to the models were made: (1) the implementation of new equations of state for the cavity gases; (2) an improved treatment of overburden pressure and (3) an improved effective stress model. The new models and their effect on source calculations for PILEDRIVER, SALMON and Rainier Mesa tuff are described.

A.2 FINAL CONTRACT REPORTS

- October 1976, "Improved Yield Determination and Event Identification Research," J. M. Savino, T. C. Bache, T. G. Barker, J. T. Cherry, D. G. Lambert, J. F. Masso, N. Rimer and W. O. Wray, SSS-R-77-3038, 61 pages.

Work performed on Contract No. F8606-75-C-0045 has been reported in detail in a series of twelve topical and quarterly technical reports. This final report summarizes the material covered in each of the technical reports and discusses the conclusions obtained. The primary objective of the program is to develop methods for estimating the yield of underground nuclear explosions. The topics addressed include the modeling of both single and multiple explosions, propagation of the resultant stress waves through realistic earth structures, and prediction of short- and long-period explosion seismograms recorded at teleseismically located receivers. The results of these investigations provide a theoretical framework for expressing uncertainties in explosion yield estimates in terms of uncertainties in the near source material properties, local source and receiver crustal structures, and the upper mantle structure of the earth.

- July 1977, "Seismic Ground Motion from Free-Field and Underburied Explosive Sources," J. T. Cherry, T. G. Barker, S. M. Day and P. L. Coleman, SSS-R-77-3349, 44 pages.

Small-scale laboratory experiments were conducted and analyzed to study the effect of the proximity of the free surface on the seismic ground motions. Two classes of experiments were done. In one the charges were far from the free surface and the free-field displacement-time histories were measured. In the second class the charges were near the surface and were either fully contained or formed a crater. The charges were 0.25 g of PETN in concrete cylinders,

120 cm in diameter and 33 to 60 cm thick. In all experiments displacements were measured 30.5 cm directly below the charges. The experiments produced consistent and repeatable data. A striking feature of the ground motions for the near surface experiments is a large long-period negative pulse which is present whether or not cratering occurred.

The results were studied by comparing to numerical simulations of the experiments using a Lagrangian finite difference program and published properties of the concrete and PETN. The calculations are in good agreement with the laboratory data, providing verification of both the constitutive models and the methods.

The large, long-period negative pulse can be explained in the context of linear elasticity. It is due to the near-field interaction of the spherical wave front with the free surface. Therefore, it does not propagate to the far-field and is not important for teleseismic magnitudes.

A.3 TECHNICAL REPORTS

- September 1975, "Seismic Coupling from a Nuclear Explosion: The Dependence of the Reduced Displacement Potential on the Nonlinear Behavior of the Near Source Rock Environment," J. T. Cherry, N. Rimer and W. O. Wray, SSS-R-76-2742, 68 pages.

The objective of the research presented in this report is to determine the dependence of teleseismic magnitudes on the nonlinear behavior of the near source rock environment. Such information enables one to express uncertainties in explosive yield estimates in terms of uncertainties in the material properties and provides insight concerning the requirements for collection of geophysical data at a specific test site.

A series of spherically symmetric calculations have been performed in which the properties of the near source

material were varied systematically. Output from these calculations enables one to determine the relative teleseismic coupling efficiency of a given near source material. Also, since seismic magnitudes are directly related to explosive yield, this parameter study permits an assessment of uncertainties in the estimated yield in terms of uncertainties of the material properties of the test site.

- October 1975, "Constitutive Equations for Fluid-Saturated Porous Media," S. K. Garg, SSS-R-76-2766, 12 pages.

This report developes constitutive relations for fluid-saturated porous media, suitable for inclusion in standard hydrodynamic codes (e.g., CRAM or SKIPPER). The theoretical formulation is based on the models for fluid-saturated rock aggregates previously developed by Garg and Nur (1973) and Garg, et al. (1975).

- February 1976, "Prediction and Matching of Teleseismic Ground Motion (Body and Surface Waves) from the NTS MAST Explosion," T. G. Barker, T. C. Bache, J. T. Cherry, N. Rimer and J. M. Savino, SSS-R-76-2727, 60 pages.

This report presents the results of a theoretical prediction of the teleseismic body and surface wave signatures of the recent underground explosion, MAST, and a detailed comparison of the predicted waveforms with seismograms recorded at stations of the Special Data Collection System (SDCS). This study represents a comprehensive analysis of the MAST event involving computer modeling of the close-in nonlinear ground motion produced by the explosion, propagation of the resultant stress waves through the appropriate earth structures and computation of seismograms recorded at designated teleseismic stations.

- February 1976, "Teleseismic Coupling from the Simultaneous Detonation of an Array of Nuclear Explosions," J. T. Cherry, T. C. Bache, W. O. Wray and J. F. Masso, SSS-R-76-2865, 26 pages.

This report presents the results of a theoretical study undertaken to determine if teleseismic ground motion may be enhanced by the simultaneous detonation of a closely spaced array of nuclear explosions. The specific array analyzed consisted of three 15 kt explosions equally spaced 165 meters apart. The explosive array was assumed contained, i.e., coupling effects due to cratering were not included in the analysis.

- May 1976, "Comparison of Theoretical and Observed Body and Surface Waves for KASSERI, an Explosion at NTS," T. C. Bache, T. G. Barker, N. Rimer and J. M. Savino, SSS-R-76-2937, 44 pages.

This report presents the results of a theoretical calculation of the teleseismic body and surface waves for the NTS KASSERI explosion, and a detailed comparison of the synthetic seismograms with those recorded at stations of the Special Data Collection System (SDCS). This study is a comprehensive analysis of the KASSERI event including modeling of the close-in nonlinear ground motion produced by the explosion, propagation of the resulting seismic waves through the earth and computation of synthetic seismograms at designated teleseismic stations.

- May 1976, "Teleseismic Verification of Data Exchange Yields," T. C. Bache, T. G. Barker, J. T. Cherry and J. M. Savino, SSS-R-76-2941, 55 pages.

This working paper addressed the possibility of directly inverting teleseismic ground motion in order to obtain explosion yield. We accomplished this inversion via a deterministic

model which predicts the teleseismic ground motion for a nuclear explosion. Our intent is to use the data to choose an analog rock whose material properties are consistent with the data furnished in the exchange.

- November 1976, "The Dependence of Body Wave Magnitude on Yield for Underground Explosions in Salt," T. C. Bache, J. T. Cherry and B. F. Mason, SSS-R-77-3057, 36 pages.

In this report we address the dependence of body wave magnitude (m_b) on yield for explosions in salt. Our objective is to compare salt events in Eurasia to similar, though hypothetical, events at NTS and to granite events at NTS. Our study uses deterministic computational methods and our results are based on time domain measurements from synthetic seismograms. The methods have been shown to give theoretical seismograms that agree quite well with observations when appropriate model parameters are included in the calculations.

- January 1977, "Theoretical Body and Surface Wave Magnitudes for Twelve Numerically Simulated Cratering Explosions," T. C. Bache, J. F. Masso and B. F. Mason, SSS-R-77-3119, 142 pages.

The results of the Systems, Science and Software (S^3) contribution to a study of cratering explosions are presented. A series of twelve numerical simulations of 150 kt cratering explosions in three materials at several depths were carried out by Applied Theory, Inc. The data from these calculations were processed to compute theoretical far-field body and surface wave seismograms and from these to determine m_b and M_s. The m_b and M_s data are to be analyzed by Pacific Sierra Research.

The theoretical seismogram calculations are done in a two-step process. First, an equivalent elastic source representation of the cratering event is obtained. The wave field is then propagated through realistic layered earth models to

teleseismic distances. For this application the procedure is found to be more accurate for the shorter period body waves than for the surface waves. The m_b and M_s values are presented for the twelve 150 kt sources and for these sources scaled to 37.5 and 600 kt. Also given are the values for contained explosions of the same yield in the same emplacement material. The contribution of the ejecta fallback is studied and is found to be insignificant for teleseismic magnitude values.

- February 1977, "Comparison of Theoretical and Observed Short Period Seismograms for Soviet Explosions in Salt," T. C. Bache, SSS-CR-77-3136. (Classified Report, Unclassified Title and Abstract), 44 pages.

In this report we direct our attention to five specific Soviet explosions in salt. These were PNE events and the Soviet estimates for the yield and depth of burial are available. The contracting officer has also provided us with estimates of the near-source crustal layering for these events. The question to be addressed in our report is then, with all this information, how well can we match the recorded waveforms and amplitudes of these events?

- March 1977, "A Review of the Nature and Variability of the Anelastic Properties of the Upper Mantle Beneath North America and Eurasia," B. J. Mitchell and T. C. Bache, SSS-R-77-3164, 25 pages.

All reasonable mechanisms for producing low-velocity zones in the upper mantle should also produce zones of low Q. The available studies of upper mantle Q and the velocity for the same regions suggest that a coincidence of low velocity and low Q zones does indeed occur.

Seismic body- and surface-wave data indicate a substantial low velocity, low Q zone in the upper mantle beneath

western North America. The zone appears to be 150 km thick or more, the velocities for both P and S waves being lower than typical upper mantle velocities for stable regions.

The available evidence for eastern North America indicates that a low velocity zone is either absent for that region or more poorly developed than it is in western North America. Most interpretations for P waves in eastern North America include no low velocity zone. Surface wave studies of the shear wave velocity structure beneath eastern North America indicate the possibility of a low velocity zone for S waves, at least in some regions.

The available data for northern Europe and Asia indicate that it is a stable region with velocity and attenuative properties much like those of eastern North America. The difference in attenuative properties of the upper mantle between the western United States and northern Asia might lead to higher m_b values for the Asian nuclear events than for equivalent NTS events, if the low velocity, low Q zone beneath the western United States is sufficiently thick and has low enough values. Thickness and Q values suggested by most published research can easily cause m_b values for events in the Basin and Range province to be a few tenths of a magnitude unit lower than events in shield regions.

- June 1977, "Simulation and Decomposition of Multiple Explosions," D. G. Lambert, T. C. Bache and J. M. Savino, SSS-R-77-3194, 66 pages.

The purpose of the study is to develop procedures for using seismic measurements to verify the number and yields of individual explosions making up a multiple event. Multiple explosion seismograms are simulated by straightforward summations of single explosion records. Several types of multiple explosions are simulated. These include closely spaced equal

yield explosions (no consideration given to propagation path effects between explosions and receiver) and relatively more widely spaced explosions (propagation path effects included) of varying yields. The data employed are principally close-in seismic recordings of the Nevada Test Site explosions obtained from Sandia Laboratories in Albuquerque, New Mexico. Decomposition of the simulated multiple explosion records is accomplished using a series of narrow-band filters with center frequencies ranging from 3 to 100 Hz. In general, our results show that the narrow-band filter technique is able to achieve accurate time separation and amplitude scaling. The limitation on the technique is essentially the requirement for the presence of sufficient signal energy at frequencies greater than about 3.5 times the inverse of the lag time between arriving signals.

- October 1977, "Identification of Individual Events in a Multiple Explosion from Teleseismic Short Period Body Wave Recordings," D. G. Lambert and T. C. Bache, SSS-R-78-3421, 40 pages.

The objective of this study is to detect and identify the individual events in a hypothetical multiple explosion. The data analyzed are simulated short period body wave recordings of that event. These were, presumably, constructed by lagging, scaling and summing a single event record according to some formula unknown to the analysts. Data for two stations, including both the single event and multiple event records, were provided to Systems, Science and Software by the VELA Seismological Center.

The data were analyzed by the MARS (Multiple Arrival Recognition System) program which uses a series of narrow-band filters to identify phase arrivals. Their amplitude and arrival time are accurately preserved. The variable frequency magnitude (VFM) discriminant is also computed and

the multiple explosion records are clearly identified as being from an explosion.

For decomposition of the multiple event the MARS output for the single and multiple event records were cross-correlated. Two main groups of events separated by 6.7 to 7.8 seconds, depending on azimuth, were identified. Each of these groups appeared to include two or more explosions.

Subsequent comparison with the actual array configuration showed that the two main groups of events had been correctly identified. There were two events in each group and their lag times were correctly identified within 0.1 second. For these four events the relative amplitude estimates were correct within 10 to 20 percent. The actual array also included two other smaller and later events that were not identified by our analysis.

- April 1978, "Analysis of Two Decoupled Explosion Simulations," T. C. Bache and J. F. Masso, SSS-R-78-3627, 44 pages.

Two axisymmetric ground motion calculations were carried out by Applied Theory, Inc. to simulate 25 kt decoupled nuclear explosions in mined cavities in salt. One cavity was spherical with a radius of 66 meters while the other was a 3/1 aspect ratio ellipsoid of revolution. Both had the same volume. Results of the two calculations were analyzed to determine the character of the teleseismic body and surface waves.

The spherically symmetric portion of the field is slightly (20 to 25 percent) smaller for the spherical cavity. Comparing to results of tamped explosions, the decoupling factor for this case is about 140 at 1 Hz. The radiation from the ellipsoidal cavity is substantially perturbed from spherical symmetry; the maximum S wave amplitudes are nearly

three times as large as maximum P wave amplitudes at 1.0 Hz. However, theoretical body and surface wave seismograms indicate that the m_b and M_s values are not substantially different for the two cavities.

- June 1978, "Source Amplitudes of NTS Explosions Inferred from Rayleigh Waves at Albuquerque and Tucson," T. C. Bache, W. L. Rodi and B. F. Mason, SSS-R-78-3690, 91 pages.

Comparing observed and synthetic seismograms, source amplitudes of NTS explosions are inferred from Rayleigh wave recordings from the WWSSN stations at Albuquerque, New Mexico (ALQ) and Tucson, Arizona (TUC). The potential influence of source complexities, particularly surface spallation and related phenomena, is studied in detail.

As described in earlier work by Bache, Rodi and Harkrider, the earth model for the synthetic were converted from observations at ALQ and TUC. The agreement of observed and synthetic seismograms is quite good and is sensitive to important features of the source.

The events studied are in three distinct areas, Yucca Flat, Pahute Mesa and PILEDRIVER in climax granite. All events were below the water table and the yields varied from 40 to 200 KT. Within each group the mean static value of the reduced displacement potential (Ψ_∞) was determined at a fixed scaled yield, assuming a spherically symmetric point source. The source is then modified to study the effect of: (1) the addition of a double-couple component; (2) the addition of a surface impulse associated with impact of the material spalled from the surface; (3) loss of energy from the free surface reflected waves due to spallation. Comparing observed and synthetic seismograms, the extent of the effect of these secondary phenomena is outlined.

For Yucca Flat and Pahute Mesa events the inferred source amplitudes are in general agreement with values

obtained by other methods. The spall impulse is too small to be of much importance. More likely to be important, especially for the Pahute Mesa events, is the loss of energy from the up-going waves. For PILEDRIVER the double-couple and attenuation of up-going waves dominate the source determination. Correcting for these phenomena, the explosion source level (Ψ_∞) is considerably smaller than has usually been supposed.

- August 1978, "A Detailed Listing of the Data and Results for the Unclassified Report: Source Amplitudes of NTS Explosions Inferred from Rayleigh Waves at Albuquerque and Tucson," T. C. Bache, W. L. Rodi and B. F. Mason, SSS-CR-78-3745, 17 pages.

An analysis of Rayleigh waves at the indicated stations is presented. The objective was to infer the amplitude and character of the source function. This report is intended to serve as an Appendix to the earlier report. Detailed listings of the data and the results of the analysis are given.